APPLICATION OF STATISTICAL ENERGY ANALYSIS TO VIBRATIONS OF MULTI-PANEL STRUCTURES

ERIC E. UNGAR
NICHOLAS KORONAIOS
JEROME E. MANNING

FOREWORD

This report was prepared by Bolt Beranek and Newman Inc., Cambridge, Massachusetts, for the Aerospace Dynamics Branch, Vehicle Dynamics Division, AF Flight Dynamics Laboratory, Wright-Patterson Air Force Base, Ohio 45433, under Contract No. AF 33 (615)-2649. The research performed is part of a continuing effort to provide advanced techniques in the application of random process theory and statistics to vibration problems. This effort is part of the Research and Technology Division, Air Force Systems Command's exploratory development program. The contract was initiated under Project No. 1370, "Dynamic Problems in Flight Vehicles," Task No. 137005, "Prediction and Control of Structural Vibration." Lt. A.R. Basso of the Vehicle Dynamics Division, FDDS was the project engineer.

This report covers work conducted from February 1966 to April 1967. Contractor's report number is 1491. Manuscript released by the author in May 1967 for publication.

The authors are indebted to Drs. D.C. Karnopp, T.D. Scharton, and K.S. Lee for the ideas they contributed to the subject matter of this report and to Mr. Y. Kadman for his valuable assistance with the experimental phases of the reported work.

This technical report has been reviewed and is approved.

Howard C. Magrath

HOWARD A. MAGRATH
Chief, Vehicle Dynamics Division

ABSTRACT

Experimentally determined vibratory mean square velocity distributions on a multi-panel planar structure and on a ring-and-stringer reinforced cylindrical shell are compared with predictions obtained from statistical energy analysis. Generally good agreement is observed.

The flow of mechanical power between two panels that are separated by a reinforcing beam is studied, in order to uncover the important parameters and to provide information on the coefficients of proportionality between power flow and average modal energy difference, which one must know in order to apply statistical energy analysis. No analytical prediction methods are developed for these coefficients, but an empirical measurement technique is presented and is shown to yield consistent results.

Analyses pertaining to dynamic response concentrations in plate and shell structures are summarized, and investigations of response characteristics and response statistics which warrant further pursuit are delineated.

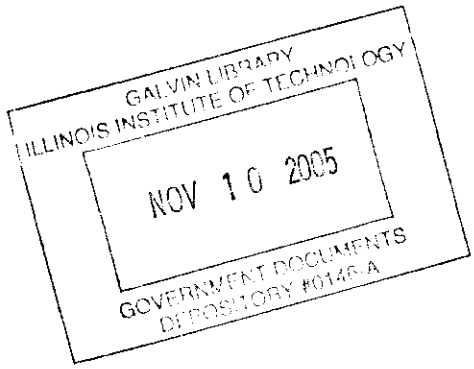

TABLE OF CONTENTS

TABLE OF CONTENTS (continued)

LIST OF ILLUSTRATIONS AND TABLES

LIST OF ILLUSTRATIONS AND TABLES (continued)

LIST OF ILLUSTRATIONS AND TABLES (continued)

LIST OF ILLUSTRATIONS AND TABLES (continued)

APPLICATION OF STATISTICAL ENERGY ANALYSIS TO VIBRATIONS OF MULTI-PANEL STRUCTURES

INTRODUCTION

Statistical energy analysis, the fundamentals of which have been presented in Ref. 1, is an analytical tool of great potential utility, since it promises to enable one to deal relatively simply with the (multi-modal) random vibrations of built-up structures and of elastic systems involving both structures and fluids. Although some basic assumptions that underlie statistical energy analysis have not been verified for the general case (see Appendix III), this approach has been applied successfully to predict the vibrational behavior of some structural and structure/fluid systems of limited complexity (Refs. 2-4).

The present report describes the results of study that had the two-fold purpose of (1) verifying the applicability of the statistical energy analysis approach to relatively realistic multi-panel structures, and (2) developing additional information to make this approach and its results more useful in practice.

The first of the following sections compares experimentally observed results with statistical energy predictions for two multi-panel structures. The second section describes a study of the coefficients that pertain to power flow between two panels, which coefficients must be known before one can perform statistical analysis calculations. The final section summarizes some thoughts on extensions of statistical energy analysis, pertaining to response concentrations and response statistics.

VIBRATION DISTRIBUTIONS IN MULTI-PANEL STRUCTURES

The following paragraphs describe a study that was carried out on two structural configurations in order to obtain an indication of how well statistical energy analysis can predict the mean-square vibrations of multi-panel structures, when these structures are excited at one point.

Test Structures

Two structural configurations were selected for extensive study: a fin-like structure made up of beam-reinforced flat plates, and a ring-and-stringer-reinforced cylindrical shell (Fig. 1). These configurations were chosen because they are reasonably realistic, yet simple enough so that their analysis does not require an excessive amount of computation.

Both structures of Fig. 1 were made of 1/16-inch thick aluminum, and all reinforcing beams and rings were of aluminum, with 1/2-inch × 3/4-inch rectangular cross-sections. These reinforcements were attached (along their 1/2-inch wide faces) by means of a rigid epoxy (Allaco 20-20).

The "fin" was assembled from two plates; one comprises the rectangular base plate G, the other the trapezoidal fin itself. Three layers of two-inch wide damping tape (Minnesota Mining and Manufacturing Co. 428 B) were applied along the edges of the base plate, in order to simulate the loss of vibratory energy that the fin would experience if it were attached to some larger structure. A weld was used to strengthen the joint between the fin and the beam at its base, since the epoxy was found to have insufficient strength to support the structure. For the same reason, bolts were used in addition to the epoxy to secure the junction beam to the base plate.

The cylindrical shell was assembled from two separate segments, one 25 inches, and the other 48 inches high. The two shell segments were joined via a ring epoxied to the adjacent edges of the segments.

Statistical Energy Analysis

In order to apply the statistical energy approach to the fin structure one may consider each of the seven panels that comprise that structure as a separate elastic system (or "mode set" within a given frequency band). One may then draw a power flow diagram as shown in Fig. 2, if one makes the reasonable assumption that the power flow between panels that touch each other only at their corners is negligible. The notation used in Fig. 2 and in the subsequent analysis is essentially that of Ref. 1; A_α denotes the time-average power supplied to panel α, D_α denotes the time-average power dissipated by that panel, and $P_{\alpha\beta}$ denotes the time-average power transferred from panel α to panel β.

By considering the energy balance of each of the seven fin panels one may obtain the following seven relations:

$$\begin{aligned} A_A &= D_A+P_{AB}+P_{AF} \quad , & A_E+P_{FE} &= D_E+P_{ED}+P_{EG} \quad , \\ A_B+P_{AB} &= D_B+P_{BC} \quad , & A_F+P_{AF} &= D_F+P_{FE} \quad , \\ A_C+P_{BC} &= D_C+P_{CD} \quad , & A_G+P_{EG}+P_{DG} &= D_G \quad . \\ A_D+P_{CD}+P_{ED} &= D_D+P_{DG} \quad , \end{aligned} \tag{1}$$

If the conditions (Ref. 1) hold under which the power flow between two panels is proportional to the difference between their average modal kinetic energies, then one may write

$$P_{\alpha\beta} = \phi_{\alpha\beta}(T_\alpha - T_\beta) \quad , \tag{2}$$

where T_α and T_β represent the average modal kinetic energies of panels α and β, respectively, and where the constant of proportionality $\phi_{\alpha\beta}$ is known as the power flow coefficient. It is also convenient to set

$$D_\alpha = d_\alpha T_\alpha \quad , \tag{3}$$

where d_α is related to the panel loss factor η_α, to the center frequency f_o and bandwidth Δf of the frequency band under consideration, and to the modal density n_α (number of modes per unit frequency interval) of the panel as (Ref. 1)

$$d_\alpha = 4\pi\, f_o\, \eta_\alpha\, n_\alpha(f_o)\Delta f \quad . \tag{4}$$

By substituting Eqs. (2) and (3) into (1) one finds that each of Eqs. (1) may be expressed in the form

$$T_j\left[d_j + \sum_k \phi_{jk}\right] - \sum_k \phi_{jk}\, T_k = A_j \quad , \tag{5}$$

where j=A,B,...,G refers to the elements whose energy balance is being considered and k=A,...,G to elements which are connected in the power flow diagram to the element under consideration. The summation on k is to be performed over all elements which are directly connected to the element being considered. Specifically, Eqs. (1) become

$$
\begin{aligned}
T_A\left(d_A+\phi_{AB}+\phi_{AF}\right)-T_B\phi_{AB}-T_F\phi_{AF} &= A_A \\
T_B\left(d_B+\phi_{AB}+\phi_{BC}\right)-T_A\phi_{AB}-T_C\phi_{BC} &= A_B \\
T_C\left(d_C+\phi_{BC}+\phi_{CD}\right)-T_B\phi_{BC}-T_D\phi_{CD} &= A_C \\
T_D\left(d_D+\phi_{CD}+\phi_{DG}+\phi_{ED}\right)-T_C\phi_{CD}-T_G\phi_{DG}-T_E\phi_{ED} &= A_D \qquad (6) \\
T_E\left(d_E+\phi_{ED}+\phi_{EG}+\phi_{FE}\right)-T_D\phi_{ED}-T_G\phi_{EG}-T_F\phi_{FE} &= A_E \\
T_F\left(d_F+\phi_{AF}+\phi_{FE}\right)-T_A\phi_{AF}-T_E\phi_{FE} &= A_F \\
T_G\left(d_G+\phi_{EG}+\phi_{DG}\right)-T_E\phi_{EG}-T_D\phi_{DG} &= A_G \quad .
\end{aligned}
$$

It is of interest to note that the form of Eqs. (5) and (6) may also be deduced by observing the analogy between a power flow diagram like that of Fig. 2 and the type of diagram one usually draws to study heat flow (and temperature distribution) problems by lumped-parameter approximations. Relations like Eq. (5) are typical of heat transfer problems (for example, see Ref. 5).

Equations (6) constitute seven linear equations in terms of the seven unknowns $T_A, T_B, \ldots T_G$, and may be solved for these unknowns by any of several well-known techniques. Numerical methods, such as matrix inversion, or — in analogy to heat transfer — relaxation techniques, appear to be most efficient here. Such techniques, of course, require that the numerical

values of all coefficients and of all "external inputs" A_α be known.

Once these average modal kinetic energies have been determined, one may calculate the mean-square velocities of the various panels from

$$\langle v_\alpha^2 \rangle = 2T_\alpha n_\alpha(f_o)\ \Delta f/M_\alpha \tag{7}$$

where M_α represents the mass of panel α.

The analysis of the cylindrical shell structure may be carried out much like that of the fin. The power flow diagram for the shell is shown in the lower portion of Fig. 2, and the energy balance relations are found to yield the following ten relations in the ten unknown average modal kinetic energies:

$$\begin{aligned}
T_A(d_A+\phi_{AB}+\phi_{AJ}+\phi_{AD}) - \phi_{AB}T_B - \phi_{AD}T_D - \phi_{AJ}T_J &= A_A \\
T_B(d_B+\phi_{BA}+\phi_{BE}+\phi_{BC}) - \phi_{BA}T_A - \phi_{BE}T_E - \phi_{BC}T_C &= A_B \\
T_C(d_C+\phi_{CB}+\phi_{CF}+\phi_{CK}) - \phi_{CB}T_B - \phi_{CF}T_F - \phi_{CK}T_K &= A_C \\
T_D(d_D+\phi_{DH}+\phi_{DA}+\phi_{DE}) - \phi_{DH}T_H - \phi_{DA}T_A - \phi_{DE}T_E &= A_D \\
T_E(d_E+\phi_{ED}+\phi_{EB}+\phi_{EF}) - \phi_{ED}T_D - \phi_{EB}T_B - \phi_{EF}T_F &= A_E \\
T_F(d_F+\phi_{FE}+\phi_{FC}+\phi_{FG}) - \phi_{FE}T_E - \phi_{FC}T_C - \phi_{FG}T_G &= A_F \\
T_G(d_G+\phi_{GF}+\phi_{GK}+\phi_{GH}) - \phi_{GF}T_F - \phi_{GK}T_K - \phi_{GH}T_H &= A_G \\
T_H(d_H+\phi_{HG}+\phi_{HJ}+\phi_{HD}) - \phi_{HG}T_G - \phi_{HJ}T_J - \phi_{HD}T_D &= A_H \\
T_J(d_J+\phi_{JK}+\phi_{JH}+\phi_{JA}) - \phi_{JK}T_K - \phi_{JH}T_H - \phi_{JA}T_A &= A_J \\
T_K(d_K+\phi_{KC}+\phi_{KG}+\phi_{KJ}) - \phi_{KC}T_C - \phi_{KG}T_G - \phi_{KJ}T_J &= A_K
\end{aligned} \tag{8}$$

Measurements

Vibration distribution and input power. Vibration measurements were performed with the test structures suspended from the laboratory ceiling by means of thin wires or strings. A typical experiment consisted of exciting the test structure at one point of one of the panels by means of an electrodynamic shaker, and of measuring the accelerations at one point on each panel. In an experimental series these measurements were repeated for different driving points on a given panel and for different measuring points on the other panels.

In all cases the mechanical power supplied to the structure at the driving point was also measured by means of an impedance head (connected between the excitation source and the driven point on the structure) and attendant electronic instrumentation.

All of the aforementioned measurements were carried out in one-third-octave bands: the shaker used to excite the structure was activated by a signal that was generated by a white-noise source, passed through a 1/3-octave filter, and suitably amplified; the outputs of the various accelerometers were filtered in the same 1/3-octave bands as the excitation signal, before they were fed to a voltmeter. For each excitation condition, meter readings corresponding to the excitation force amplitude F, to the driving point velocity amplitude V, and to the product FV were obtained, as well as a reading for the (average) phase angle between the force and velocity. In addition, readings corresponding to the accelerations of points on the various panels were taken, and various signals were monitored on an oscilloscope to ensure that the instrumentation system was operating properly.

Instrumentation. The instrumentation system used in the previously described measurements is diagramed in Fig. 3, and the specific items of electronic instrumentation are further identified in Table I, which appears right after Fig. 3. As indicated in Fig. 3, the impedance head provides two signals: one corresponding to the driving force, the other to the acceleration at the driving point. These signals were fed to phase-matched high impedance amplifiers which have gain controls that permit the signal levels to be adjusted to the ranges best suited to the power meter. The amplified acceleration signal was integrated by an operational amplifier, so that one could obtain a signal proportional to velocity; the power meter in effect formed the (time-averaged) product of the force and velocity signals, and thus measured the mechanical power supplied to the test structure.

The outputs of the various accelerometers attached to the test structure were connected to an rms-voltmeter via a selector switch. This voltmeter, which is provided with an averaging-time adjustment, was used also to read the force and velocity signals derived from the impedance head.

All accelerometers were calibrated at 1g and at 100 Hz, as connected to the entire circuit, by attaching them to the vibrating platforms of a (General Radio Corp. Model 1557-A) vibration calibrator. The accelerometer outputs also were compared to that of the impedance head accelerometer over a range of frequencies up to 5000 Hz, by mounting them directly on the impedance head. For calibration of the force gage of the impedance head, a 100 gm weight was attached to the impedance head and shaken at 1g at several frequencies. Proper operation of the power meter was verified by operating the system with only a pure mass attached to the impedance head and noting the very low corresponding power readings and the 90° phase angles between the force and velocity signals.

Auxiliary measurements. In order to provide the information required as input to the theoretical caculations, the panel loss factors and the power flow coefficients were determined.

Loss factor measurements were made in the various 1/3-octave bands (by means of the well-established decay-rate technique) on each of the two panels that comprise the fin and on each of the two shells that make up the cylindrical shell structure. The results of these measurements, which were made before assembly of the structures, with no reinforcements added, but with the damping tapes in place on panel G, are indicated in Figs. 4 and 5.

Values for the power flow coefficients were obtained from a separate series of measurements, carried out on two panels separated by a reinforcing beam, as described in detail in the next major section of this report. The average values of these coefficients, which were used in the numerical calculations discussed later, are presented in Fig. 6.

Calculations

Procedure. Numerical calculations corresponding to the fin and cylindrical shell test structures were carried out, based on Eqs. (6) and (8), and using the values of the loss factors and power flow transmission coefficients indicated in Figs. 4-6. Because all of the reinforcements had the same cross-section, all of the beams and rings, except the ring that coupled the two shell portions, were taken to have the same power flow transmission coefficient (given by the solid curve of Fig. 6, which corresponds to the case where the structure is continuous under a reinforcement). For the latter ring the dotted curve of Fig. 6 was used, which corresponds to the case where the structure is not continuous under the reinforcing beams.

In these calculations Eq. (4) was used to change the loss factor data into values of the damping coefficient d_α, and the modal densities of the various panels were calculated from the expression (Ref. 1)

$$n(f_o) = A_s\left[3\left(1-\nu^2\right)\right]^{1/2}\left(h\, c_L\right)^{-1} \quad , \tag{9}$$

where A_S denotes the surface area and h the thickness of the panel, and where ν denotes Poisson's ratio and c_L the longitudinal wave velocity of the panel material. Although Eq. (9) applies strictly only for flat plates and for shells at high frequencies, it was used for the cylindrical shell throughout the entire frequency range studied.

If all input power terms of Eqs. (6) or (8), except one, are set equal to zero, in order to make these equations conform to the experimental conditions, then one may most conveniently solve these equations for the various values of T_α/A, where A is the one non-zero input power. If one uses the definition for the average modal kinetic energy T_α and expresses A in terms of the driving point resistance R and mean-square velocity v_o^2 of the driving point, one finds that

$$\frac{T}{A} = \frac{M_\alpha \langle v_\alpha^2 \rangle / 2 n_\alpha(f_o)\Delta f}{R\, v_o^2} \tag{10}$$

where $\langle v_\alpha^2 \rangle$ represents the spatial average mean-square velocity of panel α. Thus, T_α/A may be directly interpreted in terms of the velocity ratio $\langle v_\alpha^2 \rangle / v_0^2$, if the various panel parameters are known.

Calculated values of T_α/A for the various panels as a function of frequency are shown in Figs. 7 and 8 for the fin excited at panels B and E, respectively, and in Fig. 9 for the cylindrical shell excited at panel A.

Discussion of results. All of the curves of Figs. 7-9 may be seen to exhibit an average slope of approximately -2. Some of this very strong frequency-dependence of T_α/A is due to the Δf term that appears on the right-hand side of Eq. (10); curves of $\langle v_\alpha^2 \rangle / v_0^2$ would have an approximate shape of only -1, if all of the other parameters of Eq. (10) were independent of frequency.

Inspection of Eq. (4) reveals that the dissipation factor d_α is proportional to the square of frequency, whereas Fig. 6 shows that the power flow coefficients vary only as roughly the first power of frequency. With increasing frequency one would therefore expect local power dissipation to take on increasing importance relative to power transmission, thus justifying the observed decrease of $\langle v_\alpha^2 \rangle / v_0^2$ with increasing frequency.

Comparison of the various theoretical curves of Fig. 7 reveals that the curve for the externally excited panel B is highest, and that the curves lie below each other in the following order, proceeding from top to bottom: B, A, C, F, D, E, G. The curves for panels A through E are seen to be not widely separated from each other, whereas that for panel E is found to lie markedly below the rest. The observed rank-ordering of the vibration levels of the panels agrees with what one expects from energy considerations, which require the directly excited panel B to have the highest modal energy and the highly damped panel G (which is also relatively far from the directly excited panel) to have a relatively low modal energy. The relative magnitudes of the energies of the other panels lie between those of panels B and G, with panels closer to B and farther from G having higher energies.

Analysis of the theoretical curves of Fig. 8 leads one to essentially the same conclusions as those obtained from Fig. 7. For Fig. 8, however, panel E of the fin structure was the directly excited one, and the panel energies are arranged in the

order E, F, A, D, C, B, G. The curves for panels A, B, C, D, are all clustered together, and the curve for the highly damped panel G lies closer to that for the directly excited panel E than is the case in Fig. 7 (where the B panel is directly excited). This greater proximity again agrees with what one expects, since panel G is geometrically nearer to panel E than to panel B.

For the cylindrical shell structure (Fig. 9) one finds that all of the theoretical curves are closely clustered, except that the curve for the directly excited panel A lies somewhat above the rest. In this shell structure, all of the panels have nearly the same damping; there is no region of high damping, which would serve to decrease the energy levels markedly. Only a slight decrease of energy level with increasing distance from the driving point is evident, as expected. (For this lightly damped structure a simplified analysis based on equipartition of modal energy would have yielded nearly the same results.)

Experimental Results

The results of all of the previously described experimental measurements are summarized in Figs. 10-12, together with the corresponding calculated results, in terms of plots of T_α/A versus frequency. Each of these figures consists of several sheets (essentially one per panel), in order to present all of the information in readily interpretable form.

Figures 10 and 11 pertain to the fin; Figure 10 corresponds to excitation applied to panel B, and Fig. 11 to excitation applied to panel E. Figure 12 pertains to the cylindrical shell, excited at panel A. Because of the symmetry of the shell, it was necessary to analyze only one half of it; hence for the shell the figure has fewer pages than there are panels.

Comparison of Theoretical Predictions and Experimental Results

Inspection of Figs. 10-12 reveals that there exist general agreement between the theoretical and the experimental results. This agreement appears even better if one recalls that statistical energy analysis gives one only spatial averages, whereas the experimental data were obtained at discreet measurement points.

The scatter of the experimental results may be ascribed largely to the spread in the velocities one measures at different points on a structure. Such spreads in velocities have also been observed in experiments on simpler structure. (For example, see Fig. 17.)

The scatter of the experimental points for panel A in Figs. 10 and 11 is seen to be somewhat larger than that for the other panels. A similar statement holds also for panel F, except that the scatter for panel F is less than that for panel A. As evident from Fig. 1, panels A and F are the smallest panels of the fin structure. They thus have the smallest modal densities [see Eq. (9)], and one would expect them to exhibit the least uniform velocity distributions, and hence the greatest data scatter.

Nearly all of the theoretical curves of Figs. 10 and 11 agree reasonably well with the average values of the experimental data. Notable exceptions are the curves for panels D and E. Since D and E are those panels which are directly connected to the highly damped panel G, and the theoretical calculations yielded vibration levels which are lower than those that were measured, it is likely that too large values for the coupling of panels D and E to panel G were used in the calculations. This conjecture is plausible: in the calculations the same power flow coupling coefficient was used between all panels, but at the connection of panels E and D to panel G the panels are joined at right angles, whereas panels A through F lie in the same plane — coupling across a beam-reinforced right-angle joint is very likely to be poorer than that across a similar in-plane joint.

The theoretical curve of Fig. 10f, which pertains to the response of fin panel F with the excitation applied at panel B, also lies generally below the experimental data points. No explanation of this anomalous behavior is available, and such behavior is not apparent in Fig. 11f.

If one compares the theoretical curves and experimental points for the cylindrical shell (Fig. 12), one finds that on the whole the measured vibration levels were lower than those which were predicted theoretically. This discrepancy is believed to be due to use of too low damping (loss factor) values in the theoretical calculations, and to the sensitivity of the vibration levels to damping in the presence of only lightly damped structural components. Loss factors measured on the bare, unreinforced, cylindrical shells were used in the calculations. It is likely

that the addition of the reinforcing beams increased the damping sufficiently to account for the observed discrepancy.

In a cylindrical shell one usually expects to observe a transition from shell-like to flat-plate-like vibratory behavior as the frequency is increased beyond the "ring frequency" (at which the shell circumference is equal to the wavelength of a longitudinal wave in the shell material). For the 2-ft diameter test shell the ring frequency is about 2700 Hz; inspection of Fig. 12 reveals no significant difference in the behavior of the data below and above that frequency. It should be noted that the calculations for the cylindrical shell were formulated as if it were a flat plate — no curvature effects were taken into account. It thus appears likely that consideration of such effects constitutes a refinement which is not warranted, in view of the various other inaccuracies that are inherent in the practical application of the statistical energy approach to the vibration analysis of built-up structures.

Driving Point Resistance

As evident from Eq. (10), one must know the driving point resistance R, i.e., the real part of the driving point impedance (Ref. 6), if one desires to interpret the T_α/A ratios of Figs. 10-12 in terms of velocity ratios $\langle v_\alpha^2 \rangle / v_0^2$. This resistance may in principle be calculated by classical means from a complete modal analysis of the structure of interest. However, for realistic structures such calculations are prohibitively lengthy and complex.

However, it has been pointed out (Ref. 7) that at high enough frequencies the driving-point impedance of any finite uniform elastic structure approaches that of a similar structure of infinite extent. The impedances of infinite structures are relatively easy to determine, and for the most part are available in texts and handbooks (Ref. 8). It is of considerable interest, therefore, to compare the driving-point resistances measured on the test structures with those calculated for infinite plates. Such a comparison appears in Fig. 13.

The various points indicated in that figure correspond to various individual experimental determinations of driving-point resistance (calculated essentially from measured values of input power and driving-point velocity); the solid dots refer to data obtained on the fin structure (at several locations, including

two different panels) and the open-circle dots refer to data obtained on the cylindrical shell (at three locations on a single panel). Since the fin and the cylindrical shell both were constructed from 1/16-inch thick aluminum, the same infinite-structure impedance corresponds to both; the (frequency-independent) driving-point resistance of an infinite 1/16-inch thick aluminum plate is indicated by the horizontal line of Fig. 13.

From the figure one may observe that the experimental data always are within an order of magnitude of the infinite-plate value, that the data points generally lie below that value, and that the data cluster more closely about the infinite-plate value for higher frequencies. This closer clustering at higher frequencies is as expected from theory. The fact that the experimental driving-point resistance values generally are lower than the infinite-plate one leads one to conclude that use of the infinite-plate value in calculations would have caused one to predict vibration levels that are somewhat too high, and thus to err on the conservative side for design purposes.

POWER FLOW COEFFICIENTS

As evident from Eqs. (6) or (8), one must know the values of the various power flow coefficients $\phi_{\alpha\beta}$ before one can solve such sets of equations for the modal kinetic energies. For some cases of sound-to-structure coupling (e.g., Refs. 9,10) and for some geometrically simple cases of structure-to-structure coupling (Refs. 2,11) the interactions are understood well enough so that one may determine the corresponding power flow coefficients from theoretical considerations.

However, no valid approach exists as yet for the theoretical prediction of the coefficient that pertains to power flow between two panels that are separated by a reinforcing beam. A study of these coefficients was undertaken because of the great importance of this problem, and because values of such power flow coefficients were needed as inputs for the investigation described in the previous section. This study was partly theoretical and partly empirical. The theoretical portion attempted to derive power flow coefficients on the basis of a generalization of Heckl's study of wave propagation across a finite reinforcing beam (Ref. 12), and by use of relations for the flexural wave transmission coefficients across an infinite beam (Ref. 13). However, the theoretical developments were unsuccessful, since their

results disagreed excessively with the results of experimental measurements. Because these theoretical approaches apparently have little merit, they are not reported here; the following paragraphs discuss the results of the experimental study and the basis for them.

Basis for Experimental Measurements

The flow of mechanical power across a reinforcing beam can most readily be measured on a two-panel system like that sketched in Fig. 14. Such a configuration, when suspended from long strings, eliminates the extraneous effects that other connected structures might have; the irregular shapes of the panels encourage the establishment of reverberant vibration fields (in which waves impinge on the test beam relatively uniformly distributed over a wide range of angles of incidence).

The power flow coefficient $\phi_{\alpha\beta}$ is related to the power flow $P_{\alpha\beta}$ between the panels and to their average modal kinetic energies T_α and T_β as indicated by Eq. (2). The kinetic energies may be obtained according to Eq. (7) from measured mean-square velocity values, from known values of the band frequencies and panel masses, and from modal densities, which may be calculated from Eq. (9). The primary problem thus consists of measuring the power flow $P_{\alpha\beta}$.

If only panel α of Fig. 14 is excited by an external source, then in the steady state the time-average power $P_{\alpha\beta}$ supplied to panel β must be equal to the time-average power D_β dissipated by it; that is

$$P_{\alpha\beta} = D_\beta = 2\pi f_o \eta_\beta M_\beta \langle v_\beta^2 \rangle \quad . \tag{11}$$

The right-hand expression here follows from Eqs. (90) and (94) of Ref. 1 and indicates how one may evaluate $P_{\alpha\beta}$ from measured values of the mean-square velocity $\langle v_\beta^2 \rangle$ and from known values of the panel mass M_β and loss factor η_β. (The latter may be determined from separate measurements carried out on panel β in absence of any attached structures.)

If only panel α is directly excited, then one may also note that in the steady state the power A_α supplied to panel α from an external source must be equal to the power D_α dissipated

by it plus the power $P_{\alpha\beta}$ transferred to panel β. Thus,

$$P_{\alpha\beta} = A_\alpha - D_\alpha = A_\alpha - 2\pi f_o \eta_\alpha M_\alpha \langle v_\alpha^2 \rangle \quad . \tag{12}$$

This relation indicates how one may determine $P_{\alpha\beta}$ from measurements taken only on panel α. Such measurements may be expected to be more complex than those related to Eq. (12), but should serve as a check on the validity of the general approach.

A third means for determing the power flow coefficient $\phi_{\alpha\beta}$ involves measurement of the apparent loss factor $\eta_{\alpha app}$ of panel α. This loss factor, which can be measured rather simply by measuring the decay rate of panel α (as part of the experimental two-panel system), may be found from Eq. (103) of Ref. 1 to obey

$$\eta_{\alpha\ app} = \eta_\alpha + \left[\Psi + n_\alpha(f_o)/n_\beta(f_o)\eta_\beta\right]^{-1} \tag{13}$$

where

$$\Psi \equiv 4\pi\ f_o n_\alpha(f_o)/\phi_{\alpha\beta} \quad . \tag{14}$$

Experimental Configuration

Measurements were conducted on several panel-and-beam configurations like those shown (to scale) in Fig. 14. All test panels were made of 1/16-inch thick aluminum, and all test beams were attached by means of a rigid epoxy. Two sets of test panels were used; in one the α and β panels were of the same continuous sheet of metal (the beam there was merely cemented to that sheet to form the two panels) in the other the two panels were cut apart (and joined via the cemented-on beam). Layers of damping tape (Minnesota Mining and Manufacturing Co., No. 428A) were attached to panel β in the locations shown in Fig. 14, and carefully smoothed by a roller, to obtain good reproducibility of the damping.

The loss factors of the separate sub-panels were measured by means of the decay-rate technique, with the results as indicated in Fig. 15.

Effects of Some Beam and Panel Parameters

Figures 16a through 16j summarize the results of an extended series of apparent loss factor measurements. The data indicated in these figures were calculated according to Eq. (13), using the average values of dissipation loss factors presented in Fig. 15 and modal densities calculated from Eq. (9). In order to save computational effort, the data of Fig. 16 are presented in terms of the transmission function Ψ of Eq. (14) instead of the power flow coefficient $\phi_{\alpha\beta}$ itself.

By comparing Figs. 16a and 16b (or 16c and 16f, or 16d and 16g, or 16h and 16j) one may note that the transmission function for a steel beam is higher than for a similar aluminum beam, so that in view of Eq. (14) the steel beam results in a lower power flow coefficient $\phi_{\alpha\beta}$. Since the steel beam is heavier and stiffer, this result seems reasonable.

From Figs. 16b and 16c (or from Figs. 16d and 16e, or Figs. 16a and 16f) it appears that a continuous panel and an epoxied-together one result in roughly similar transmission.

The effect of increasing the damping of the β plate may be judged by comparing Figs. 16c and 16d (or Figs. 16f and 16g, or 16i and 16j). Except in a portion of the mid-frequency region, the effect appears to be of a minor nature.

The effects of beam cross-section changes may be studied by comparing Fig. 16a with 16h, Fig. 16e with 16i, or Fig. 16b with 16j. On the whole, the beam cross-section changes investigated appear to have relatively little effect on transmission.

Correlation of Apparent Loss Factor and Velocity Ratio Data

By equating the expression for the power flow $P_{\alpha\beta}$ given in Eq. (2) to that of Eq. (11) and substituting for T_α and T_β the relations implied by Eq. (7) one finds that one may obtain

$$\frac{\langle v_\alpha^2 \rangle}{\langle v_\beta^2 \rangle} \frac{M_\alpha / n_\alpha(f_o)}{M_\beta / n_\beta(f_o)} - 1 = \frac{4\pi f_o \Delta f \eta_\beta n_\beta(f_o)}{\phi_{\alpha\beta}} = \Psi \frac{\eta_\beta n_\beta(f_o)}{n_\alpha(f_o)} \quad , \qquad (15)$$

where the last form follows from Eq. (14). The foregoing expression establishes a relation between the steady-state mean-square velocity ratio $\langle v_\alpha^2 \rangle / \langle v_\beta^2 \rangle$ and the power flow coefficient for a pair of panels. Such velocity ratios were measured for several of the experimental configurations and are reported in Fig. 17. Each sheet of this figure shows three different solid curves; these correspond to three different measurement positions on the test panels. The dotted curve on each sheet indicates velocity ratio values calculated according to Eq. (15) from the corresponding average values of Ψ indicated in Fig. 16. The agreement between the two sets of results appears to be reasonably good, on the whole.

Correlation of Apparent Loss Factor and Input Power Measurements

An additional reexamination of some of the previously obtained transmission function values was thought in order — this time in terms of measured values of the mechanical power that is supplied to the directly excited panel — in order to obtain yet another check on the consistency of the various possible measurement approaches, and to generate increased confidence in results based on the various measured values.

The results of direct input power measurements and of corresponding calculations based on Eqs. (11) and (12), in conjunction with Eqs. (2) and (14), are presented in Fig. 18. In each of these five graphs the solid line represents the average of six values. These six values correspond to three accelerometer positions, and to two $P_{\alpha\beta}$ calculations [Eqs. (11) and (12)] per position. The two long-dashed lines delineate the region within which the data fall within one standard deviation from the average. The short-dashed lines in Fig. 11 represent the average values previously obtained (Fig. 16) from apparent loss factor measurements. (For the configuration of Fig. 11e, no precisely comparable prior data were available. In that figure the dash-dot-dash line corresponds to the same geometry, but with lesser added damping. Reasonable agreement may still be expected, since variations in damping were previously found to have relatively little effect on the transmission function Ψ.) The agreement between the power-flow coefficient values obtained by the various methods studied is seen to be generally reasonably good.

Figure 19 gives one an idea of the variability of the data for a given test configuration. The two dotted lines indicate the two different values obtained with the same pair of accelerometer positions (one accelerometer on plate α, the other on β), but using the two different aforementioned ways of obtaining $P_{\alpha\beta}$ [i.e., from Eq. (11) and from Eq. (12)]. The average of these two curves is also indicated, as are similar averages for two other pairs of accelerometer positions. The variability of the data in Fig. 19 is of the same order as that of the data of Fig. 17.

EXTENSIONS

Statistical energy analysis, as initially developed, is suitable for dealing only with mean-square response quantities. And even in regard to these, the mathematical foundation is not complete, in spite of recent efforts (Refs. 1, 11, 23) to clarify and complete it. For many practical applications one needs to know more than mean-square quantities; for example, in many instances one might be interested in the probability of exceeding a given displacement or stress level, or in the variances of response quantitites. The following paragraphs describe the results of some initial attacks on these very complex problems.

Response Concentrations

As a first step toward obtaining an estimate of the maximum response levels one is likely to encounter in a given situation, one may determine the amount by which the spatial maximum of the time-average response exceeds the root-mean-square response (averaged with respect to both space and time), as obtained from statistical energy analysis. Means for determining such "response concentrations" applicable to regions far from the boundaries of elastic systems are presented in Appendix I.

Neither the response concentrations of Appendix I, nor the mean square response calculations of statistical energy analysis, provide any information about the stresses near the boundaries of a structure, where fatigue failures occur most often. Relations between the response quantities at a boundary and those in the interior regions of a plate or shell may be studied by application of the "dynamic edge effect" concept developed by Bolotin (Ref. 16). An introduction to this concept is presented in Appendix II (since this work is not fully explained in the literature and is

as yet largely unavailable in English), but a detailed investigation of dynamic stress concentrations at system boundaries could not be undertaken within the scope of the present contract. Elements of such an investigation, and some related results, appear in Ref. 17.

Response Statistics

As has been mentioned, it is often not enough to know the mean-square velocities, stresses, etc. which one may obtain from straight-forward application of statistical energy analysis. For example, for the development of estimates of structural safety or fatigue life one needs to know the statistics of the maximum stresses.

Analysis of multi-modal response statistics presents great problems, primarily because even the mathematical basis for calculating mean-square responses of multi-modal systems is still incomplete. Although several investigators (Refs. 1, 11, 23) have dealt with two coupled modes, the step to two coupled multi-modal systems has always been made by the introduction of assumptions, the general validity of which has not been verified. (The best currently available justification for these assumptions lies in the reasonable correlations between experimental observations and statistical energy predictions that have been obtained to date.) As a step toward clarifying the mathematical basis for dealing with multi-modal systems, a study of power flow in a system of three coupled oscillators was begun, as described in Appendix III. Unfortunately, this study encountered excessive mathematical manipulative difficulties, which prevented its completion.

Attempts have been made to estimate some statistical properties of structural responses (Refs. 2,14), but these attempts have involved assumed probability densities of the responses and require a considerable amount of experimental verification before they can be given any general credence.

CONCLUDING REMARKS

The results presented in this report indicate that statistical energy analysis can be applied to obtain useful quantitative predictions of the mean-square vibratory responses of multi-panel structures. These predictions can be obtained without much computational effort. However, in order to obtain them one must know the damping (loss factors) of all panels and the coefficients that pertain to power flow between all adjacent pairs of panels.

The loss factors of structural components usually may be estimated on the basis of available information (e.g., Refs. 26, 27) or may be obtained from relatively simple measurements. Means are available for estimating the coefficients that pertain to power flow from an acoustic space to a vibrating structural surface, or vice versa, (Refs. 9,10), but nonempirical means for estimating the coefficients that pertain to power flow between two realistic structural components are unavailable.

An approach has been described for measuring the power flow coefficient pertaining to two panels that are separated by a reinforcing beam. The self-consistency of this approach has been verified by means of several independent types of measurements. The dependence of this power flow coefficient on such parameters as beam material and stiffness, and plate continuity and damping, has been partially explored, but the results are inconclusive and further work is indicated along these lines.

An analysis has been presented which may serve as a basis for estimating space-wise response maxima (response concentrations) in regions far from the boundaries of vibrating structures. The suggestion has also been made that these estimates may be extended into regions at and near the structural boundaries by application of the "dynamic edge effect" concept. Additional work in these areas seems warranted, in that it promises to lead to information of great practical utility.

Too little is as yet known about the statistics of systems responses that one may evaluate from statistical energy analysis, so that one cannot extract such important information as the probability density of maximum stresses. The response statistics of coupled systems depend not only on the statistics of the excitation, but also on the statistics of the coupling. At present the mathematical basis for calculating the mean-square responses of coupled multi-modal systems is still incomplete, and without

such a basis calculation of other statistical properties of the responses is impossible. Clearly, much work remains to be done in completing the aforementioned basis and in developing means for estimating the salient statistical properties of the responses of coupled structures.

In spite of its obvious shortcomings, statistical energy analysis is still a uniquely simple and powerful tool, not only for providing one with a qualitative understanding of the most important aspects of the vibrations of complex systems, but also for obtaining quantitative answers to complex vibration problems that practically cannot be attacked in any other way.

APPENDIX I

RESPONSE CONCENTRATION ESTIMATES

Introduction

Application of the basic statistical energy approach to vibration analysis permits one to obtain estimates of the mean square responses (e.g., velocities), averaged with respect to time and over the entire elastic system under consideration. However, one often may need to know the maximum values of the response variables, in addition to the aforementioned mean square values. The present appendix outlines an approach to obtaining estimates of these maxima.

Mean Square Responses

It is well known that one may express a response (velocity) distribution $v(x,t)$ in terms of system modes (Ref. 1), as

$$v(x,t) = \sum_{j=1}^{\infty} V_j(t)\, \psi_j(x) \qquad (16)$$

where the $\psi_j(x)$ are the mode shapes, and $V_j(t)$ the modal amplitude coefficients. Equation (16) is written for a one-dimensional system; the analogous expression for a two-dimensional system involves mode shape functions $\psi_{jk}(x,y)$ and coefficients $V_{jk}(t)$ with double subscripts, and a double instead of a single summation. The present discussion is carried out in the notation of one-dimensional systems for the sake of simplicity. Extensions to two- and three-dimensional systems can readily be obtained by analogy.

For a one-dimensional system of length L, having a uniform mass distribution, one may obtain the space-wise average value

of $v^2(x,t)$ from*

$$\langle v^2(x,t)\rangle_x \equiv \frac{1}{L}\int_0^L v^2(x,t)dx = \sum_{j=1}^{\infty} V_j^2(t) \quad , \tag{17}$$

where use has been made of orthogonality of the mode shapes and of the normalization

$$\frac{1}{L}\int_0^L \psi_j(x)\,\psi_k(x)dx = \begin{cases} 1 & \text{for } j=k \\ 0 & \text{for } j\neq k \end{cases} \quad . \tag{18}$$

Averaging Eq. (17) with respect to time yields the space-and-time mean square velocity v_{st}^2:

$$v_{st}^2 \equiv \langle\langle v^2(x,t)\rangle\rangle_{x,t} = \sum_{j=1}^{\infty} \langle V_j^2(t)\rangle_t \quad . \tag{19}$$

For the case where one is concerned only with the modes which respond at resonance to an excitation of bandwidth Δf and where all modes respond at approximately the same amplitude, one finds that $n(f)\Delta f$ modal resonances lie within the excitation band, where $n(f)$ denotes the modal density (number of modes per unit frequency interval) for the system under consideration, and that Eq. (19) reduces to

$$v_{st}^2 \approx n(f)\ \Delta f\ \langle V_j^2\rangle_t \quad . \tag{20}$$

In the subsequent paragraphs the mean square values of Eqs. (19) and (20) are used as reference values, and estimates are presented of the factors by which the maximum responses of a system exceed the space-and-time mean square values. The present discussion deals only with response concentrations due

---

*The brackets <...> indicate averaging with respect to the subscripted parameter appended to them.

to superposition of modal responses, but does not consider modal excitation and response statistics. The latter problem is complex and has not been treated adequately, although good strides forward have been made recently (Ref. 14).

Response Concentration Due to a Single Mode

For a single mode one may write

$$v(x,t) \approx V_j(t)\sqrt{2}\ \sin(k_j x-\phi) \tag{21}$$

where a purely sinusoidal mode shape with an arbitrary phase angle ϕ has been assumed. The numerical coefficient in Eq. (21) was chosen so as to satisfy the normalization of Eq. (18); $k_j=2\pi/\lambda_j$ is the wavenumber, where λ_j denotes the wavelength of the sinusoid.

Clearly, not all modes can be represented by spatial sinusoids. However, such sinusoids are good approximations to those portions of the mode shapes which correspond to regions several wavelengths removed from all system boundaries (Refs. 15,16). Equation (21) thus may be taken to be a reasonable estimate of the vibrations in the system "interior" associated with higher order modes. If the system encompasses many modal wavelengths λ_j, the deviations from sinusoidal behavior near the boundaries have little effect on the spatial mean square value, and one may find from Eq. (21) that

$$\langle v^2(x,t)\rangle_x = V_j^2(t)\ \frac{2}{L}\ \int_0^L \sin^2(k_j x-\phi)dx \approx V_j^2(t) \quad . \tag{22}$$

From Eq. (21) one may observe that the space-wise maximum value of $v^2(x,t)$ is given by

$$v_{max}^2(t) \approx 2V_j^2(t) \quad . \tag{23}$$

By averaging Eqs. (22) and (23) with respect to time, one readily obtains

$$v^2_{max} \equiv \langle v^2_{max}(t) \rangle_t \approx 2v^2_{st} \tag{24}$$

for a single mode of a one-dimensional system.

For a two-dimensional system, Eq. (21) would contain the product of two sinusoids (involving the two orthogonal coordinate directions); spatial averaging would then be performed over both coordinates, and an additional factor of $\sqrt{2}$ would be required in Eq. (21) in order to satisfy the prescribed normalization. A similar argument holds for a three-dimensional system. One may hence generalize Eq. (24) to apply to systems of any dimensionality. Thus, one finds that in the interior of a d-dimensional system, due to a single higher-order mode,

$$v^2_{max}/v^2_{st} \approx 2^d \quad . \tag{25}$$

Response Concentrations of Correlated and Uncorrelated Groups of Modes

It is convenient here to obtain first the time-average of $v^2(x,t)$, in order to take into account the possible temporal correlation of modal responses. (The order of averaging is, of course, immaterial, since averaging is essentially a summation process.) From Eq. (16) one obtains

$$\langle v^2(x,t) \rangle_t = \sum_{j=1}^{\infty} \sum_{k=1}^{\infty} \langle V_j(t) V_k(t) \rangle_t \, \psi_j(x) \psi_k(x) \quad . \tag{26}$$

If the modal responses are uncorrelated, which means that

$$\langle V_j(t) V_k(t) \rangle_t = 0 \quad \text{for} \quad j \neq k \quad , \tag{27}$$

then Eq. (26) reduces to

$$\langle v^2(x,t) \rangle_t = \sum_{j=1}^{\infty} \langle V^2_j(t) \rangle_t \, \psi^2_j(x) \quad . \tag{28}$$

For sinusoidal mode shapes, as indicated in Eq. (21), the greatest possible value of $\langle v^2(x,t)\rangle_t$ occurs where all sinusoids have the value of unity. Thus, from Eq. (28)one finds that for a system of d-dimensions

$$v_{max}^2 \approx 2^d \sum_{j=1}^{\infty} \langle V_j^2(t)\rangle_t \approx 2^d \, N_u \langle V_j^2(t)\rangle_t \quad . \tag{29}$$

The last approximate expression of Eq. (29) pertains to the case where only N_u modes respond significantly, and those with approximately equal amplitudes, as in the case where similar modes respond to the same excitation in a limited frequency band.

On the other hand, if the modal responses are highly correlated and of approximately equal amplitudes, so that

$$\langle V_j(t) V_k(t)\rangle_t \approx \langle V_j^2(t)\rangle_t \quad \text{for all } j,k \quad , \tag{30}$$

then Eq. (26) may be reduced to

$$\langle v^2(x,t)\rangle_t \approx \langle V_j^2(t)\rangle_t \sum_{j=1}^{\infty} \sum_{k=1}^{\infty} \psi_j(x) \, \psi_k(x) \quad . \tag{31}$$

If N_c modes respond in a correlated manner, one then finds that (for the previously mentioned d-dimensional sinusoidal mode shapes) the space-wise maximum value of Eq. (31) may be written as

$$v_{max}^2 \approx 2^d \, N_c^2 \langle V_j^2(t)\rangle_t \quad . \tag{32}$$

Since the space-and-time-average mean square velocity is given by Eqs. (19) or (20), one may now readily determine the "response concentrations" v_{max}^2/v_{st}^2. However, instead of setting down the results for these very special cases, it is useful to turn to consideration of a more general one.

Response Concentrations in Systems Excited by Bands of Noise

A pure tone (single frequency) or narrow-band noise excitation acting on an elastic system may be expected to excite only those modes significantly whose response peaks (resonant frequencies) occur "close enough" to the exciting frequency. Usually the modal bandwidth B is taken as a measure of "close enough." If the modal frequency spacing $1/n$ (where n denotes modal density, as previously mentioned) is greater than the modal bandwidth B, then a narrow band of noise will excite only one mode at resonance. Excitation by a broad band of noise then essentially amounts to each mode being excited by a different narrow-band source; the modal responses may then be expected to be uncorrelated.

If, however, the modal responses "overlap," i.e., if the modal frequency spacing is less than the modal bandwidth, then one may expect nB modes (the number of modes per bandwidth) to respond "resonantly" to a narrow band of noise. Since all of these nB modes have nearly the same resonance frequency and are similarly excited, their responses will be highly coherent. Since the responses of modes whose resonances are more than a modal bandwidth apart will still be uncorrelated, one may consider the total response to excitation having a broad bandwidth Δf to be made up of the responses of a number N_G of groups of modes, where the responses of modes within a group are highly correlated with each other, but uncorrelated with responses of modes outside the group.

The number N_G of uncorrelated mode groups may be estimated to be equal to the number of separate response bandwidths B that can occur within the excitation bandwidth Δf; i.e., $N_G \approx \Delta f/B$. The number of coherently excited modes per mode group is $N_m \approx nB$, of course.

For the case where modal overlap occurs (that is, for $1/n<B$), one thus may write

$$\langle V_j(t)V_k(t)\rangle_t \approx \begin{cases} \langle V_j^2(t)\rangle_t & \text{if j and k belong to the same mode group} \\ 0 & \text{otherwise} \end{cases} . \qquad (33)$$

Then, if one computes the time-average of $v^2(x,t)$, one obtains

$$\langle v^2(x,t)\rangle_t = \sum_{j=1}^{\infty}\sum_{k=1}^{\infty} \langle V_j(t)V_k(t)\rangle_t \, \psi_j(x)\, \psi_k(x)$$

$$\approx \langle V_j^2(t)\rangle_t \cdot \sum_{\text{group 1}}\sum \psi_j(x)\, \psi_k(x) + \langle V_j^2(t)\rangle_t \cdot \sum_{\text{group 2}}\sum + \cdots \tag{34}$$

$$\psi_j(x)\, \psi_k(x) \approx \langle V_j^2(t)\rangle_t \, N_G \sum_{\substack{\text{typical}\\ \text{group}}}\sum \psi_j(x)\, \psi_k(x) \quad ,$$

where it has been assumed that all modal response amplitudes are equal and that all groups are similar. For sinusoidal mode shapes one may then obtain the space-wise maximum response as

$$v_{max}^2 \approx N_G \, 2^d \, N_m^2 \langle V_j^2(t)\rangle_t \approx 2^d \, \Delta f \, n^2 B \langle V_j^2(t)\rangle_t \quad . \tag{35}$$

For the case where no modal overlap occurs (that is for $1/n>B$), one finds that $N_u=n(f)\Delta f$ modes are excited incoherently, and that in view of Eq. (29)

$$v_{max}^2 \approx 2^d \, n(f)\Delta f \, \langle V_j^2(t)\rangle_t \quad . \tag{36}$$

By use of Eq. (20) one may then determine that the mean square response concentrations for systems excited by a band of noise obey

$$\frac{v_{max}^2}{v_{st}^2} \approx \begin{cases} 2^d \, nB & \text{for } 1/n<B \\ 2^d & \text{for } 1/n>B \quad . \end{cases} \tag{37}$$

Remarks

It is useful to reiterate that the present appendix only deals with response concentrations (in the plate interior region, at several wavelengths from the plate boundaries) of the type of v^2_{max}/v^2_{st}, where v^2_{max} denotes the time-average of the spatial maximum of $v^2(x,t)$ and where v^2_{st} denotes the average value of $v^2(x,t)$ with respect to both space and time. These response concentrations provide some information that may be useful for fatigue life estimation; however, one may for some purposes be interested in other concentrations, such as the ratio of the spatial-and-temporal maximum response to the mean square response. One may obtain an upper bound on such stress concentrations from the previously presented work, but better estimates remain to be developed.

The derivations which appear in this appendix are based on the assumption that the various mode shape sinusoids in a given situation attain their maxima in the same location on the structure. At first glance one might expect such an assumption to lead to a gross overestimate of the response concentrations; however, it has recently been shown (Ref. 14) that such coincidence of modal maxima occurs with unit probability at some position in a vibrating system.

APPENDIX II

AN INTRODUCTION TO BOLOTIN'S "DYNAMIC EDGE EFFECT" IN PLATES

Introduction

Statistical energy analysis of built-up panel structures permits one to evaluate the mean square velocities of the panels and the associated average stresses. However, the presently available techniques do not permit one to estimate the stresses near the panel boundaries, where fatigue failures are usually observed.

The concept of the "dynamic edge effect," developed by Bolotin (Ref. 16), promises to be useful for the study of mode shapes (and the associated stresses), particularly for the higher modes which are of primary interest in statistical energy analyses. The present appendix is intended to introduce and interpret Bolotin's dynamic edge effect, in order to provide a basis for further work.

Classical Plate Vibration Relations

The free motion of a thin isotropic elastic plate obeys the well-known classical equation

$$\nabla^4 w_o + \frac{m}{D} \frac{\partial^2 w_o}{\partial t^2} = 0 \qquad (38)$$

where $w_o = w_o(x,y,t)$ denotes the deflection, D the flexural rigidity, m the mass per unit area of the plate; x,y denote Cartesian coordinates in the plane of the plate, and t denotes time.

For natural vibrations, where all points on the plate move sinusoidally with the same circular frequency ω, one may set

$$w_o(x,y,t) = w(x,y) \sin \omega t \quad . \qquad (39)$$

Substitution of Eq. (39) into Eq. (38) and use of the expression for the operator ∇^4 which applies for Cartesian coordinates yields

$$\frac{\partial^4 w}{\partial x^4} + 2\frac{\partial^4 w}{\partial x^2 \partial y^2} + \frac{\partial^4 w}{\partial y^4} = \frac{m\omega^2}{D} w \quad . \tag{40}$$

The mode shape functions $w(x,y)$, in conjunction with the natural frequencies ω, must satisfy Eq. (40) and appropriate boundary conditions.

The classical approach to finding plate mode shapes and frequencies consists of solving Eq. (40) directly, subject to the appropriate boundary conditions. Bolotin's approach is based on the same equation and conditions, but provides a simple means for obtaining good approximations applicable to the higher modes.

Mode Shape in Interior Plate Regions

Rayleigh has observed (as clearly restated in Ref. 15) that the conditions along the interior modal lines (i.e. along lines of zero displacement) of a plate vibrating in one of its higher modes are those which are imposed as boundary conditions at "simply supported" edges, where both the displacement and the bending moment vanish. Hence, each interior internodal segment can be treated as if it were a simply supported plate. It thus seems reasonable to assume, as Bolotin has done, that for the higher modes the mode shapes in the region far from the edges of a rectangular plate with <u>any</u> type of edge conditions should be of the same form as those for a plate which is simply supported on all edges; namely,

$$w = A \sin k_x(x-x_o) \sin k_y(y-y_o) \quad . \tag{41}$$

Here k_x and k_y represent the wavenumbers in the coordinate directions, or

$$k_x = \pi/\ell_x \quad , \qquad k_y = \pi/\ell_y \quad , \tag{42}$$

where ℓ_x, ℓ_y denote the distances between nodal lines (Fig. 20). A, x_o, and y_o are constants.

Substitution of Eq. (41) into (40) yields an expression for the natural frequency which may be written as

$$\omega = k_p^2 \sqrt{D/m} \tag{43}$$

where k_p^2 is defined as

$$k_p^2 = k_x^2 + k_y^2 \quad . \tag{44}$$

The phase constants x_o and y_o and the wavenumbers k_x and k_y are to be evaluated on the basis of the plate edge conditions.

Asymptotic Mode Shape and Dynamic Edge Effect

In order to demonstrate that the mode shape assumption of Eq. (41) is reasonable, one may consider the more general mode shape function

$$w = X(x) \sin k_y(y-y_o) \quad , \tag{45}$$

where X(x) is an as yet undefined function of only the x-coordinate. [Equation (45) essentially applies for a plate which has simply supported edges (or corresponding nodal lines) parallel to the y-axis, but arbitrary boundary conditions on the edges parallel to the x-axis.] If one substitutes Eq. (45) into Eq. (40) one obtains

$$\frac{d^4X}{dx^4} - 2k_y^2 \frac{d^2X}{dx^2} + k_y^4 X = \frac{m\omega^2}{D} X \approx k_p^4 X \quad , \tag{46}$$

where the approximate expression on the right-hand side has been obtained by use of Eq. (43).

The general solution of Eq. (46) may be expressed as

$$X(x) = C_o \sin k_x(x-x_o)+C_1 e^{-k_o x}+C_2 e^{k_o x} \qquad (47)$$

where

$$k_o \equiv k_x\sqrt{1+2\beta^2} \quad , \quad \beta \equiv k_y/k_x \quad . \qquad (48)$$

The symbols C_o, x_o, C_1, C_2 represent constants of integration, which one may evaluate by use of the boundary conditions which apply at the edges at x=0 and x=a. However, instead of determining these constants in the classical way, it is instructive to focus on the edge at x=0 and to consider the cases where $\ell_x \ll a$, i.e. where $k_x a$ is very large. In that case C_2 must vanish, otherwise the plate deflections would increase without bound for increasing $k_x x$. Then Eq. (47) reduces to

$$X(x) = C_o \sin k_x(x-x_o)+C_1 e^{-k_o x} \quad . \qquad (49)$$

For large values of $k_x x$, the right-hand side of Eq. (49) approaches $C_o \sin k_x(x-x_o)$, which, when substituted for $X(x)$ in Eq. (45) reduces that equation to the form of Eq. (41). An analogous argument shows that the y-dependence in the interior region of the plate is of the form of $\sin k_y(y-y_o)$, indicating that assumption of the mode shape form of Eq. (41) is indeed reasonable.

The exponentially decaying term of Eq. (49) is what Bolotin has called the "dynamic edge effect"; and, since the mode shape of Eq. (41) is approached asymptotically at positions far from the boundaries, that mode shape may be called the "asymptotic mode shape."

Justification of Asymptotic Natural Frequency

One might be inclined to object to the foregoing analysis on the basis that this analysis makes use of the approximate form of Eq. (46), which was obtained by use of Eq. (43), where Eq. (43)

itself only holds for the "asymptotic" mode shape given by Eq. (41). However, application of Rayleigh's method (Ref. 18) convinces one that Eq. (43) gives a good approximation to the natural frequencies as long as the "dynamic edge effect" significantly affects only a small portion of the plate.

Rayleigh's method consists essentially of equating the maximum potential (strain) and kinetic energies of a vibrating system, where these energies are calculated on the basis of an assumed deflection shape. For a plate the strain energy V is given (Ref. 19) by

$$V = \frac{D}{2} \iint_S \left[\left(w_{xx}^2 + w_{yy}^2 \right)^2 - 2(1-\nu)\left(w_{xx} w_{yy} - w_{xy}^2 \right) \right] dx\, dy \qquad (50)$$

where the subscripts indicate partial differentiation, ν represents Poisson's ratio, and where the integration extends over the entire area S of the plate. The kinetic energy T is given by

$$T = \frac{m}{2} \omega^2 \iint_S w^2\, dx\, dy \quad . \qquad (51)$$

For w as given by Eq. (41), the foregoing procedure yields an expression for the natural frequency which corresponds exactly to Eq. (43). Changes in the mode shape [from the double-sinusoid of Eq. (41)] which are significant over only a very small portion of the total plate area may be expected to affect the values of the integrals of Eqs. (50) and (51) only to a minor extent, and hence to have little effect on the natural frequency.

Additional Remarks

Bolotin has also extended his method to shells (Ref. 20). The same general concepts, with some complications, apply for shells as for the flat plates discussed here.

Bolotin and his co-workers (Refs. 16,20,21) have shown that the asymptotic method provides very good approximations to the natural frequencies, and Bolotin has also applied his concepts to study the modal densities of plates and shells (Ref. 22).

A recent study (Ref. 17) of some special cases of flat plates has shown that Bolotin's method provides a good approximation to the exact mode shapes and stress distributions.

APPENDIX III

THE THREE OSCILLATOR POWER FLOW PROBLEM

Introduction

This appendix presents an attempt to calculate the time-average power flow between three coupled oscillators excited by independent white noise sources. The calculation is carried to the point where a 12 by 12 matrix must be inverted. Because of the difficulty of this step, however, the calculation is not carried further.

The need for the present power flow calculation arises from an effort to clarify Statistical Energy Analysis (SEA). Numerous authors have used SEA to obtain vibration levels in randomly excited complex structures. (A fairly complete list of references is given in Ref. 1). Unfortunately, however, none of these authors have been able to justify completely the assumptions required by SEA. In fact, in most cases, the assumptions are not clearly stated.

Recently several authors (Refs. 1,11,23) set out to investigate the fundamentals of SEA and to clarify the required assumptions. They found that the basic assumption in SEA is that the power flow (in a frequency band) between two coupled multimodal structures is proportional to the difference between the average energies of the modes in the band. The validity of this assumption has never been verified for the general case.

Numerous authors (Refs. 1,11,23,24) have studied the power flow between two coupled oscillators and have found it to be proportional to the difference between the modal energies. These authors have then assumed that the two-oscillator result can be used to predict power flow between sets of coupled oscillators. These investigators have qualitatively supported their assumption by stating that the power flow expression for two oscillators gives an ensemble average power flow between two out of a group of oscillators. The ensemble consists of sets of oscillators in which the resonance frequencies are random variables. The study of three coupled oscillators in this paper was undertaken to support this idea. Unfortunately, the calculation of power flow was found to be too complex to be completed within the scope of the present study.

Formulation of Analysis

Consider the problem of three oscillators (Fig. 21) coupled by purely spring-like and gyroscopic elements. The describing equations of motion are

$$\ddot{x}_1 + \beta_1\dot{x}_1 + \omega_1^2 x_1 + \frac{G_1}{M_1}\dot{x}_2 - \frac{K_{c1}}{M_1}x_2 = f_1/M_1 \qquad (52a)$$

$$\ddot{x}_2 + \beta_2\dot{x}_2 + \omega_2^2 x_2 - \frac{G_1}{M_2}\dot{x}_1 - \frac{G_2}{M_2}\dot{x}_3 - \frac{K_{c1}}{M_2}x_1 - \frac{K_{c2}}{M_2}x_3 = f_2/M_2 \qquad (52b)$$

$$\ddot{x}_3 + \beta_3\dot{x}_3 + \omega_3^2 x_3 + \frac{G_2}{M_3}\dot{x}_2 - \frac{K_{c2}}{M_3}x_2 = f_3/M_3 \quad . \qquad (52c)$$

In Eqs. (52), x_i denotes the displacement of the ith oscillator, β_i is the damping constant of the ith oscillator, ω_i is the resonance frequency of the ith oscillator when the other oscillators are held at rest, G_1 is the gyroscopic coupling between oscillator 1 and 2, G_2 is the gyroscopic coupling between oscillator 2 and 3, K_{c1} is the spring coupling between oscillator 1 and 2, K_{c2} is the spring coupling between oscillator 2 and 3, M_i is the mass of the ith oscillator, and f_i is the force exciting the ith oscillator. The excitation forces are taken to have a white spectrum and to be independent.

Proceeding, as did Lyon and Maidanik (Ref. 24), to calculate stochastic equations, one multiplies Eq. (52a) by x_1, x_2, x_3, $\dot{x}_2$, and $\dot{x}_3$, and takes the time-average. The resulting stochastic equations may be simplified by noting that

$$\overline{x_i\ddot{x}_j} = -\overline{\dot{x}_i\dot{x}_j}\ , \quad \overline{x_i\dot{x}_j} = -\overline{\dot{x}_i x_j}\ , \quad \overline{x_i\dot{x}_i} = 0\ , \quad \overline{\dot{x}_i\ddot{x}_j} = -\overline{\ddot{x}_i\dot{x}_j}\ ,$$

$$\overline{\dot{x}_i\ddot{x}_i} = 0\ , \quad \overline{x_i f_i} = 0\ , \quad \overline{\dot{x}_i f_i} = 0\ ;\ i = 1,2,3\ ;\ j = 1,2,3\ , \qquad (53)$$

where the bar designates the time-average. The simplified equations one obtains are

$$- \overline{\dot{x}_1^2} + \omega_1^2 \overline{x_1^2} + \frac{G_1}{M_1} \overline{x_1 \dot{x}_2} - \frac{K_{c1}}{M_1} \overline{x_1 x_2} = 0 \tag{54a}$$

$$- \overline{\ddot{x}_2 \dot{x}_1} - \beta_1 \overline{x_1 \dot{x}_2} + \omega_1^2 \overline{x_1 x_2} - \frac{K_{c1}}{M_1} \overline{x_2^2} = 0 \tag{54b}$$

$$- \overline{\dot{x}_3 \dot{x}_1} - \beta_1 \overline{x_1 \dot{x}_3} + \omega_1^2 \overline{x_1 x_3} - \frac{G_1}{M_1} \overline{x_2 \dot{x}_3} - \frac{K_{c1}}{M_1} \overline{x_2 x_3} = 0 \tag{54c}$$

$$- \overline{\dot{x}_1 \ddot{x}_2} + \beta_1 \overline{\dot{x}_1 \dot{x}_2} + \omega_1^2 \overline{x_1 \dot{x}_2} + \frac{G_1}{M_1} \overline{\dot{x}_2^2} = 0 \tag{54d}$$

$$- \overline{\dot{x}_1 \ddot{x}_3} + \beta_1 \overline{\dot{x}_1 \dot{x}_3} + \omega_1^2 \overline{x_1 \dot{x}_3} + \frac{G_1}{M_1} \overline{\dot{x}_2 \dot{x}_3} - \frac{K_{c1}}{M_1} \overline{x_2 \dot{x}_3} = 0 \quad . \tag{54e}$$

A similar set of equations is obtained by multiplying Eq. (52b) by x_1, x_2, x_3, $\dot{x}_1$, and $\dot{x}_3$ and Eq. (52c) by x_1, x_2, x_3, $\dot{x}_1$, and $\dot{x}_2$. Again, simplifications may be introduced.

The complete set of 15 equations can be written in matrix form as shown in Eq. (55)*, which may be reduced to the form indicated in Eq. (56)*.

The power flow P_{12} from oscillator 1 to oscillator 2 is given by

$$\begin{aligned} P_{12} &= \overline{(F_{1K}+F_{1G})\dot{x}_1} = K_{c1} \overline{(x_1-x_2)\dot{x}_1} - G_1 \overline{\dot{x}_1 \dot{x}_2} \\ &= K_{c1} \overline{x_1 \dot{x}_2} - G_1 \overline{\dot{x}_1 \dot{x}_2} \end{aligned} \tag{57}$$

where F_{1K} and F_{1G} denote the forces exerted by mass 1 on the spring and gyroscopic coupling elements, respectively, and where the second of Eqs. (53) has been applied. The time-average kinetic and potential energies of each oscillator are given by

*Because of the size of the matrix equations, they are shown on separate pages at the end of this appendix.

$$T_i = \frac{1}{2} M_i \overline{\dot{x}_i^2} \quad , \quad V_i = \frac{1}{2} M_i \omega_i^2 \overline{x_i^2} \quad ; \quad i = 1,2,3 \quad . \qquad (58)$$

Discussion

The power flow can be found in theory by solving Eq. (56) for $\overline{x_1\dot{x}_2}$ and $\overline{\dot{x}_1\dot{x}_2}$, i.e., by inverting the matrix, and then using Eq. (57). [Eqs. (58) may then be employed to express the result in terms of energies.] However, the computational difficulties in inverting this matrix algebraically are prohibitive. In order to calculate the power flow in a special case one may solve the equations numerically, but a complete study using a broad range of parameters appears not to be justified at this time.

Newland (Ref. 25) has recently studied power flow between groups of very lightly coupled oscillators. His approach leads to promising results, and at this time should be favored over attempts to solve the three-oscillator problem exactly. It is unclear, however, whether his analysis requires the coupling loss factor to be much smaller than the damping loss factor. If this is the case, then the results of his small coupling analysis are of severely limited use. This question is worthy of deeper investigation.

Eq. (55)

$\omega_1^2 - \frac{K_{c1}}{M_1}$	$\frac{G_1}{M_1}$														
	ω_1^2	$-\beta_1$	$-\frac{K_{c1}}{M_1}$	$-\frac{G_1}{M_1}$	-1										
			ω_1^2	β_1		$-\frac{K_{c1}}{M_1}$	$\frac{G_1}{M_1}$								
					ω_1^2	β_2	$\frac{G_1}{M_2}$	$-\frac{K_{c1}}{M_2}$	-1						
						ω_2^2	$-\frac{K_{c1}}{M_2}$	$-\frac{G_2}{M_2}$	$-\beta_2$	$\frac{G_2}{M_2} - \frac{G_1}{M_1}$	$\frac{K_{c2}}{M_2} - \frac{K_{c1}}{M_1}$	β_1			
							ω_2^2	β_2	$-\omega_2^2$	β_2	ω_2^2	$-\beta_1$	ω_1^2		
										$\frac{K_{c2}}{M_2} - \frac{K_{c1}}{M_1}$	$\frac{G_2}{M_2} - \frac{G_1}{M_1}$	-1			
											ω_2^2	β_2	$-\frac{K_{c1}}{M_1}$	-1	
												$\frac{G_1}{M_2}$	ω_1^2	β_1	
													$-\frac{K_{c1}}{M_1}$	$\frac{G_1}{M_1}$	
														ω_1^2	$-\beta_1$
															ω_1^2

×

$\ddot{x}_1^2$															
	$\ddot{x}_1\ddot{x}_2$														
		$\dot{x}_1\dot{x}_2$													
			$\dot{x}_2^2$												
				$\dot{x}_2\dot{x}_1$											
					$\dot{x}_2\dot{x}_3$										
						$\dot{x}_2\dot{x}_3$									
							$\dot{x}_2\dot{x}_3$								
								$\dot{x}_1\dot{x}_3$							
									$\dot{x}_1\dot{x}_3$						
										$\ddot{x}_3^2$					
											$\dot{x}_1\dot{x}_3$				
												$\dot{x}_1\dot{x}_2$			
													$\dot{x}_2\dot{x}_3$		

=

$\ddot{x}_1^2$
0
0
$\frac{G_1}{M_1}\ddot{x}_2^2$
0
0
$\ddot{x}_2^2$
0
$\frac{G_1}{M_2}\ddot{x}_1^2$
$\frac{G_2}{M_2}\ddot{x}_3^2$
0
0
$\ddot{x}_3^2$
0
$-\frac{G_2}{M_3}\ddot{x}_2^2$

$$
\begin{bmatrix}
\omega_1^2 & -\frac{K_{c1}}{M_2} & \frac{G_1}{M_1} & & & & & & & & & \\
 & \omega_1^2 & -\beta_1 & -\frac{K_{c1}}{M_1} & -1 & & & & & & & \\
 & & & & & -\frac{K_{c1}}{M_1} & -\frac{G_1}{M_1} & & -1 & -\beta_1 & \omega_1^2 & \\
 & & \omega_1^2-\omega_2^2 & & \beta_1+\beta_2 & & & & -\frac{G_2}{M_2} & \frac{K_{c2}}{M_2} & & \\
 & & \frac{K_{c2}}{M_3} & & \frac{G_2}{M_3} & & -\frac{K_{c1}}{M_1} & \frac{G_1}{M_1} & \beta_1+\beta_3 & \omega_1^2-\omega_3^2 & & \\
-\frac{K_{c1}}{M_2} & \omega_2^2 & \beta_2 & & -1 & & & & & -\frac{G_2}{M_2} & -\frac{K_{c2}}{M_2} & \\
 & -\frac{K_{c1}}{M_2} & \frac{G_1}{M_2} & \omega_2^2 & & -\frac{K_{c2}}{M_2} & -\frac{G_2}{M_2} & & & & & \\
 & & & & & \omega_2^2 & -\beta_2 & -1 & & \frac{G_1}{M_2} & -\frac{K_{c1}}{M_2} & -\frac{K_{c2}}{M_2} \\
 & & & & & & \omega_2^2-\omega_3^2 & \beta_2+\beta_3 & -\frac{G_1}{M_2} & -\frac{K_{c1}}{M_2} & & \\
 & -\frac{K_{c2}}{M_3} & \frac{G_2}{M_3} & & & & & & -1 & \beta_3 & \omega_3^2 & \\
 & & & -\frac{K_{c2}}{M_3} & & \omega_3^2 & \beta_3 & -1 & & & & \\
 & & & & & -\frac{K_{c2}}{M_3} & -\frac{G_2}{M_3} & & & & & \omega_3^2
\end{bmatrix}
\times
\begin{bmatrix}
\overline{x_1^2} \\ \overline{x_1 x_2} \\ \overline{x_1 \dot{x}_2} \\ \overline{x_2^2} \\ \overline{\dot{x}_1 \dot{x}_2} \\ \overline{x_2 x_3} \\ \overline{x_2 \dot{x}_3} \\ \overline{\dot{x}_2 \dot{x}_3} \\ \overline{\dot{x}_1 \dot{x}_3} \\ \overline{x_1 \dot{x}_3} \\ \overline{x_1 x_3} \\ \overline{x_3^2}
\end{bmatrix}
=
\begin{bmatrix}
\overline{\dot{x}_1^2} \\ \\ \\ G_1\left(\frac{\overline{\dot{x}_1^2}}{M_2} - \frac{\overline{\dot{x}_2^2}}{M_1}\right) \\ \\ \\ \overline{\dot{x}_2^2} \\ \\ G_2\left(\frac{\overline{\dot{x}_3^2}}{M_2} - \frac{\overline{\dot{x}_2^2}}{M_3}\right) \\ \\ \\ \overline{\dot{x}_3^2}
\end{bmatrix}
\qquad \text{Eq. (56)}
$$

REFERENCES

1. E.E. Ungar, "Fundamentals of Statistical Energy Analysis of Vibrating Systems," AFFDL-TR-66-52, April 1966.

2. R.H. Lyon and E. Eichler, "Random Vibration of Connected Structures," J. Acoust. Soc. Am. 36: 1344-1354 (1964).

3. E. Eichler, "Thermal Circuit Approach to Vibrations in Coupled Systems and the Noise Reduction of a Rectangular Box," J. Acoust. Soc. Am. 37: 995-1007 (1965).

4. R.H. Lyon and T.D. Scharton, "Vibrational Energy Transmission in a Three-Element Structure," J. Acoust. Soc. Am. 38: 253-261 (1965).

5. M. Jakob, Heat Transfer, Vol. I (John Wiley and Sons, Inc., New York, 1950), Chap. 18.

6. P.W. Smith, Jr. and R.H. Lyon, "Sound and Structural Vibration," NASA CR-160, Mar. 1965.

7. E. Skudrzyk, "Vibrations of a System with a Finite or an Infinite Number of Resonances," J. Acoust. Soc. Am. 30: 1140-1152 (1958).

8. E.E. Ungar, "Mechanical Vibrations," Sec. 6 of Mechanical Design and Systems Handbook (McGraw-Hill Book Co., Inc., New York, 1964).

9. G. Maidanik, "Response of Ribbed Panels to Reverberant Acoustic Fields," J. Acoust. Soc. Am. 34: 809-826 (1962).

10. J.E. Manning and G. Maidanik, "Radiation Properties of Cylindrical Shells," J. Acoust. Soc. Am. 36: 1691-1698 (1964).

11. T.D. Scharton, "Random Vibration of Coupled Oscillators and Coupled Structures," Sc.D. Thesis, Massachusetts Institute of Technology, Oct. 1965.

12. M.A. Heckl, "Wave Propagation on Beam-Plate Systems," J. Acoust. Soc. Am. 33: 640-651 (1961).

13. E.E. Ungar, "Transmission of Plate Flexural Waves through Reinforcing Beams; Dynamic Stress Concentrations," J. Acoust. Soc. Am. 33: 633-639 (1961).

14. R.H. Lyon, "Spatial Response Concentrations in Extended Structures," Paper No. 67-VIBR-22, Amer. Soc. Mech. Engrs. Vibration Conference, Boston, Mass., Mar. 1967. (To appear in Trans. ASME, J. Eng. for Ind., Series B)

15. F.V. Hunt, "Stress and Strain Limits on the Attainable Velocity in Mechanical Vibration," J. Acoust. Soc. Am. 32: 1123-1128 (1960).

16. V.V. Bolotin, "Dynamic Edge Effect in Elastic Plate Vibrations," Inzhenernyi Sbornik 31: 3-14 (1960) (In Russian).

17. E.E. Ungar and K.S. Lee, "Considerations in the Design of Supports for Panels in Fatigue Tests," Final Report, Contract AF 33(615)-5034, May 1967 (To appear as AFFDL-TR).

18. J.P. Den Hartog, Mechanical Vibrations (McGraw-Hill Book Co., Inc., New York, 1956), 4th Edition, pp. 141ff.

19. S. Timoshenko, Theory of Plates and Shells (McGraw-Hill Book Co., Inc., New York, 1940).

20. V.V. Bolotin, "The Edge Effect in the Oscillations of Elastic Shells," PMM 24, No. 5: pp. 831-834 (Translation pp. 1257-1272) (1960).

21. V.V. Bolotin, B.P. Makarov, G.V. Mishenkov, and Iu.Iu. Shveiko, "An Asymptotic Method for the Study of Natural Frequencies of Elastic Plates," Sbornik Raschety na Prochnost', Vol. 6, Mashgiz(1960)(In Russian).

22. V.V. Bolotin, "The Density of Eigenvalues in Vibration Problems of Elastic Plates and Shells," Proc. of Vibration Problems, Warsaw 4, No. 6: 341-351 (1965).

23. D.E. Newland, "Calculation of Power Flow Between Coupled Oscillators," J. Sound Vib. 3: 262-276 (1966).

24. R.H. Lyon and G. Maidanik, "Power Flow Between Linearly Coupled Oscillators," J. Acoust. Soc. Am. 34: 623-639 (1962).

25. D.E. Newland, "Power Flow Between a Class of Coupled Oscillators," Submitted to J. Acoust. Soc. Am.

26. B.J. Lazan, "Energy Dissipation Mechanisms in Structures, with Particular Reference to Material Damping," Sec. 1 of Structural Damping, J. Ruzicka, Ed., Amer. Soc. Mech. Engrs., New York, 1959.

27. E.E. Ungar and J.R. Carbonell, "On Panel Vibration Damping Due to Structural Joints," AIAA J. 4: 1385-1390, Aug. 1966.

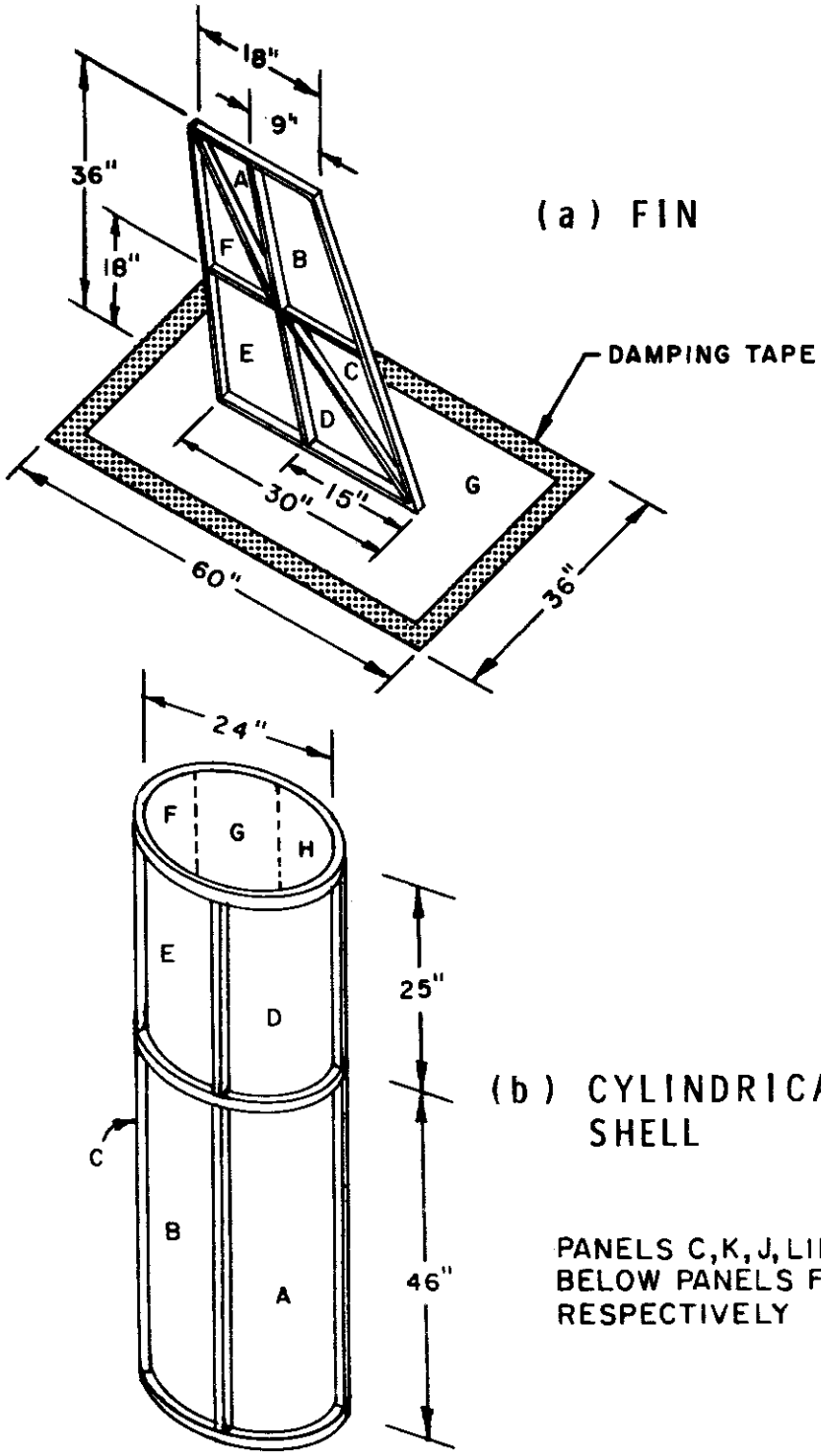

FIG. 1 MULTI-PANEL STRUCTURES

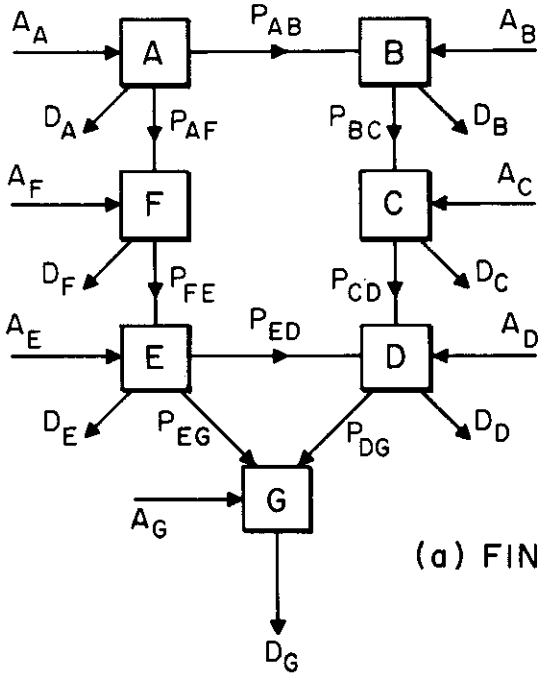

(a) FIN

(b) CYLINDRICAL SHELL

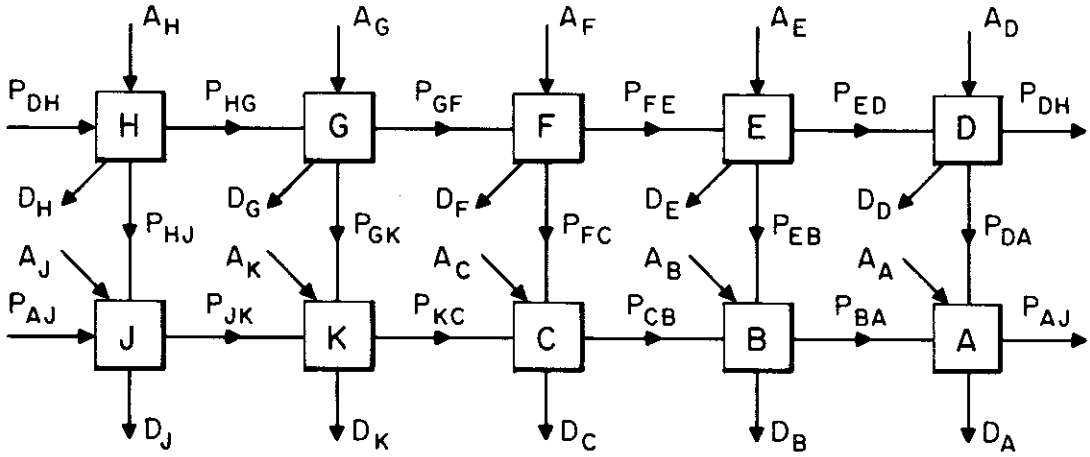

FIG. 2 POWER FLOW DIAGRAMS FOR ANALYSIS OF MULTI-PANEL STRUCTURES

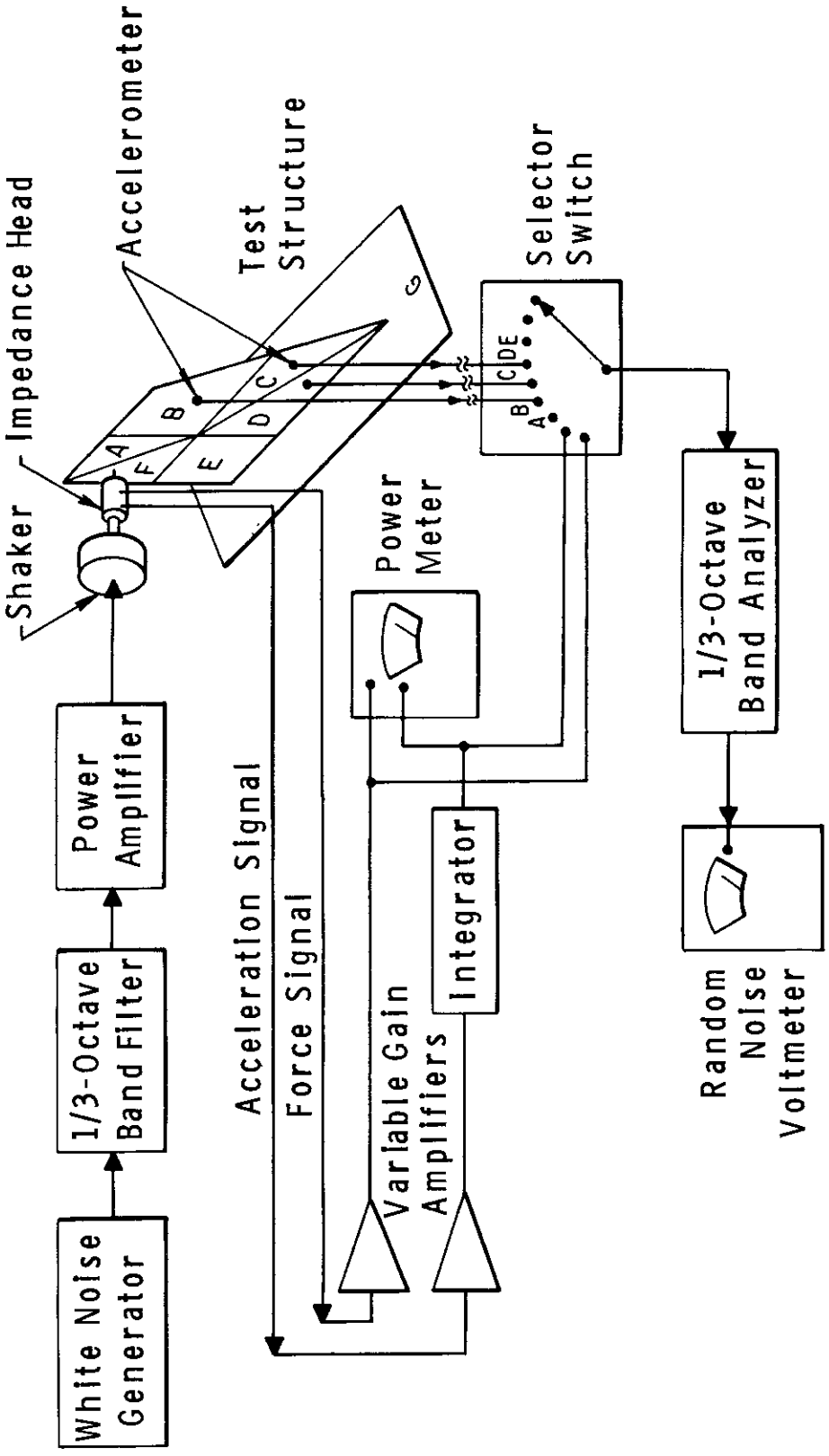

See Table I for description of components

FIG. 3 INSTRUMENTATION SYSTEM

TABLE I

INSTRUMENTATION

Designation in Fig. 3	Manufacturer	Manufacturer's Designation and Model Number		
White Noise Generator	Grason-Stadler	Noise Generator	Model 901A	Ser.178
1/3-Octave Band Filter	Bruel and Kjaer	Band Pass Filter Set	Type 1611	Ser.48592
Power Amplifier	McIntosh	30 Watt Audio Amplifier	Model MC 30	Ser.9E814
Shaker	Pye-Ling	Vibration Generator	Model V 50	Ser.252
Impedance Head	Wilcoxon Research	Impedance Head	Model Z 602	Ser.206
Variable Gain Amplifier	Ithaco	Amplifier	Model 257AM	
Integrator	Nexus	Operational Amplifier	SA-2 with capacitative feedback	
Power Meter	John Fluke	VAW Meter	Model 102	Ser.1139
Accelerometer	Bruel and Kjaer	Accelerometer	Type 4336	
Accelerometer	Wilcoxon Research	Accelerometer	Type 101	
Random Noise Voltmeter	Bruel and Kjaer	Random Noise Voltmeter	Type 2417	
1/3-Octave Band Analyzer	General Radio	Sound and Vibration Analyzer	Type 1564A	

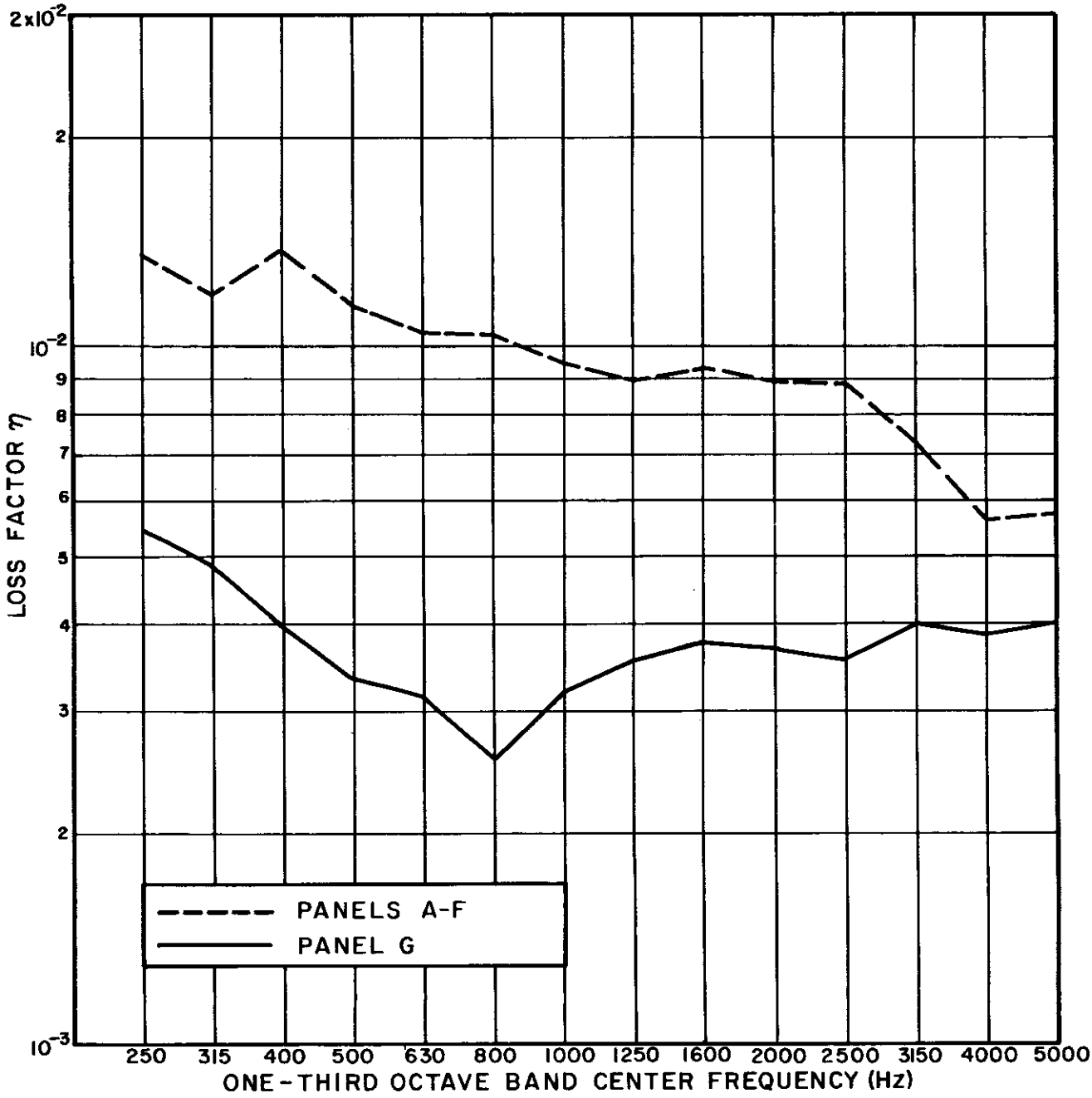

FIG. 4 LOSS FACTORS OF FIN PANELS

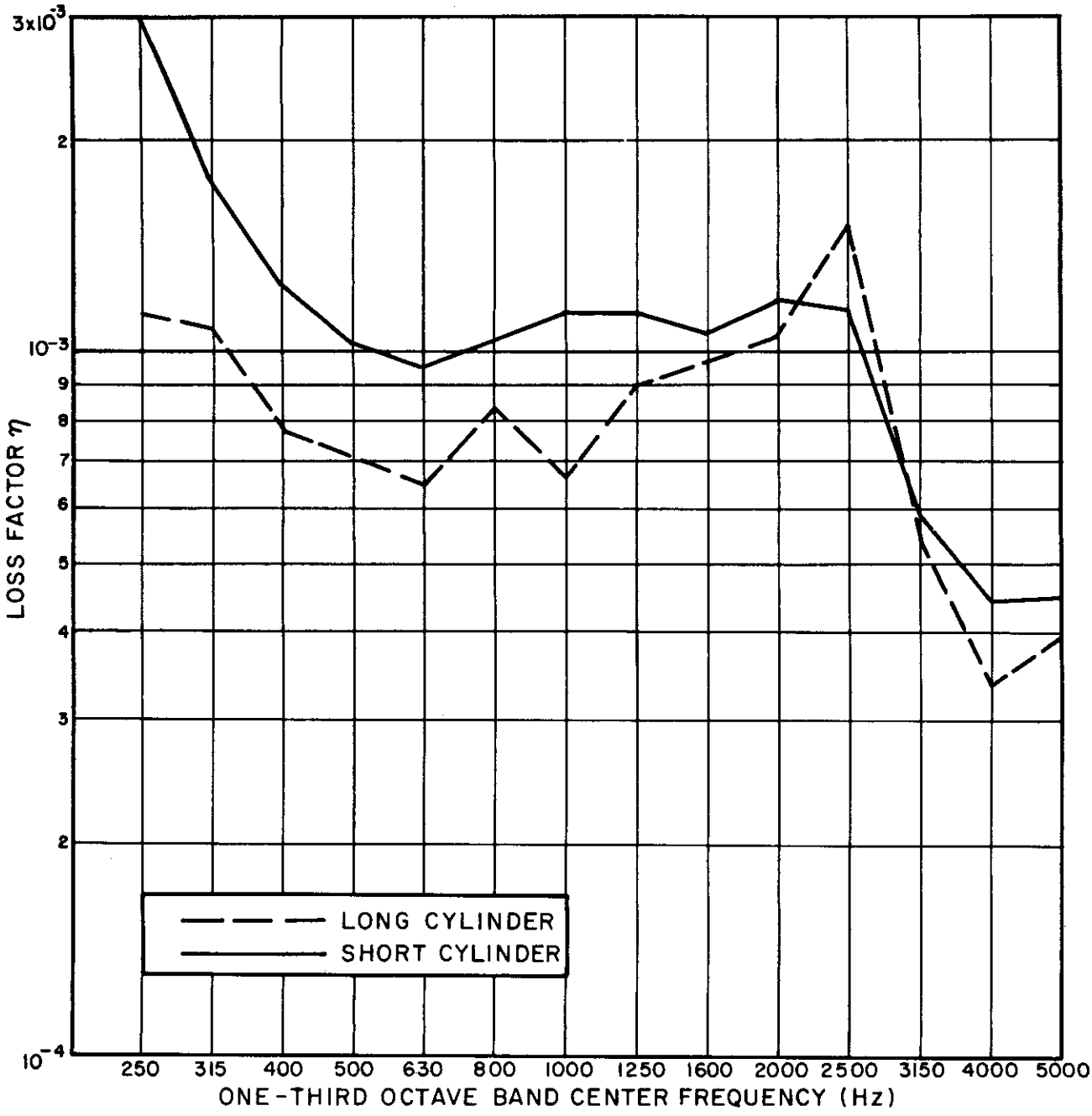

FIG. 5 LOSS FACTORS OF CYLINDRICAL SHELL PANELS

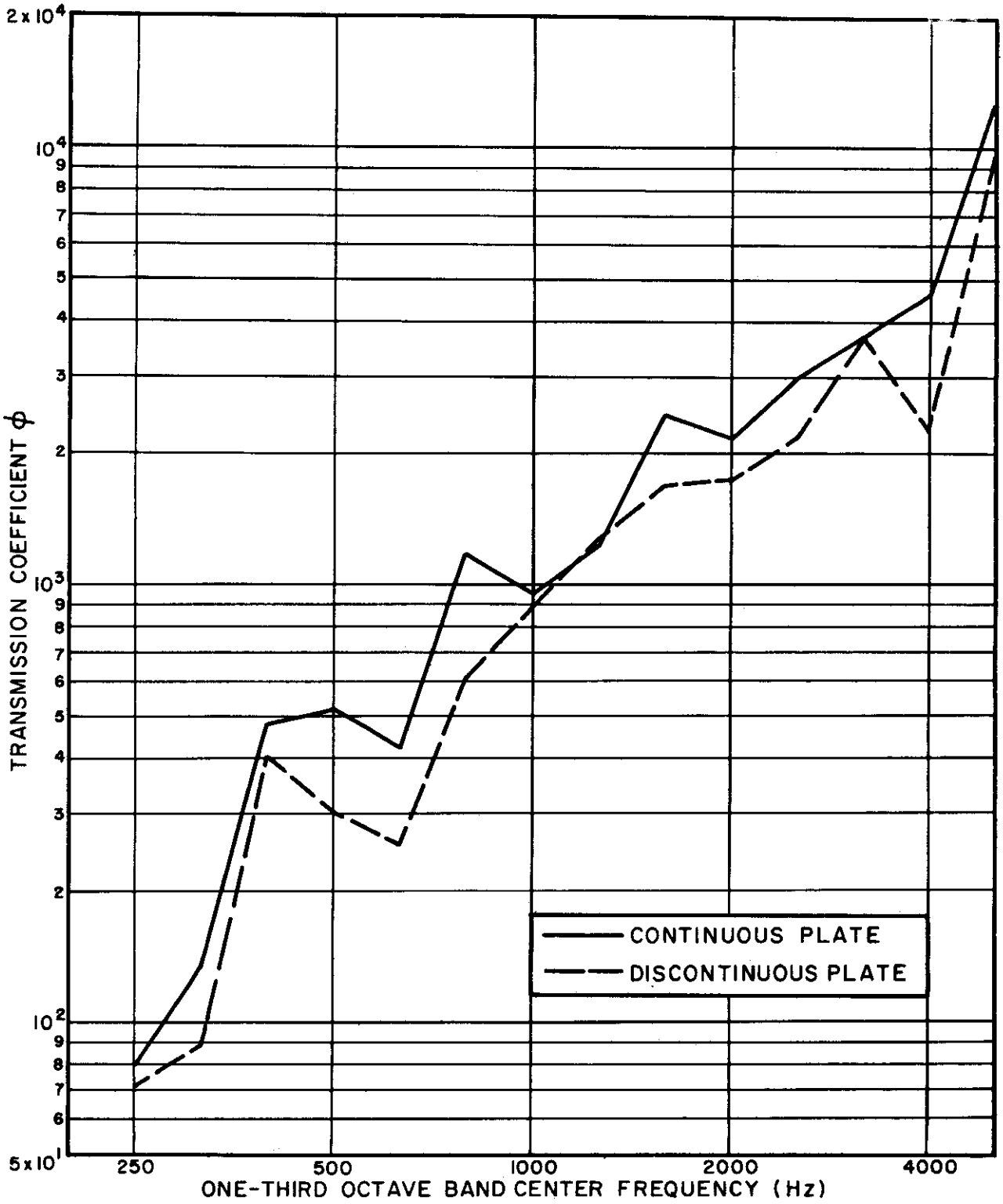

FIG. 6 POWER FLOW TRANSMISSION COEFFICIENT FOR 1/2 x 3/4" ALUMINUM BEAM ON 1/16" ALUMINUM PLATE

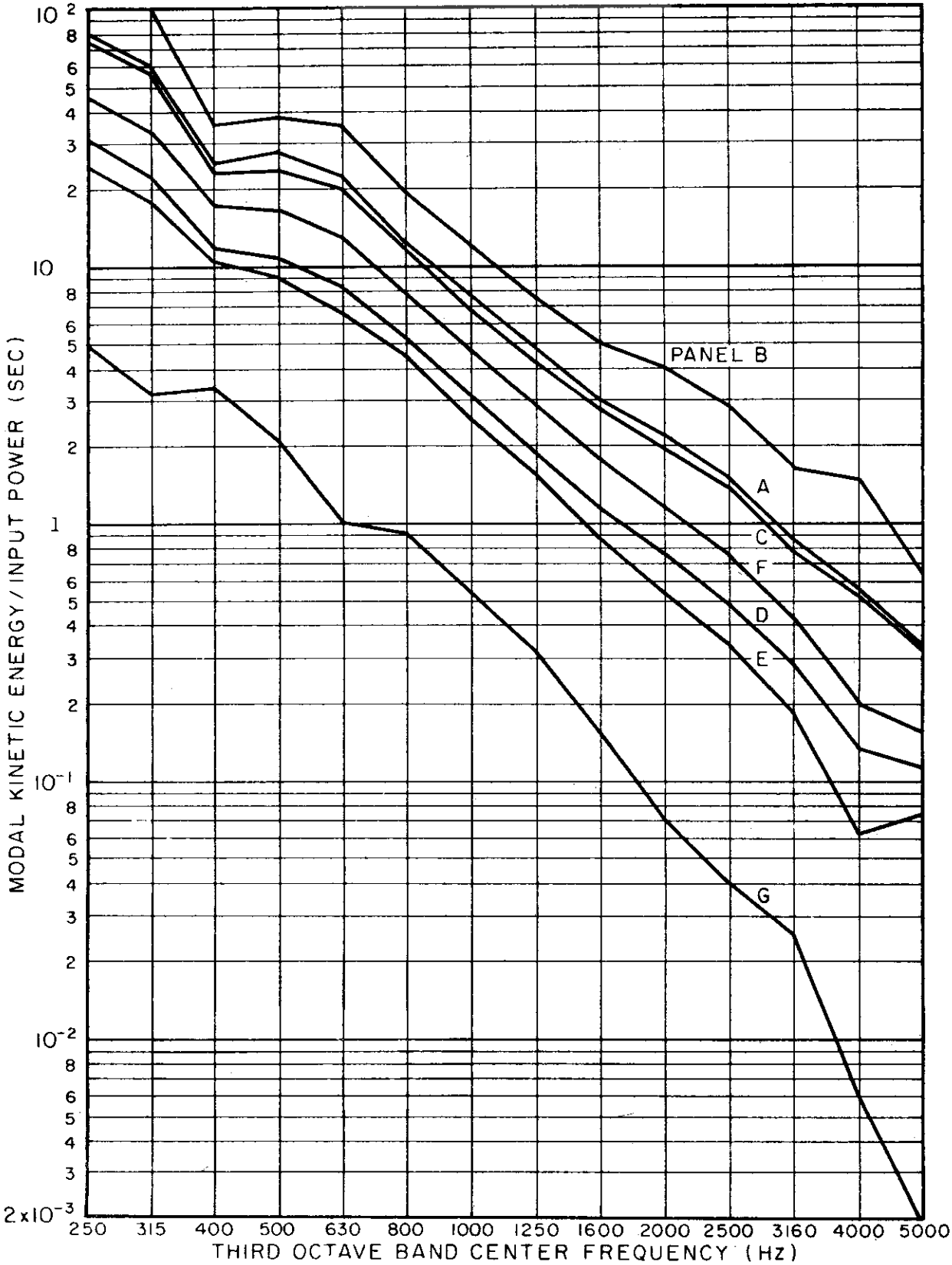

FIG. 7 CALCULATED RESPONSE OF FIN PANELS (DRIVEN AT PANEL "B")

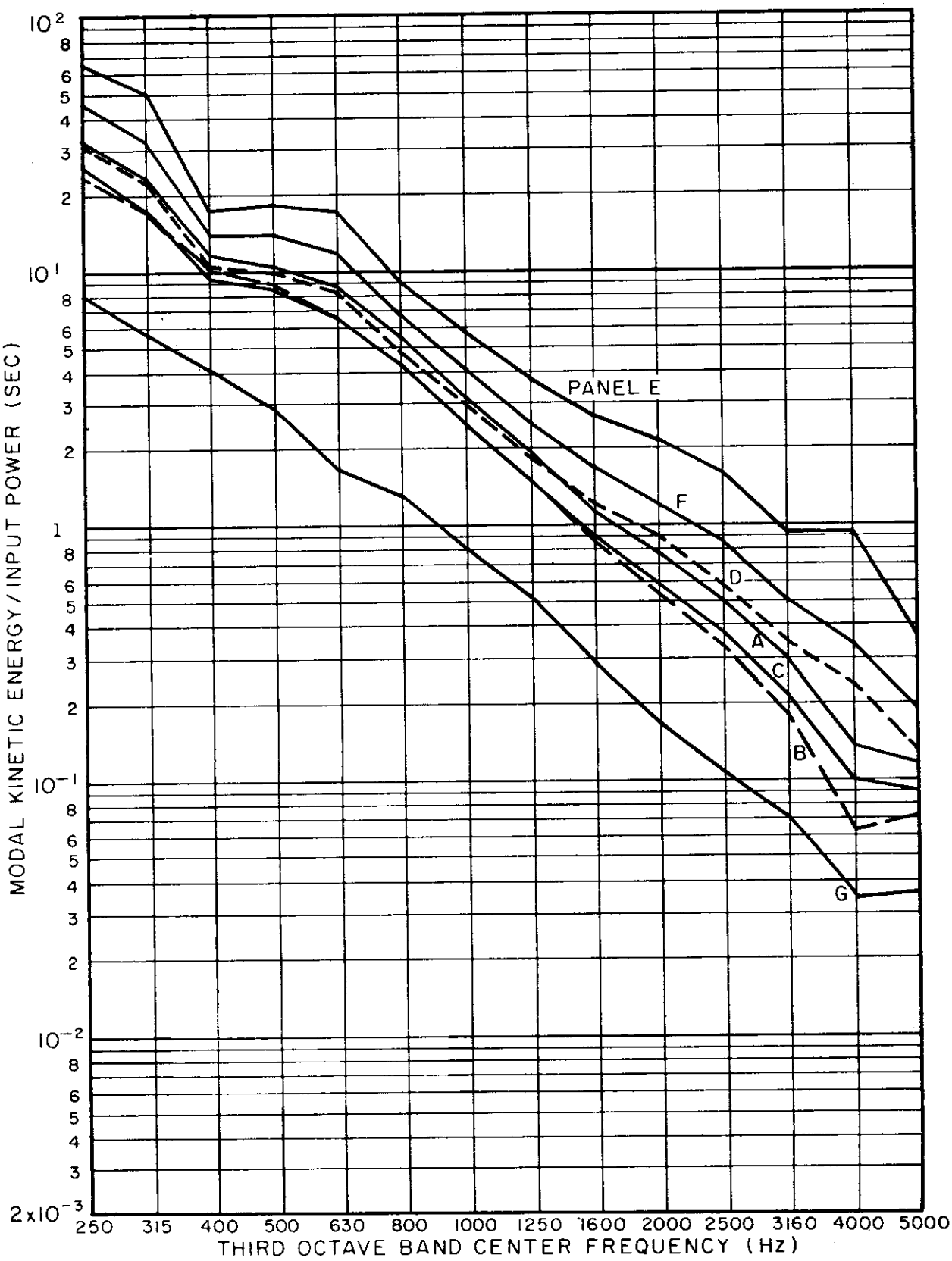

FIG. 8 CALCULATED RESPONSE OF FIN PANELS (DRIVEN AT PANEL "E")

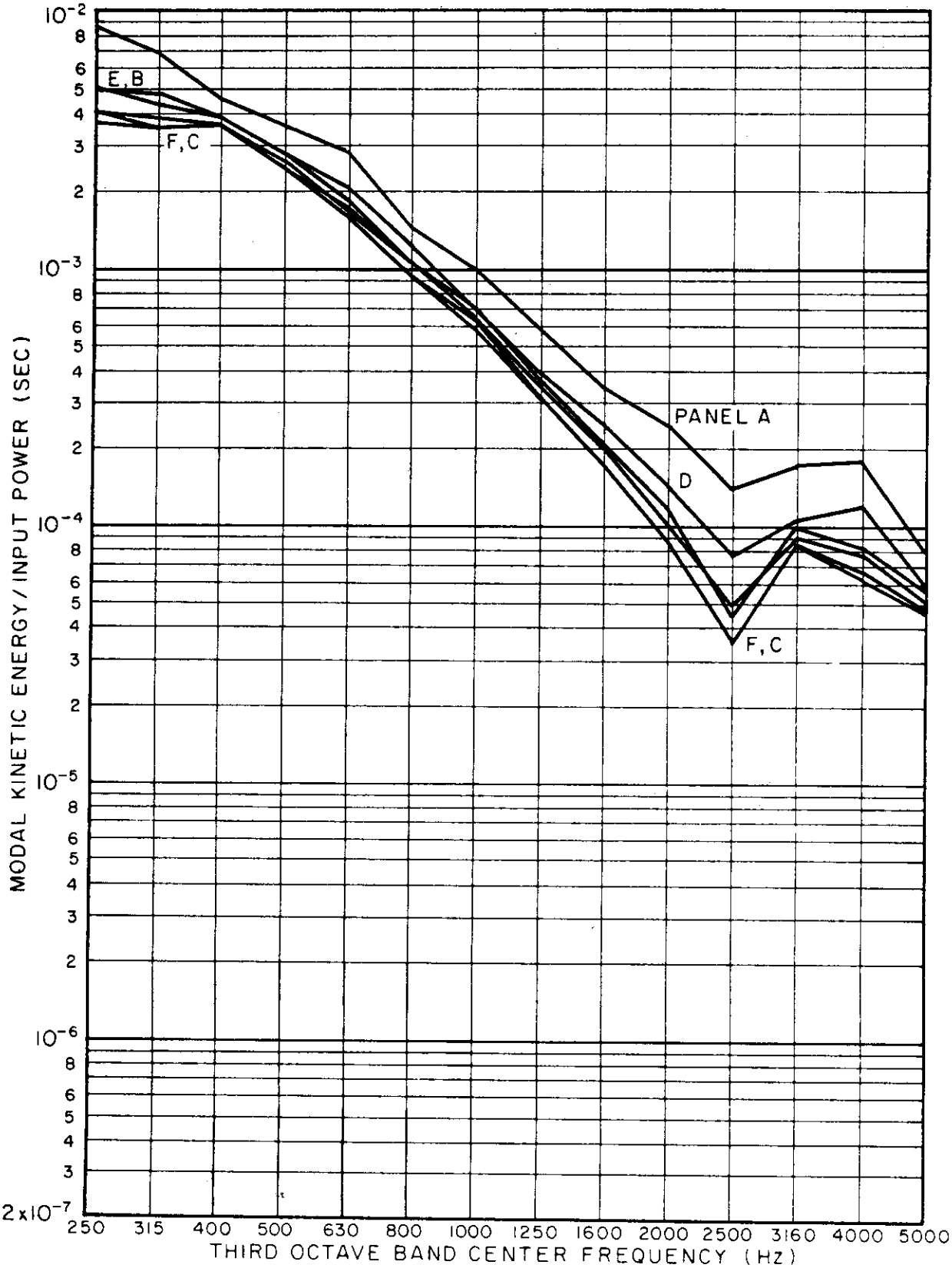

FIG. 9 CALCULATED RESPONSE OF CYLINDRICAL SHELL PANELS (DRIVEN AT PANEL "A")

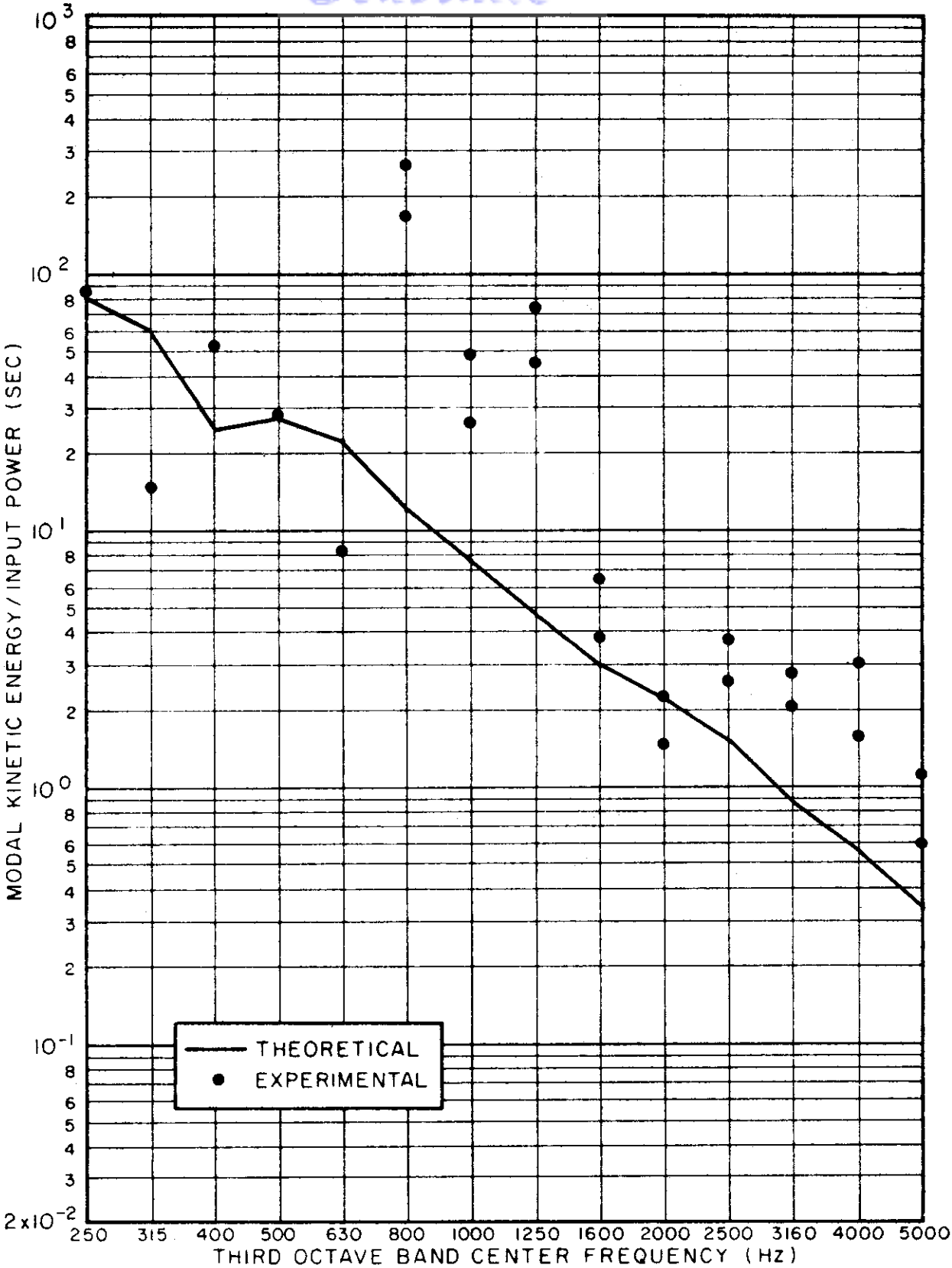

FIG. 10a RESPONSE OF PANEL "A" OF FIN STRUCTURE (DRIVEN AT PANEL "B")

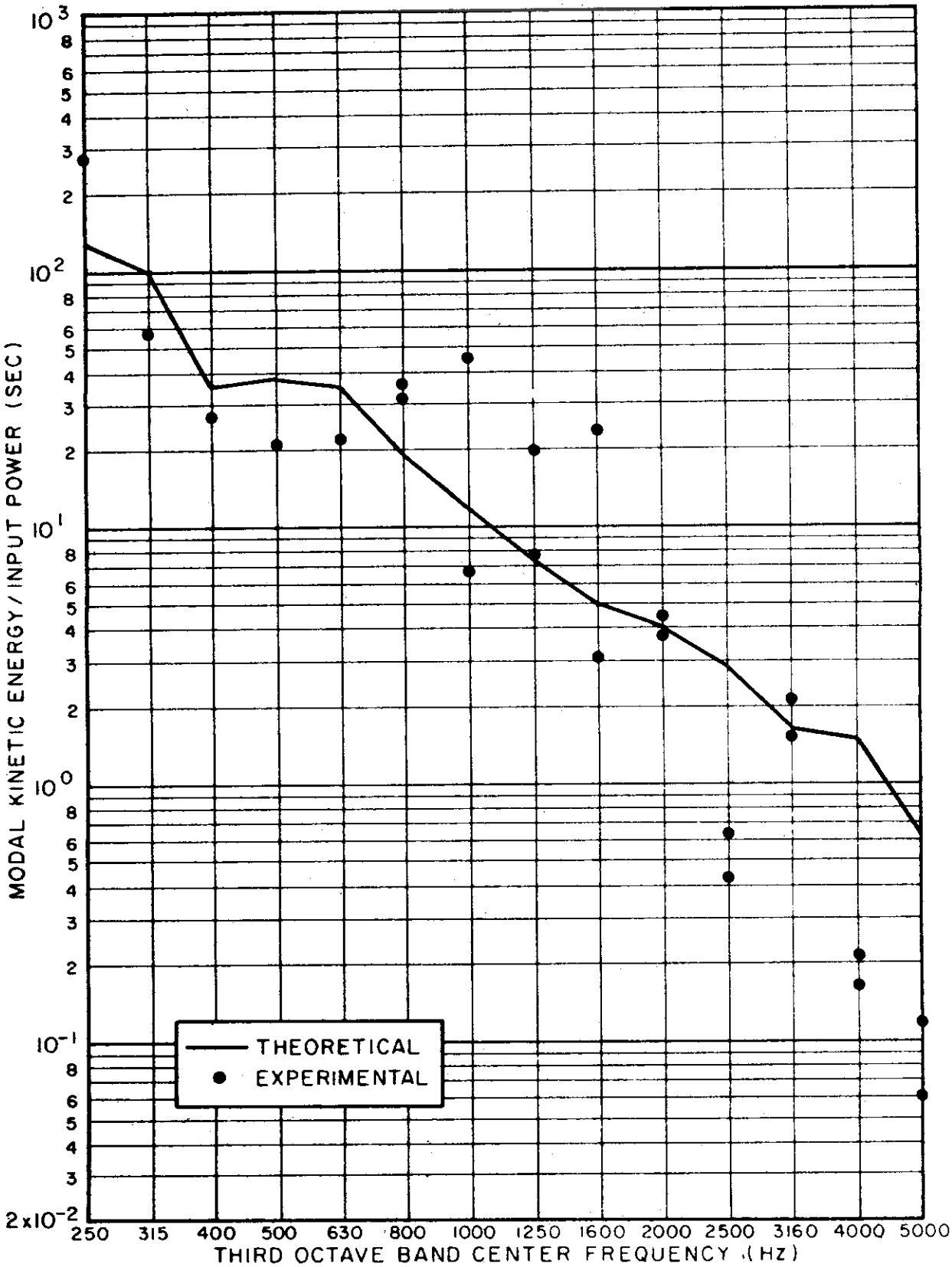

FIG. 10b RESPONSE OF PANEL "B" OF FIN STRUCTURE (DRIVEN AT PANEL "B")

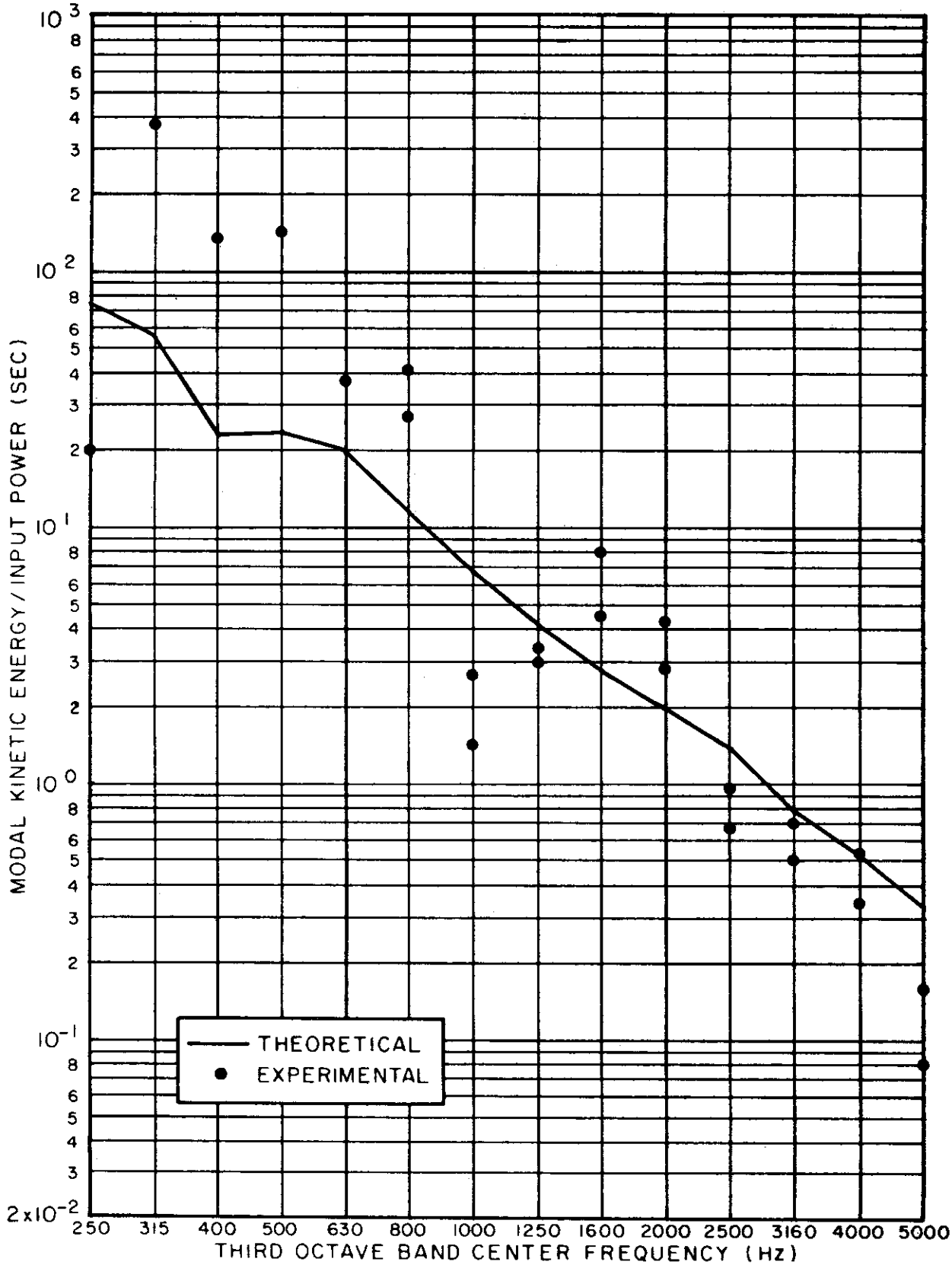

FIG. 10c RESPONSE OF PANEL "C" OF FIN STRUCTURE (DRIVEN AT PANEL "B")

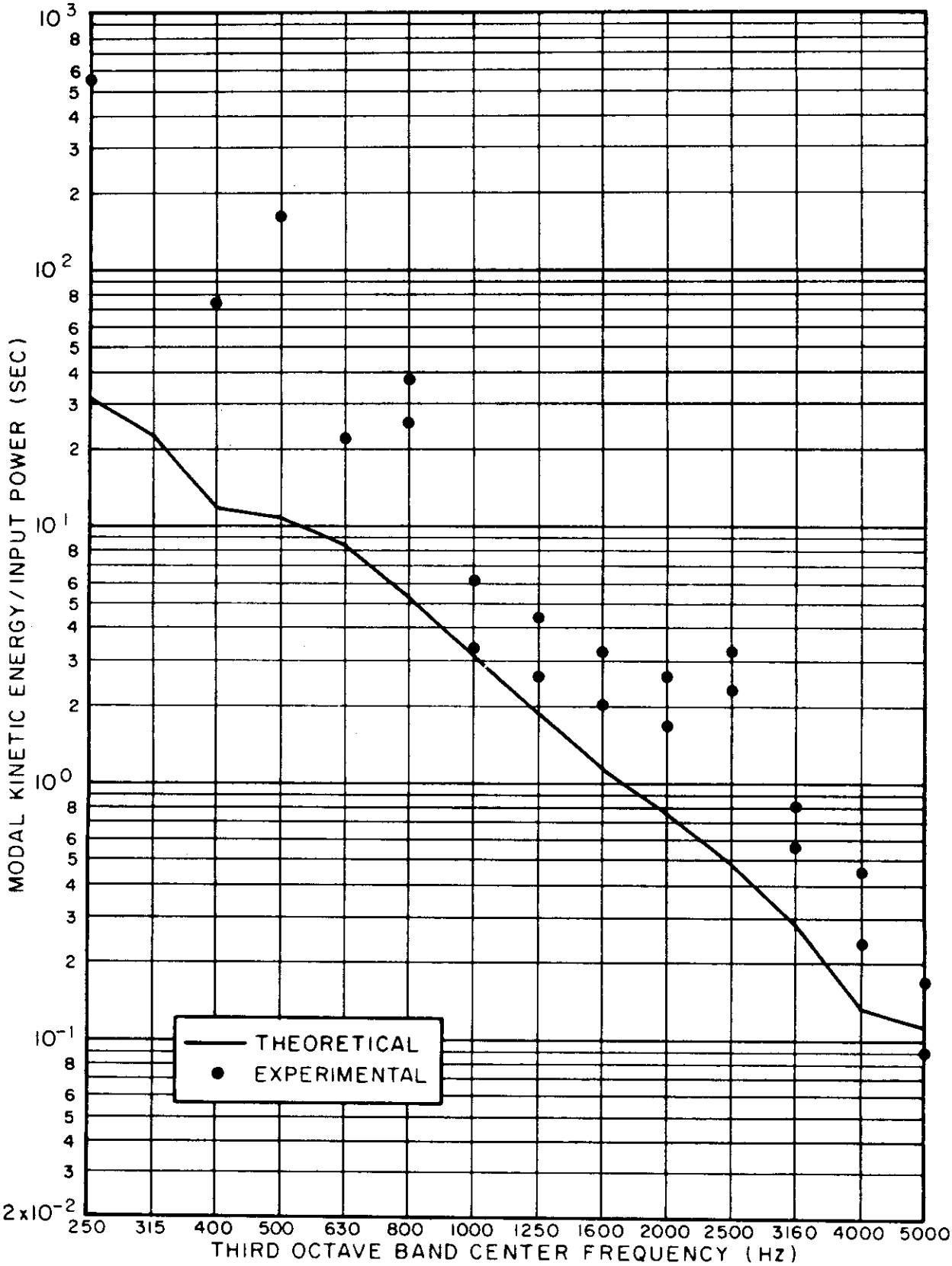

FIG. 10d RESPONSE OF PANEL "D" OF FIN STRUCTURE (DRIVEN AT PANEL "B")

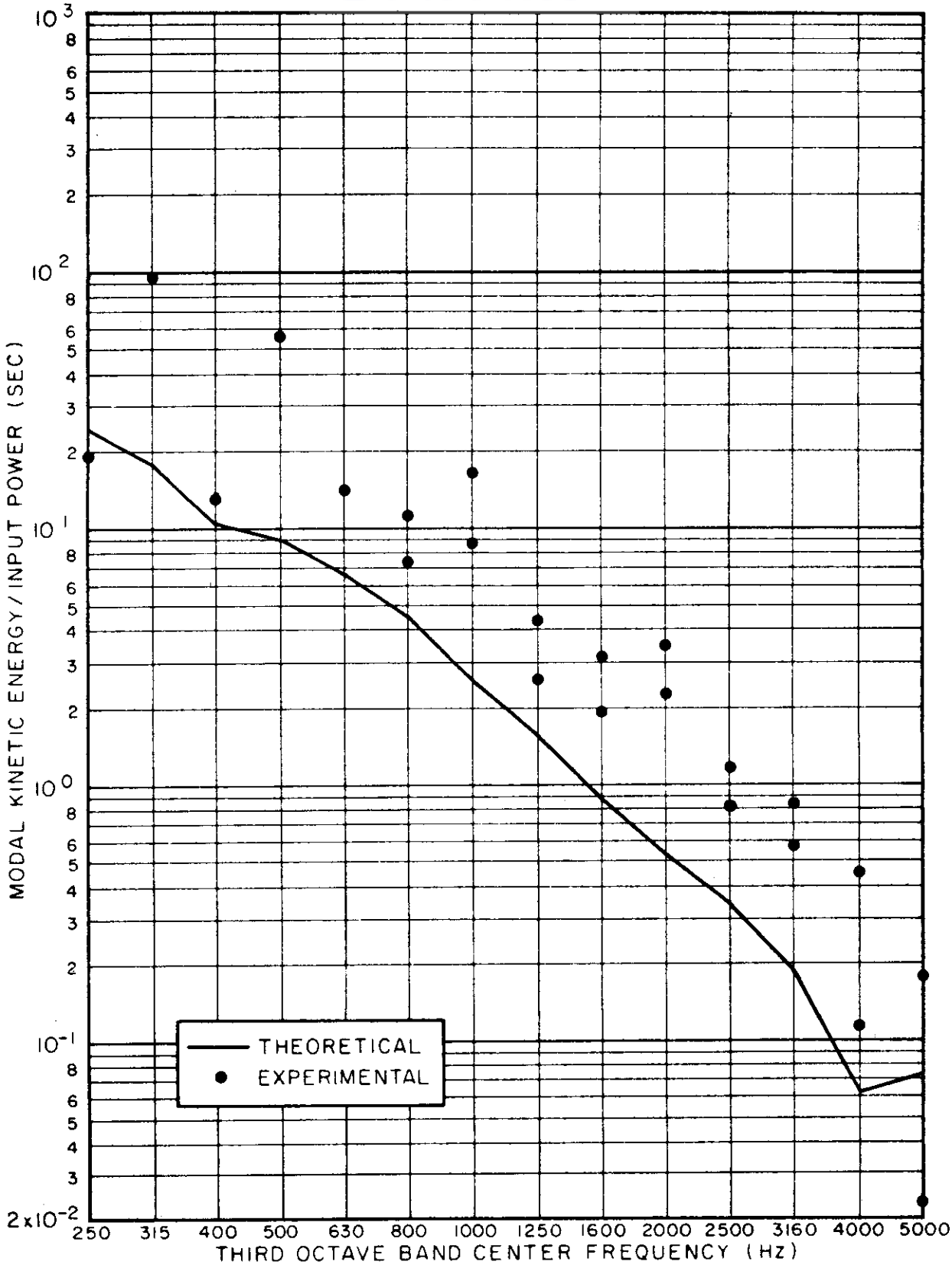

FIG.10e RESPONSE OF PANEL "E" OF FIN STRUCTURE (DRIVEN AT PANEL "B")

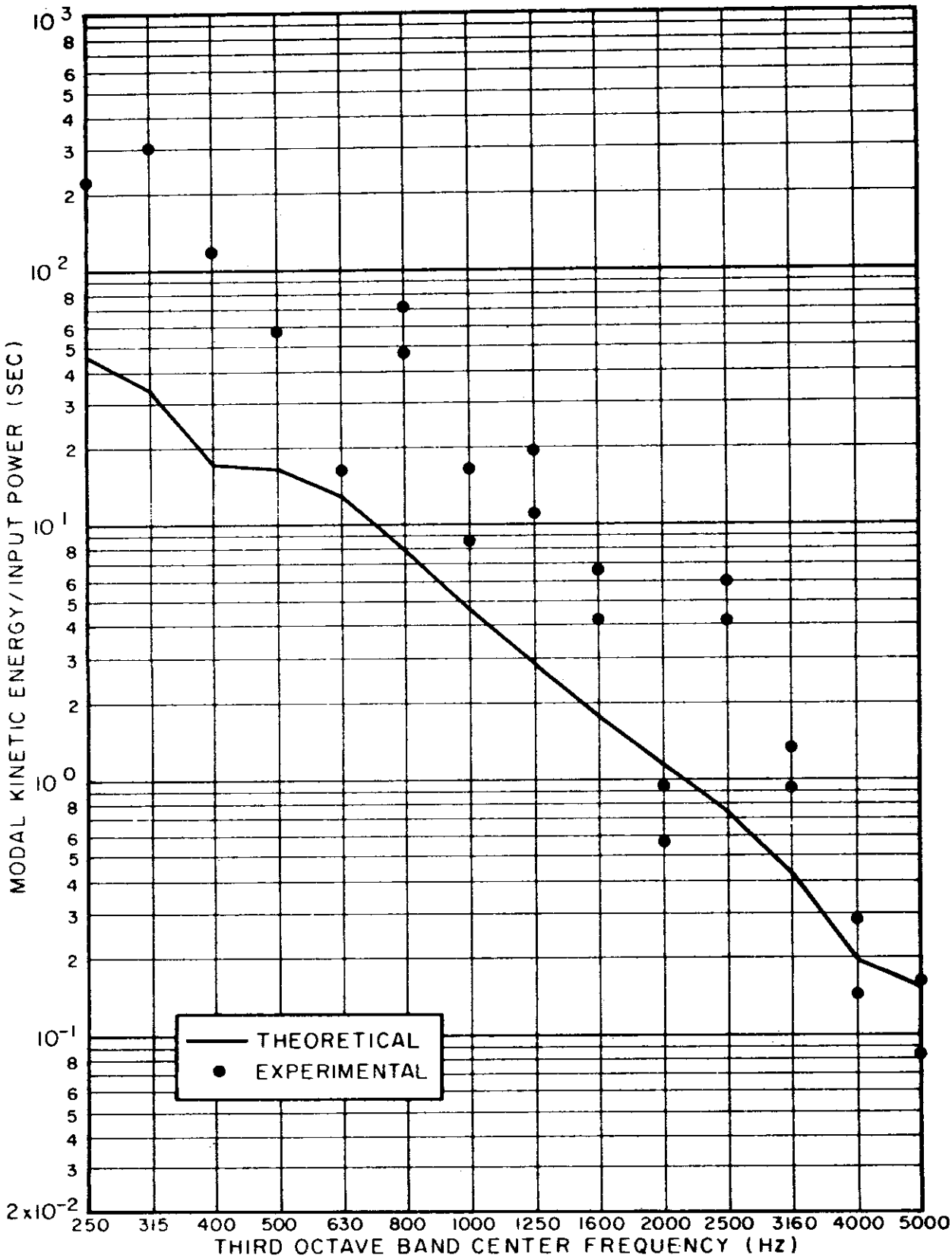

FIG. 10f RESPONSE OF PANEL "F" OF FIN STRUCTURE (DRIVEN AT PANEL "B")

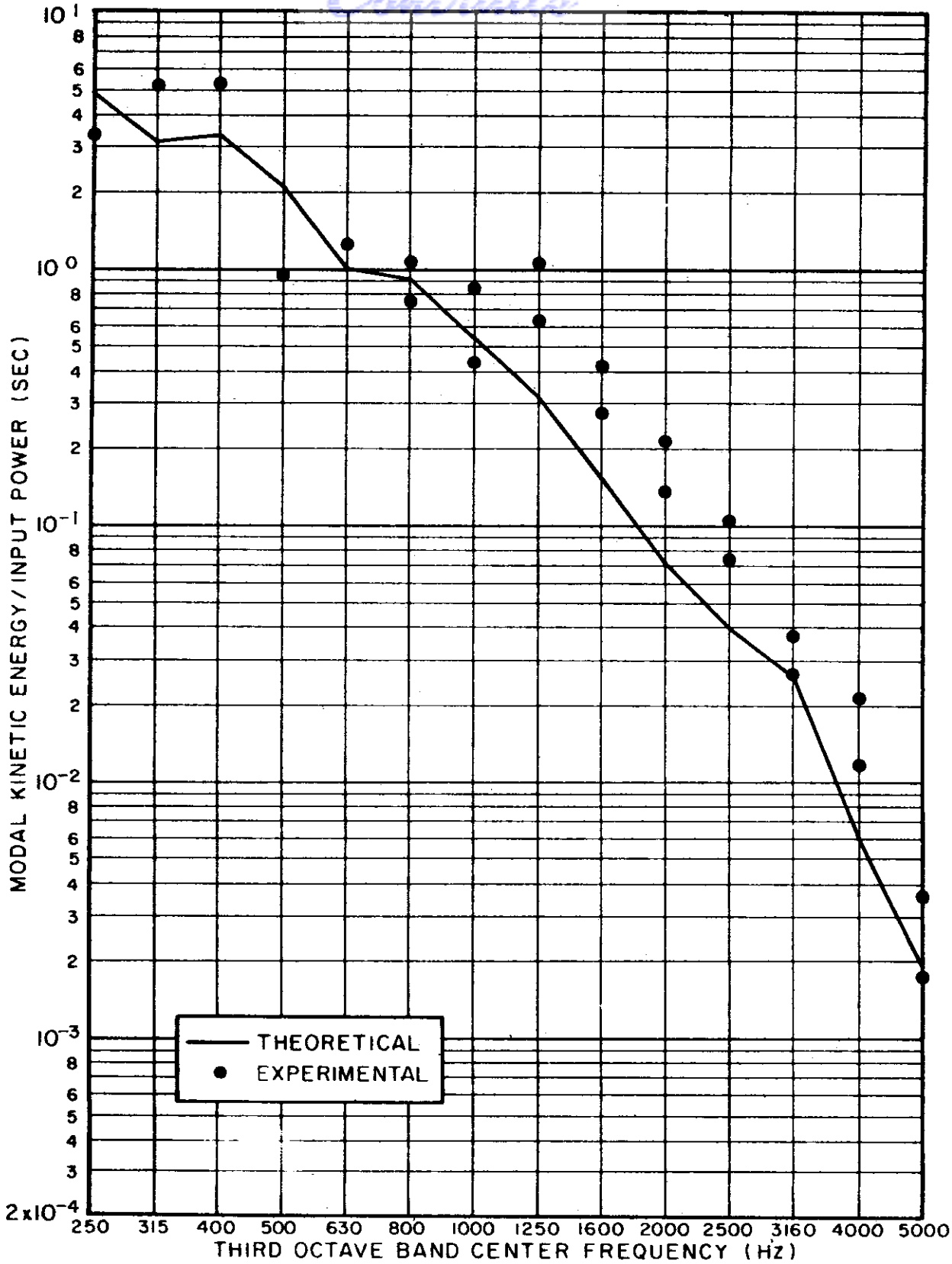

FIG.10g RESPONSE OF PANEL "G" OF FIN STRUCTURE (DRIVEN AT PANEL "B")

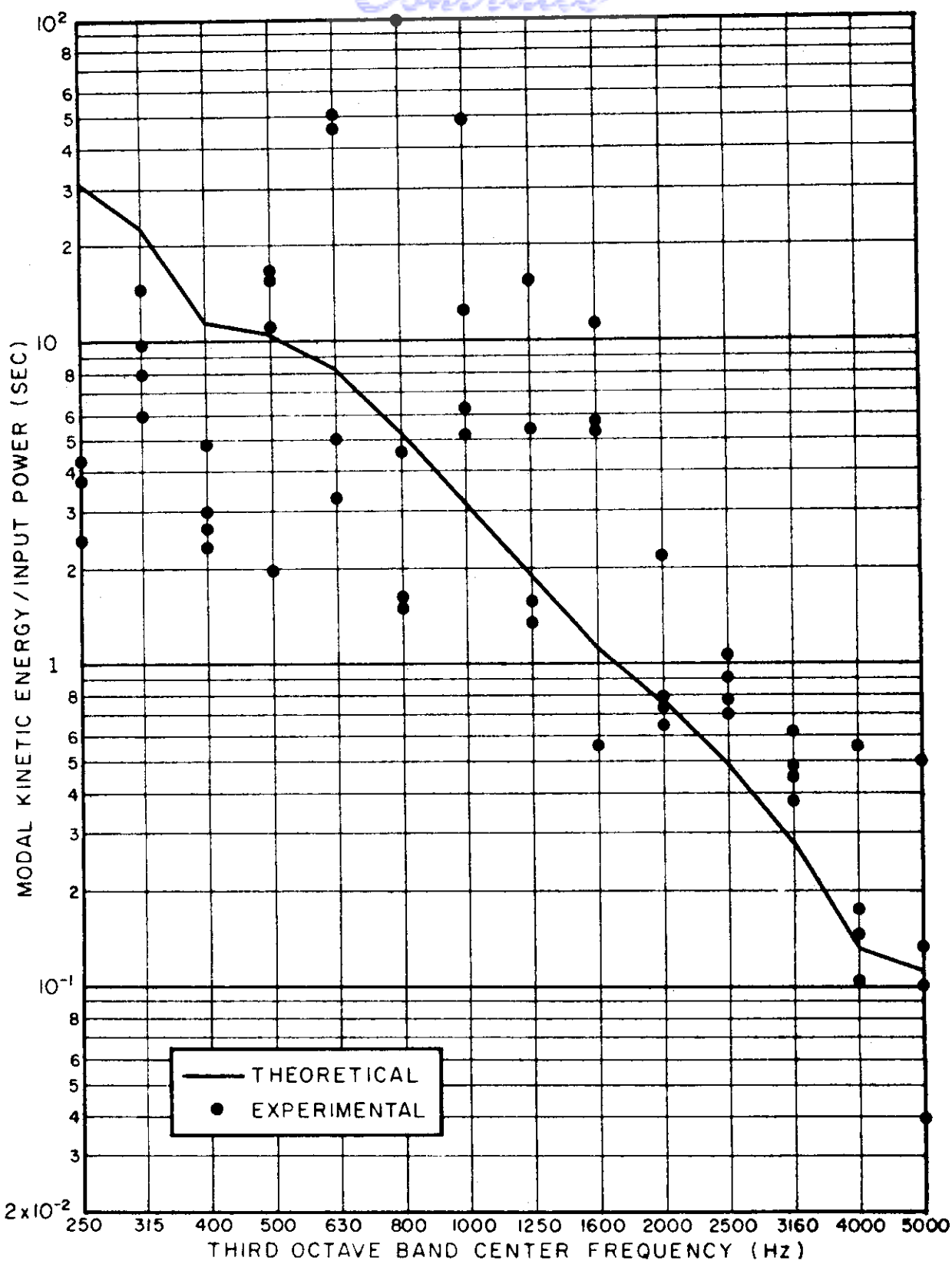

FIG. 11a RESPONSE OF PANEL "A" OF FIN STRUCTURE (DRIVEN AT PANEL "E")

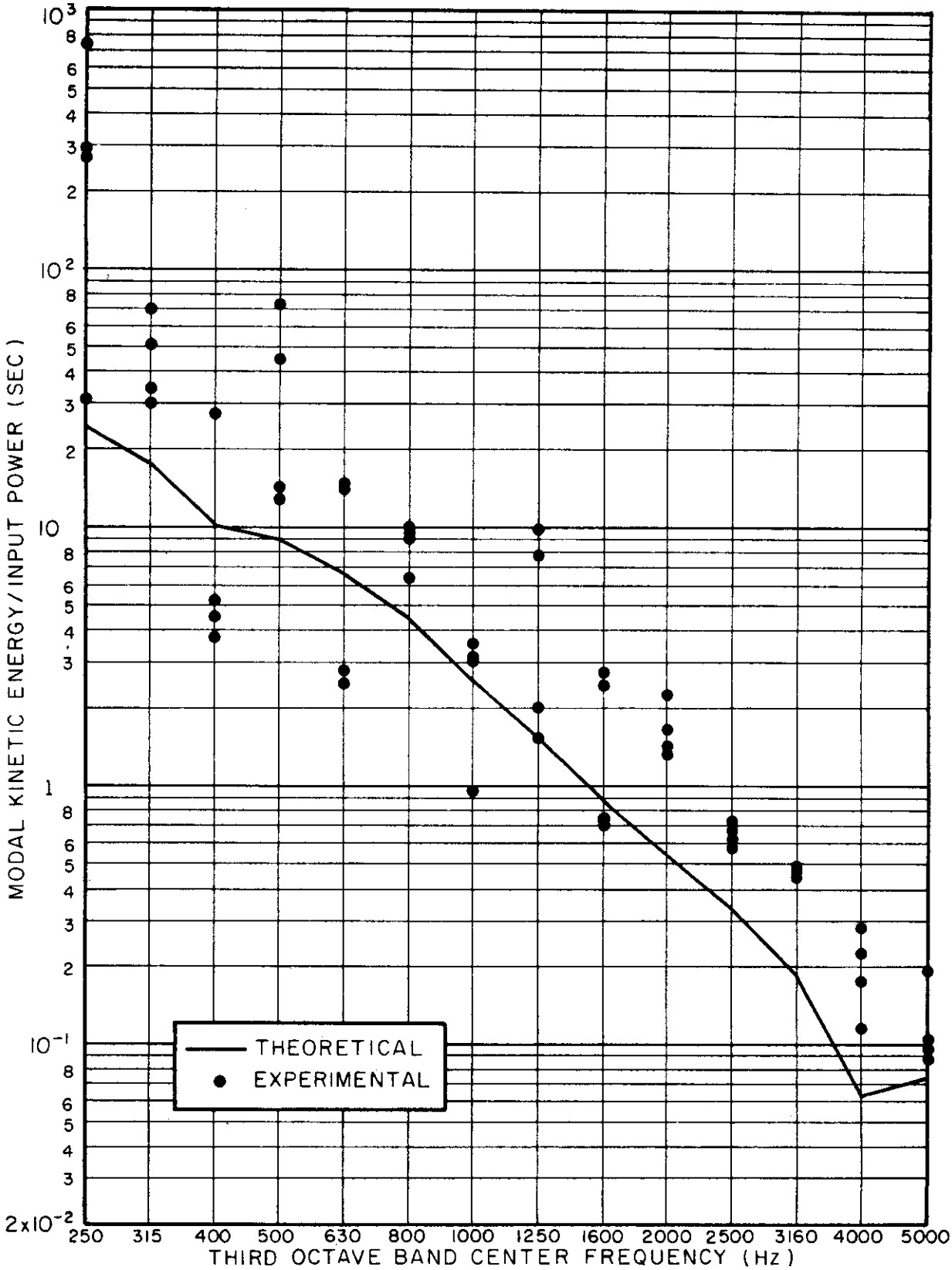

FIG. 11b RESPONSE OF PANEL "B" OF FIN STRUCTURE (DRIVEN AT PANEL "E")

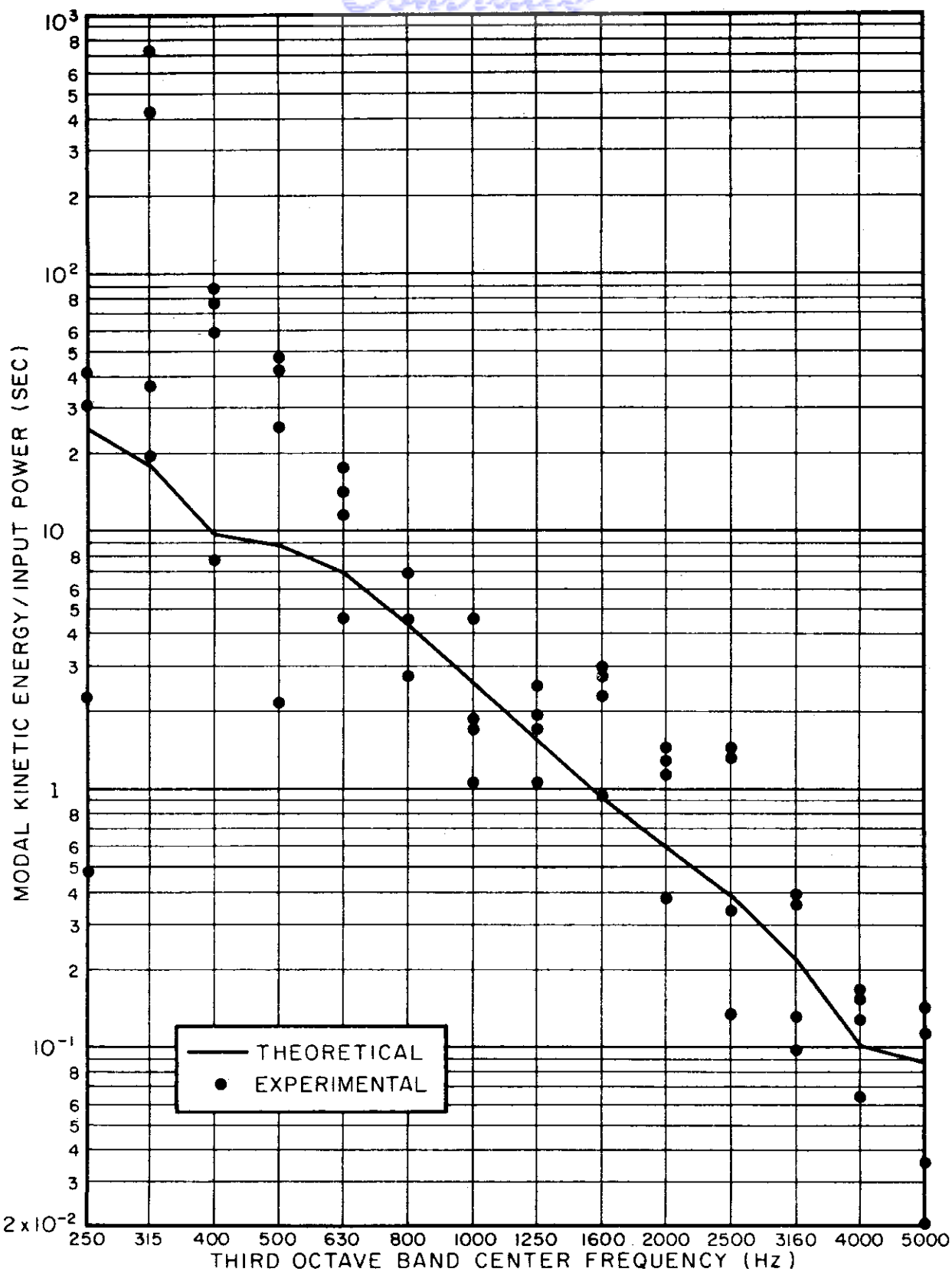

FIG. 11c RESPONSE OF PANEL "C" OF FIN STRUCTURE (DRIVEN AT PANEL "E")

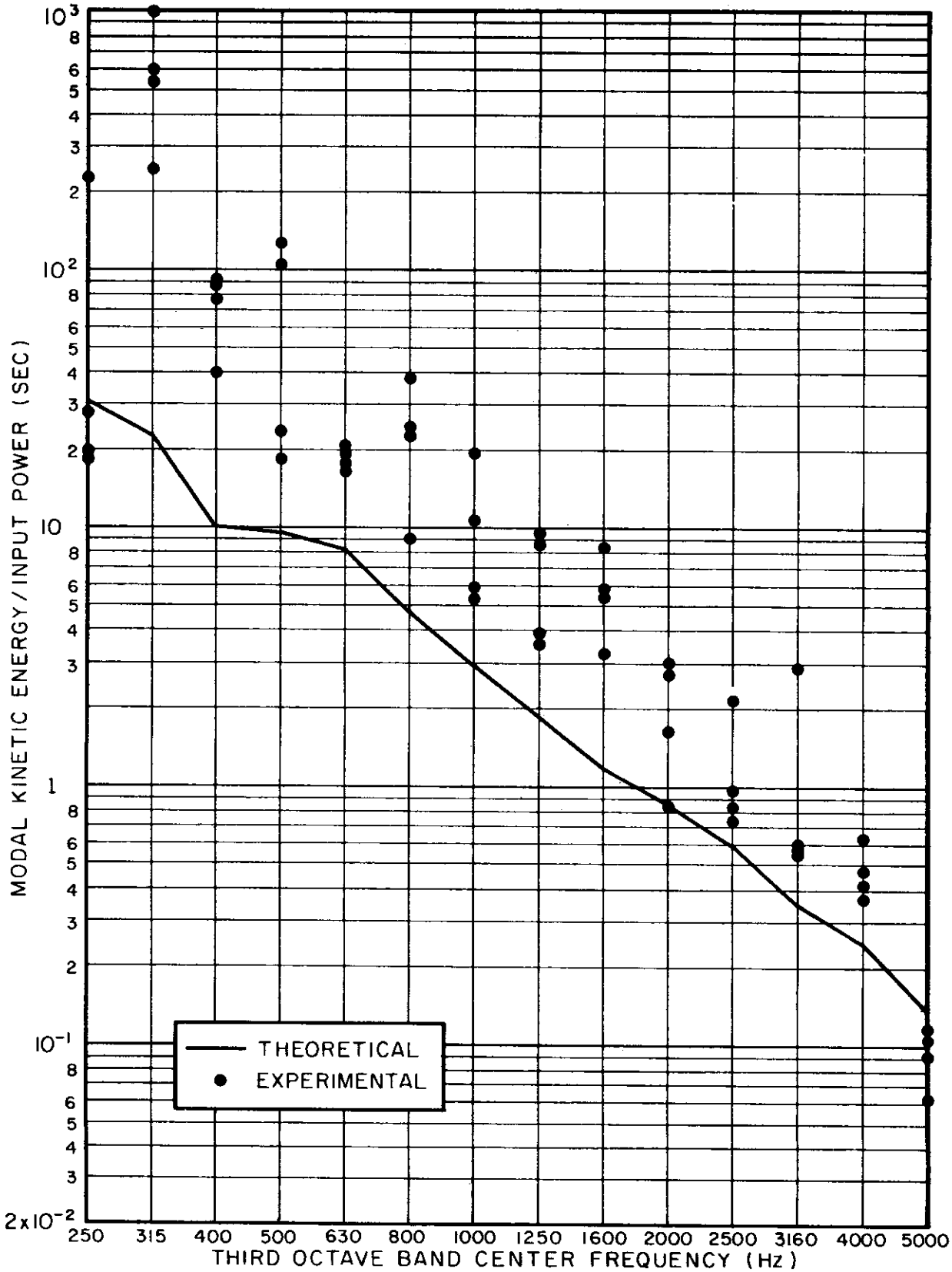

FIG. 11d RESPONSE OF PANEL "D" OF FIN STRUCTURE (DRIVEN AT PANEL "E")

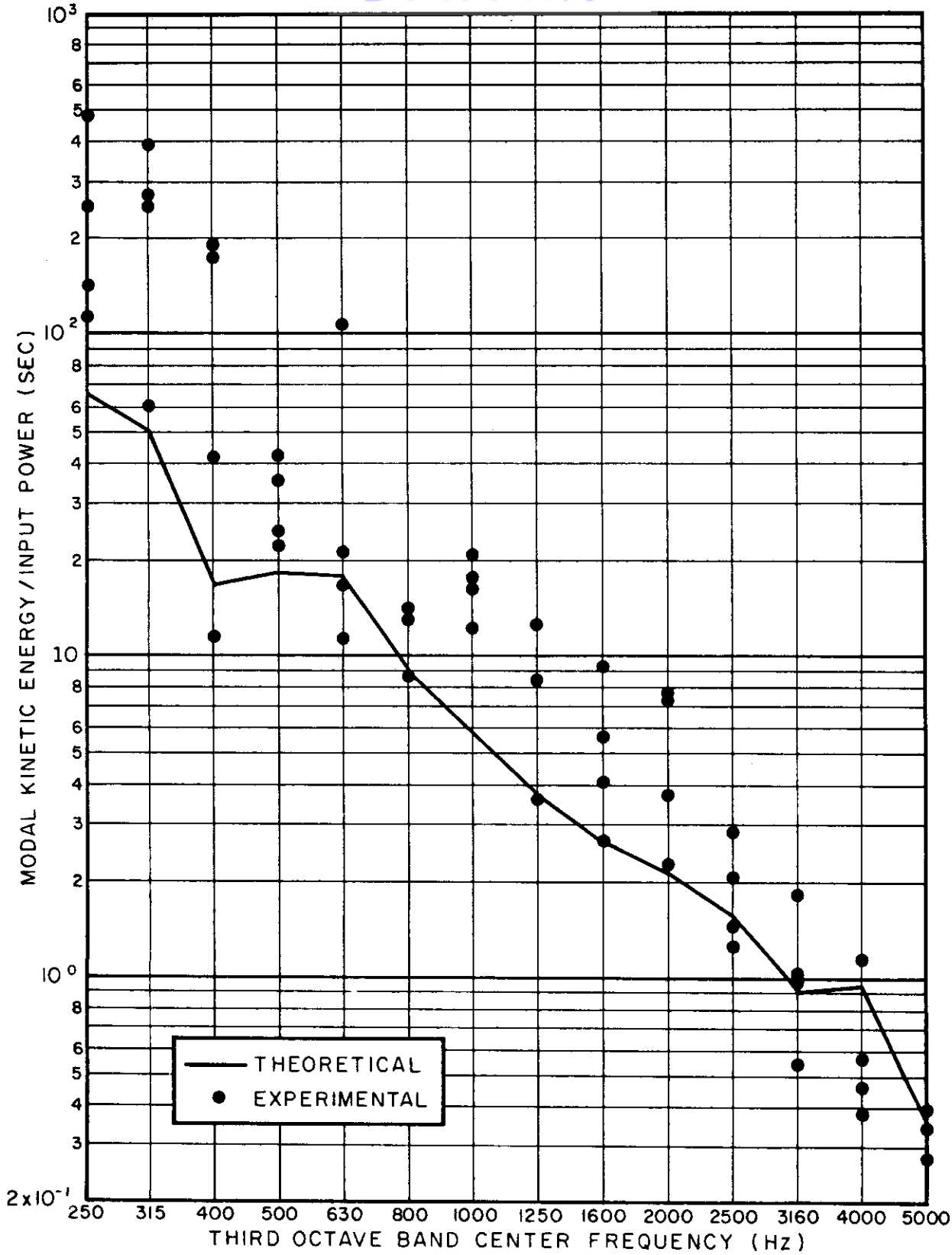

FIG.11e RESPONSE OF PANEL "E" OF FIN STRUCTURE (DRIVEN AT PANEL "E")

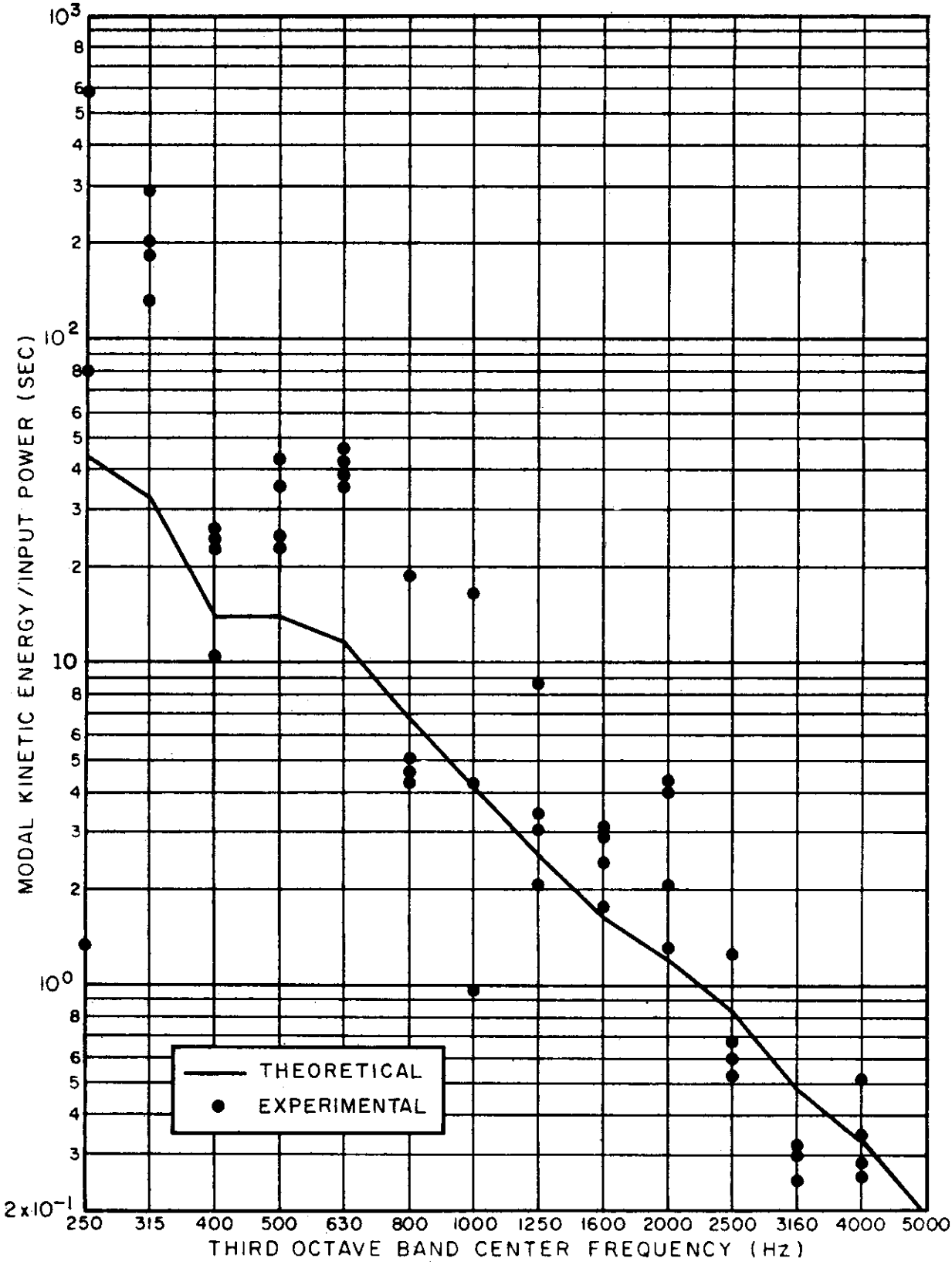

FIG. 11f RESPONSE OF PANEL "F" OF FIN STRUCTURE (DRIVEN AT PANEL "E")

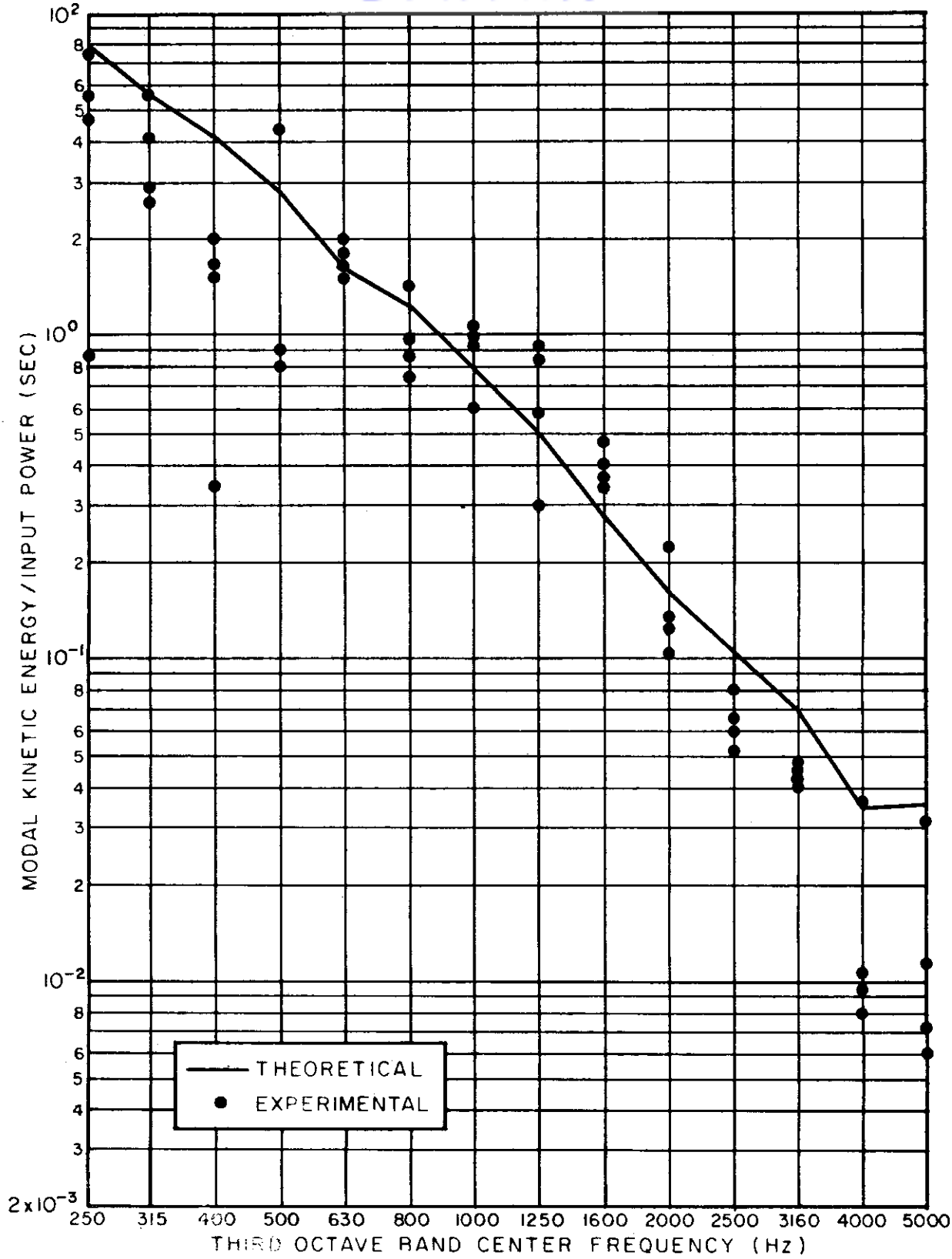

FIG. 11g RESPONSE OF PANEL "G" OF FIN STRUCTURE (DRIVEN AT PANEL "E")

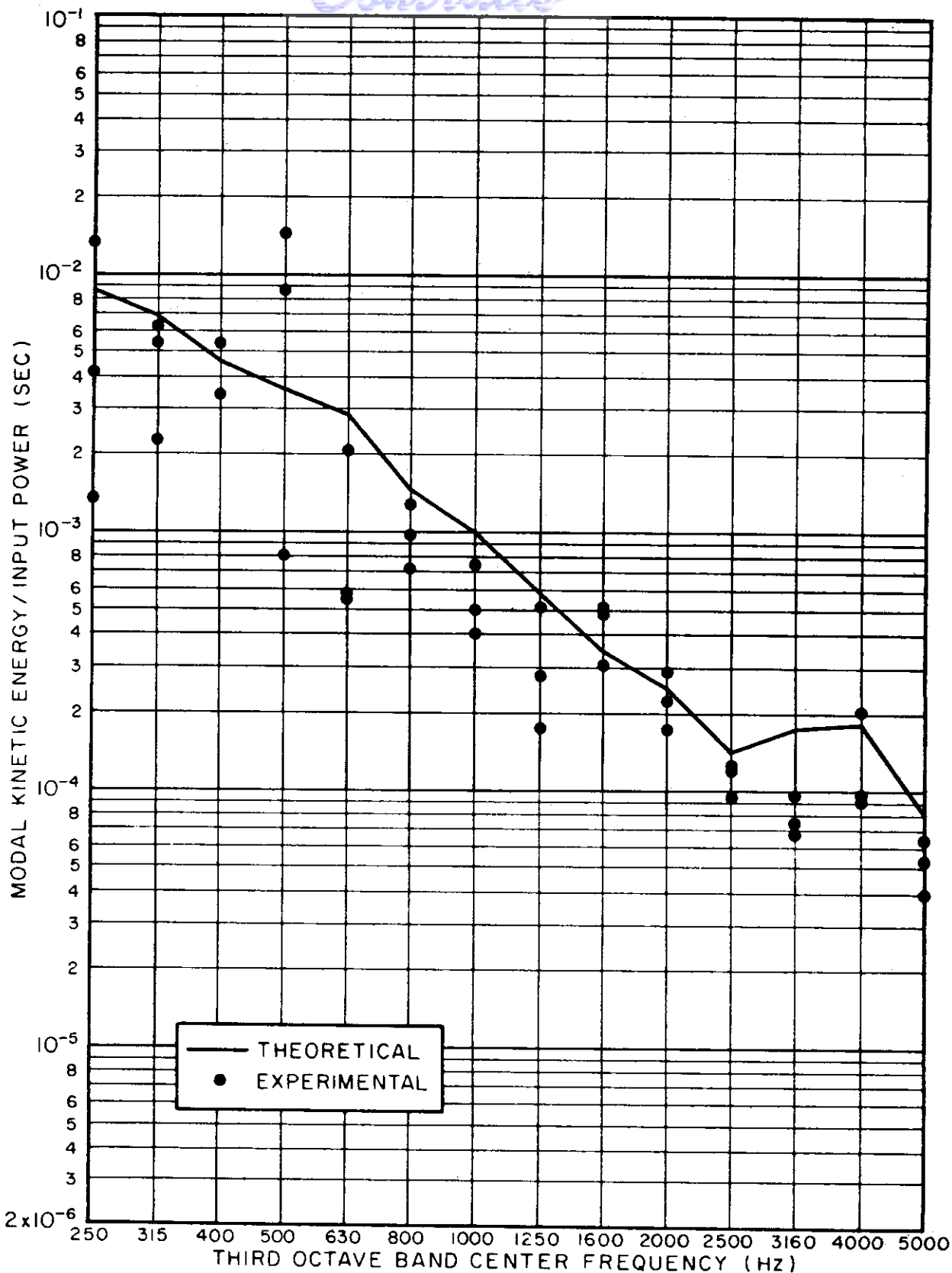

FIG.12a RESPONSE OF PANEL "A" OF CYLINDRICAL SHELL (DRIVEN AT PANEL "A")

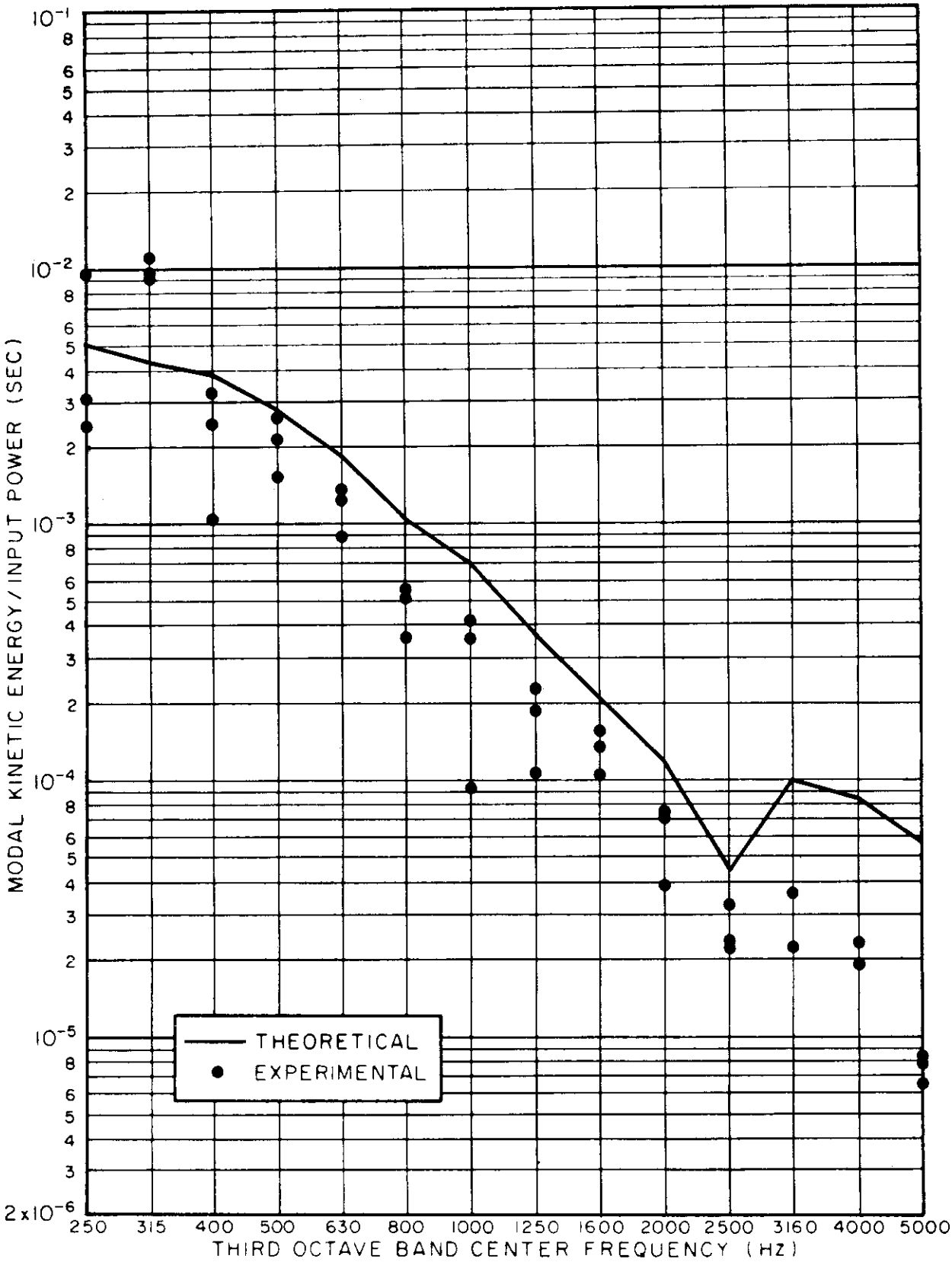

FIG.12b RESPONSE OF PANEL "B" OF CYLINDRICAL SHELL (DRIVEN AT PANEL "A")

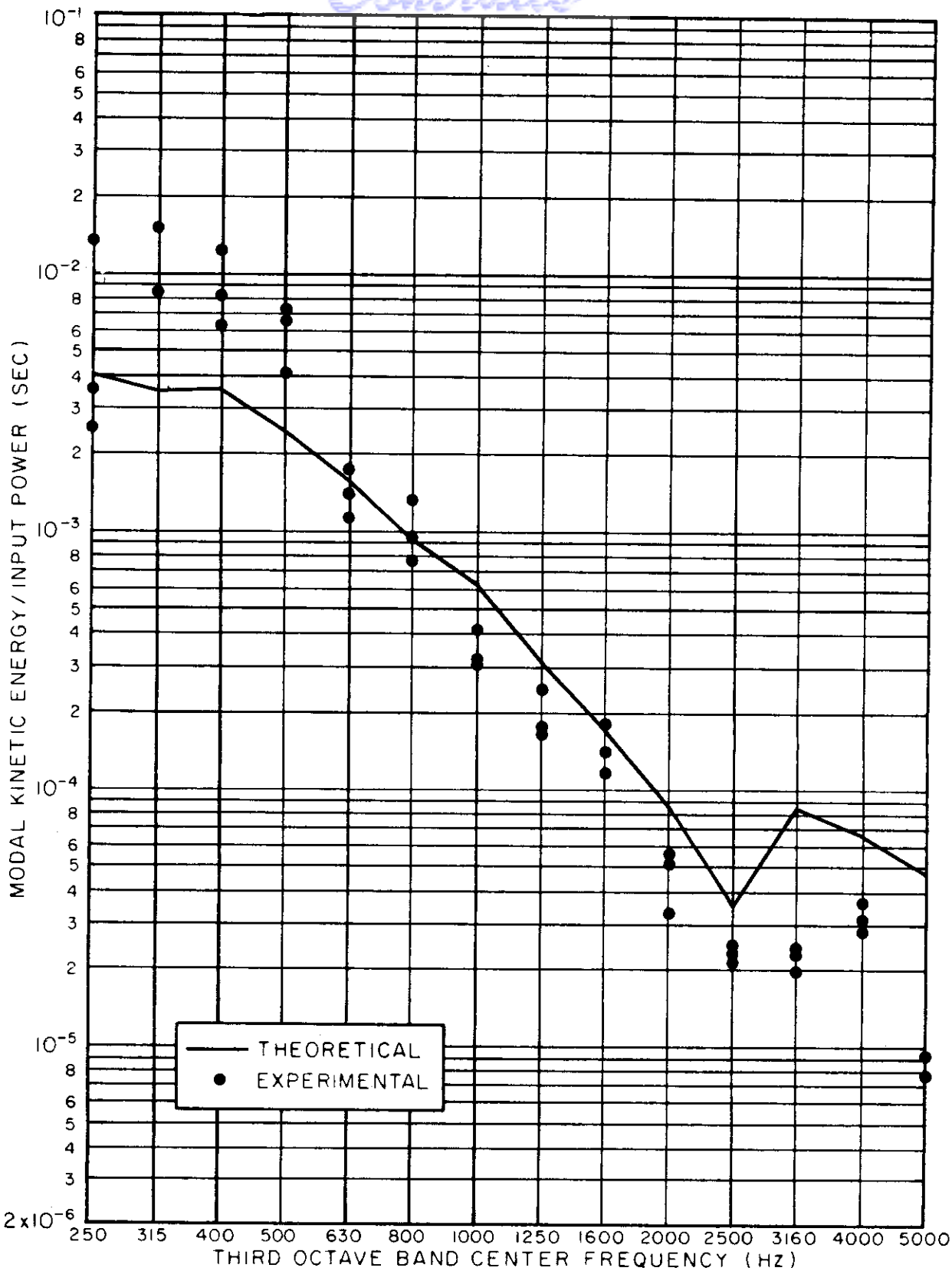

FIG.12c RESPONSE OF PANEL "C" OF CYLINDRICAL SHELL (DRIVEN AT PANEL "A")

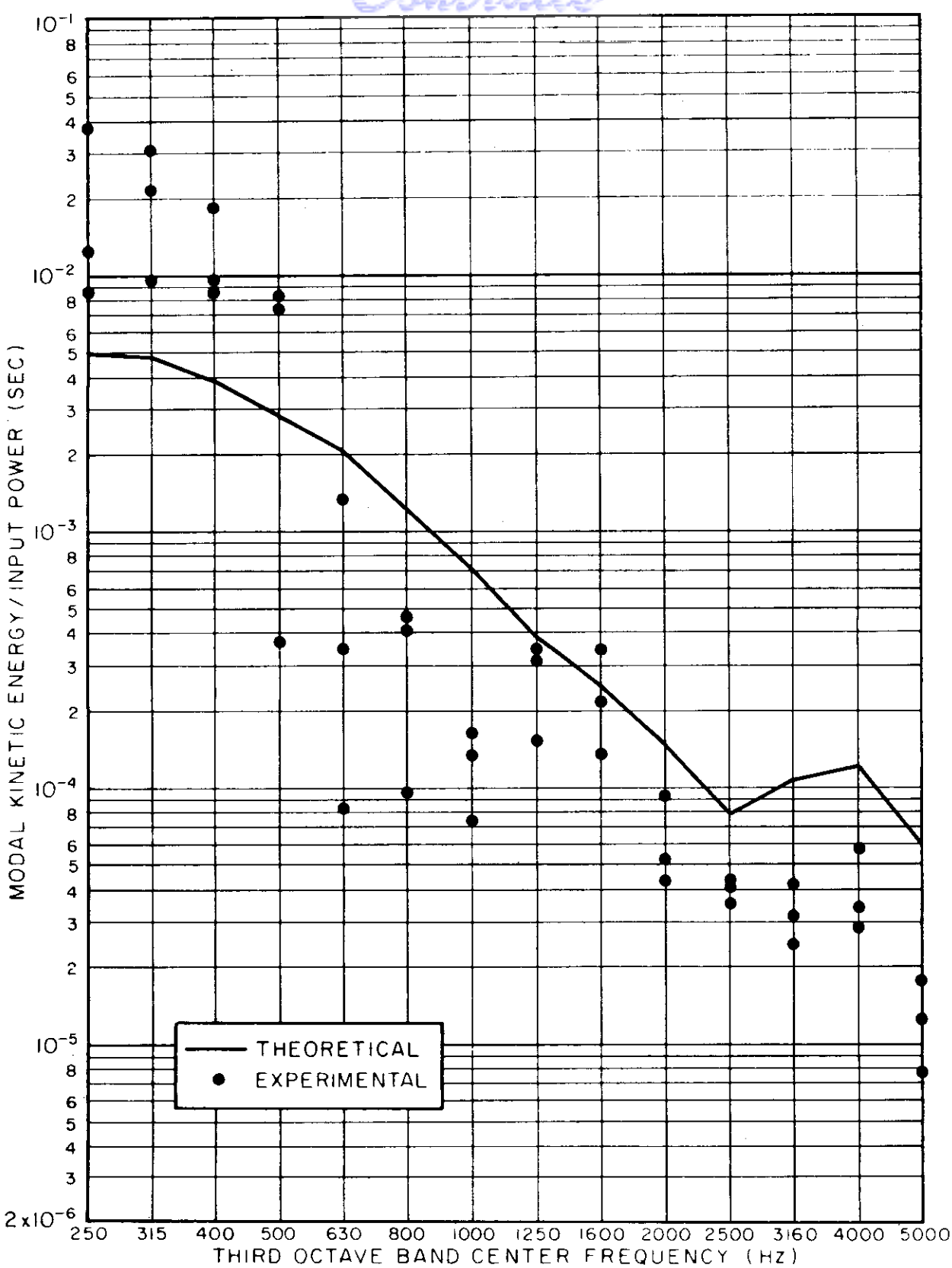

FIG. 12d RESPONSE OF PANEL "D" OF CYLINDRICAL SHELL (DRIVEN AT PANEL "A")

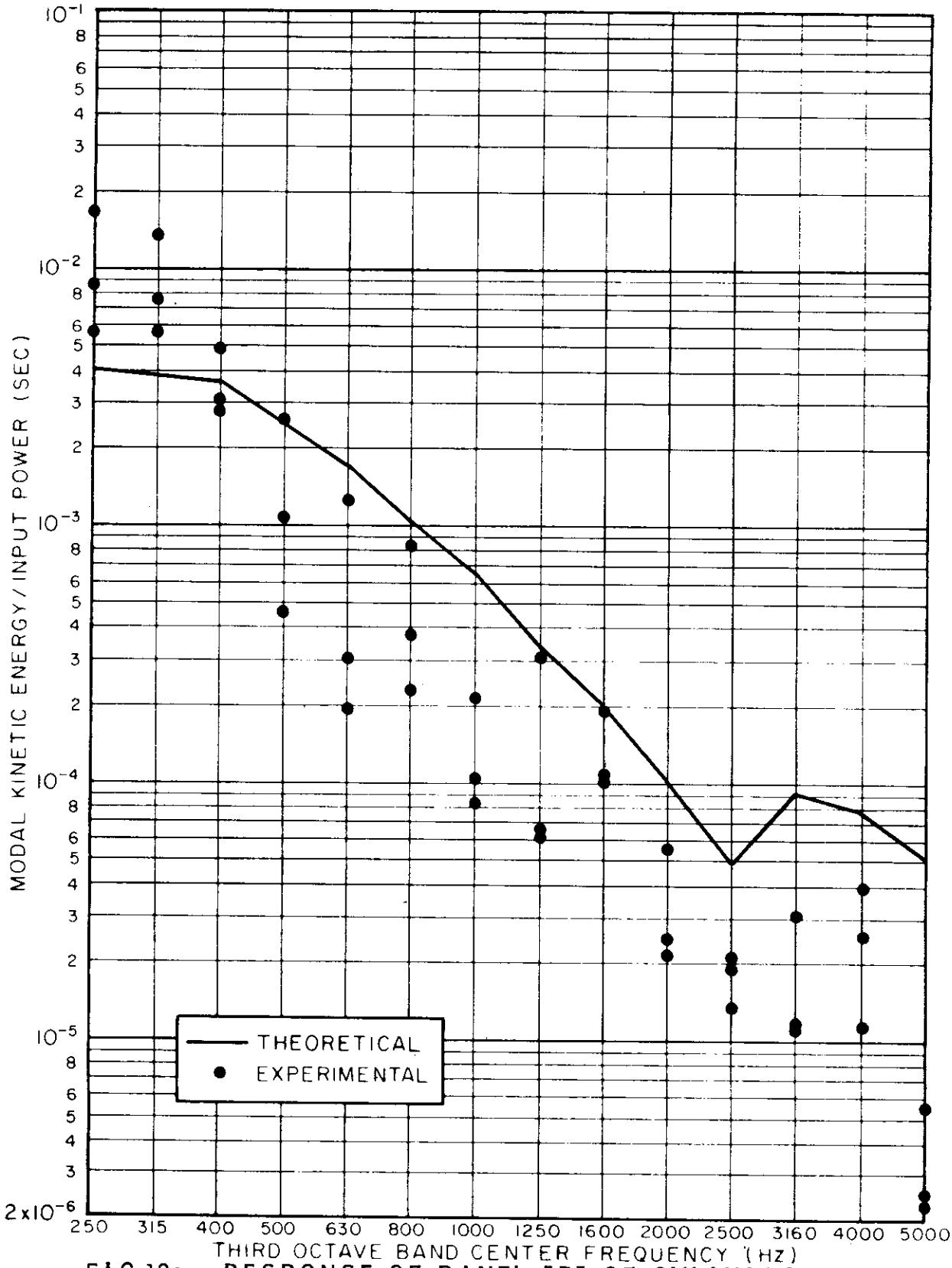

FIG. 12e RESPONSE OF PANEL "E" OF CYLINDRICAL SHELL (DRIVEN AT PANEL "A")

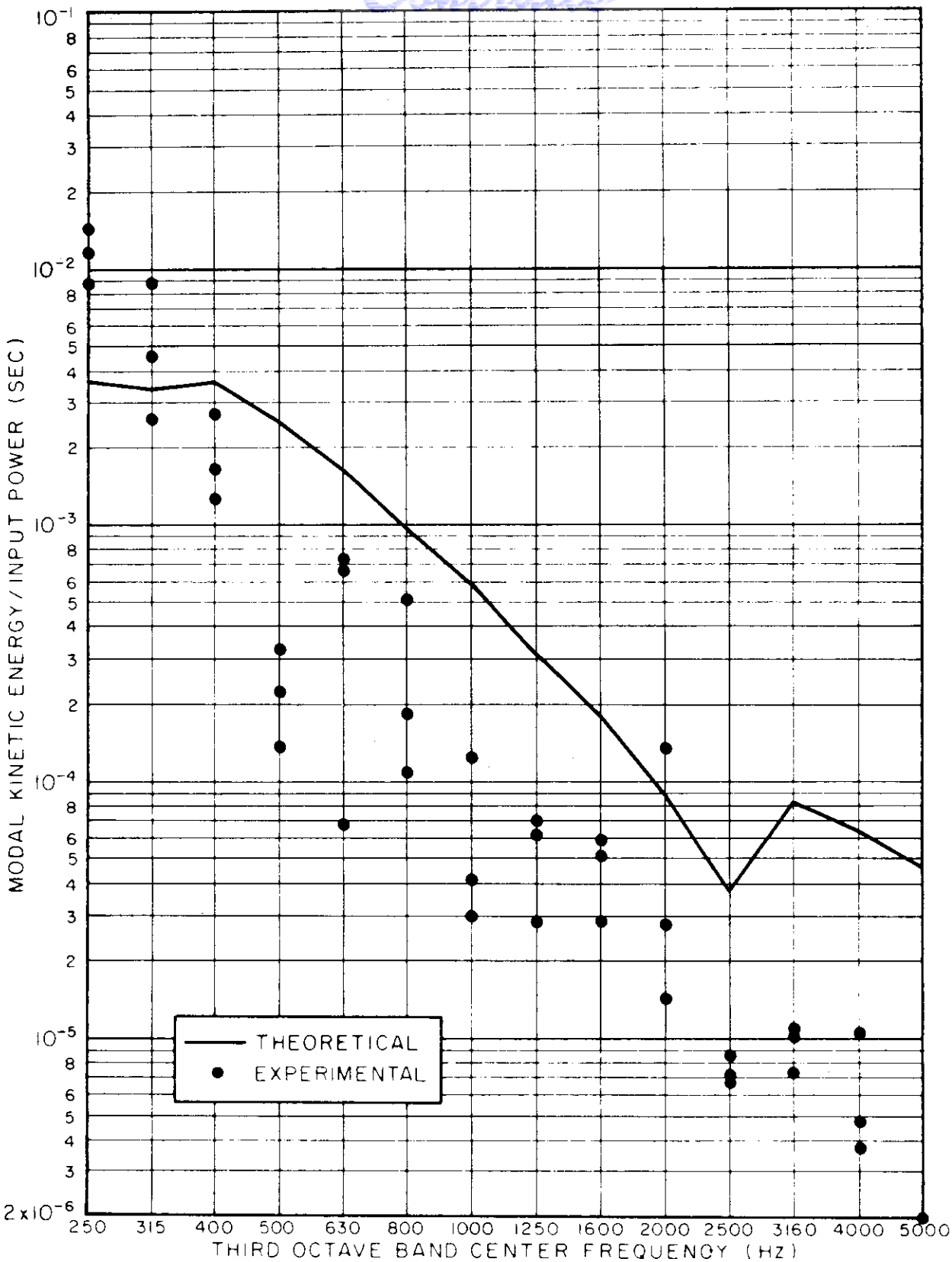

FIG. 12f RESPONSE OF PANEL "F" OF CYLINDRICAL SHELL (DRIVEN AT PANEL "A")

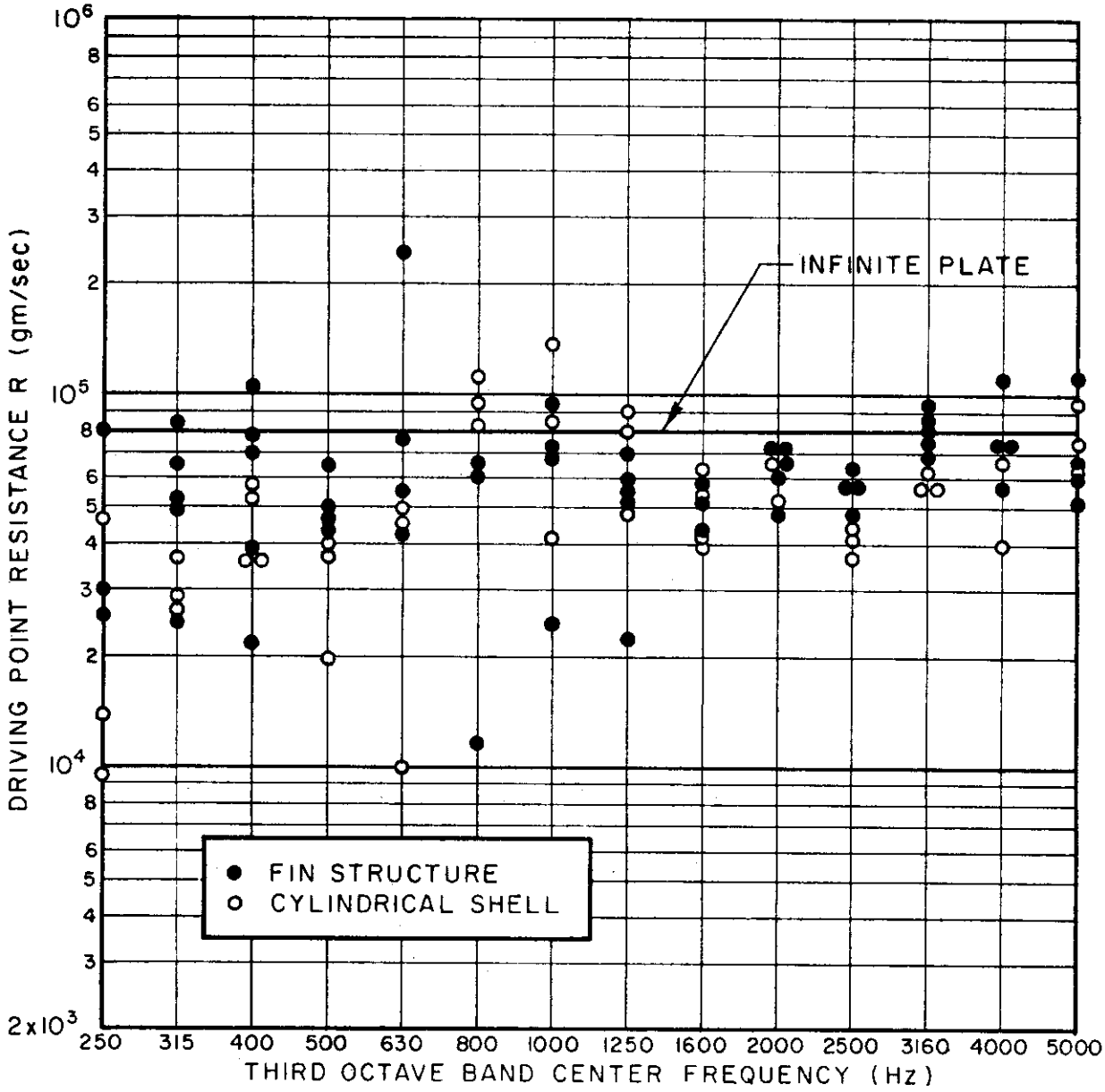

FIG. 13 DRIVING POINT RESISTANCES OF TEST STRUCTURES

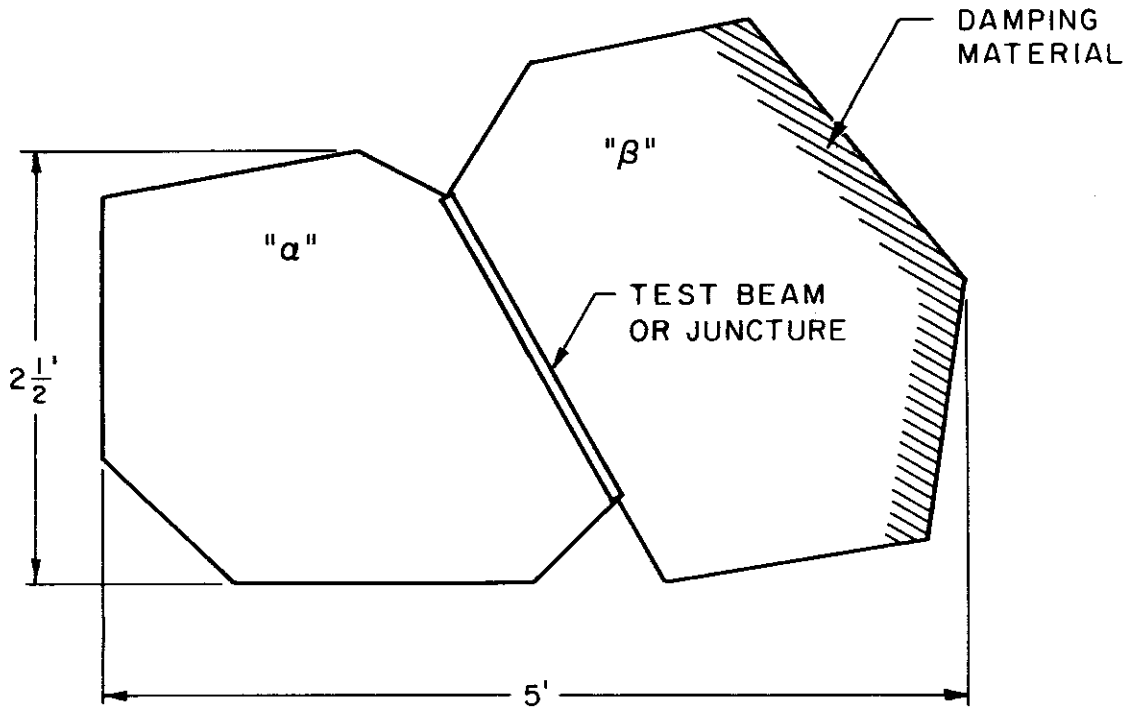

FIG. 14 EDGE-JOINED PANELS FOR MEASUREMENT OF POWER FLOW COEFFICIENTS

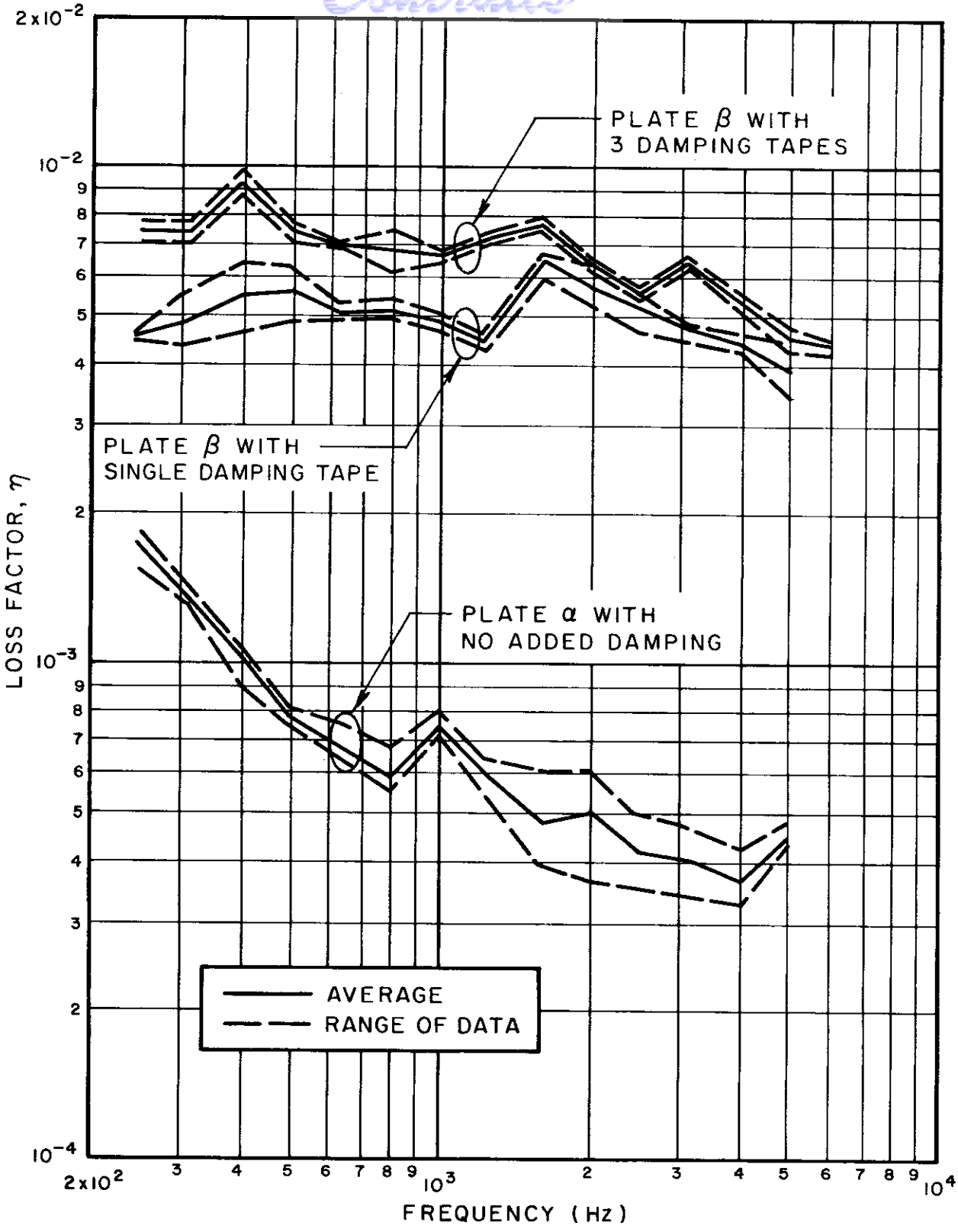

FIG. 15 DISSIPATION LOSS FACTORS OF SEPARATE PANELS

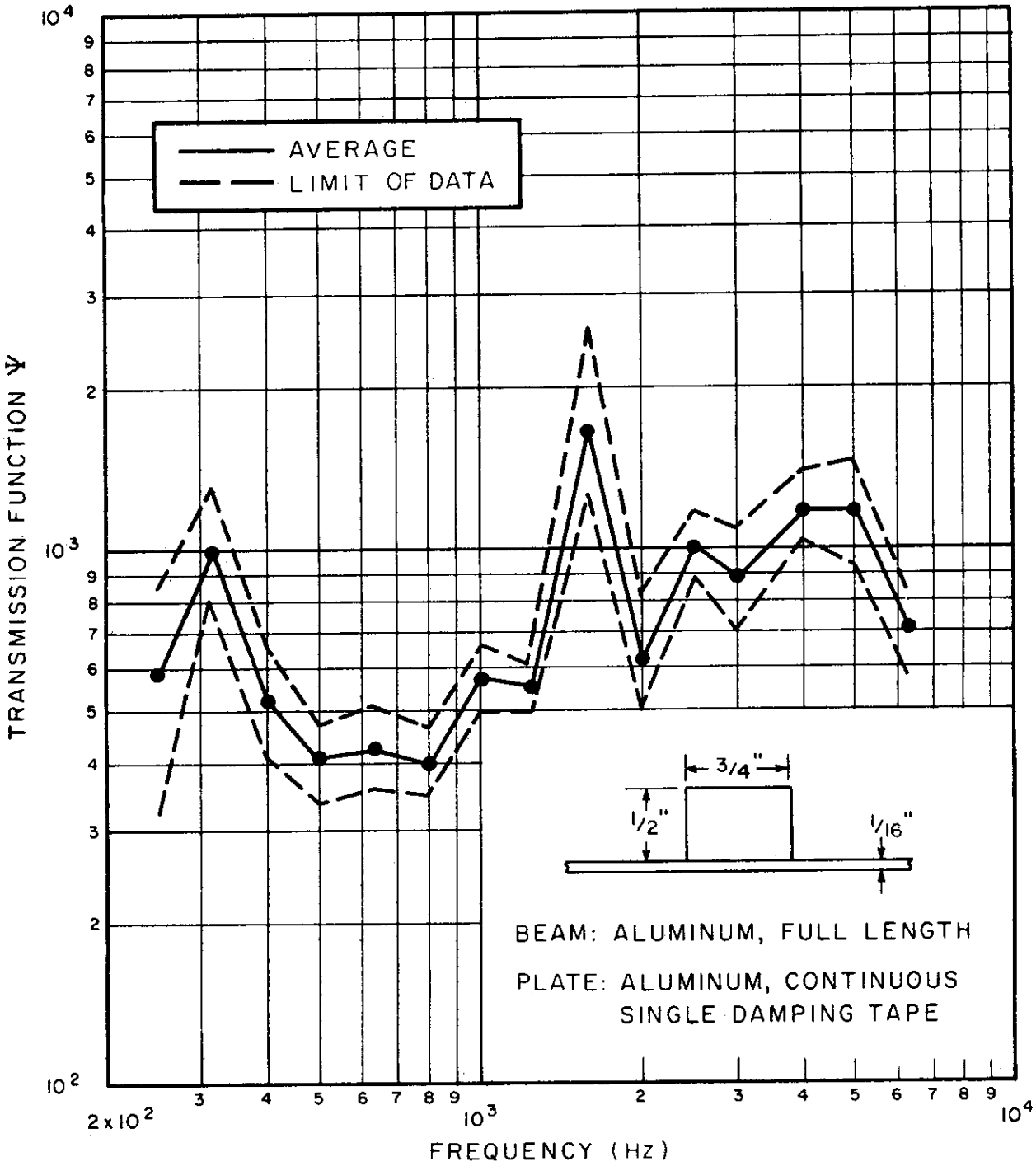

FIG. 16a POWER FLOW ACROSS A BEAM ON A PLATE

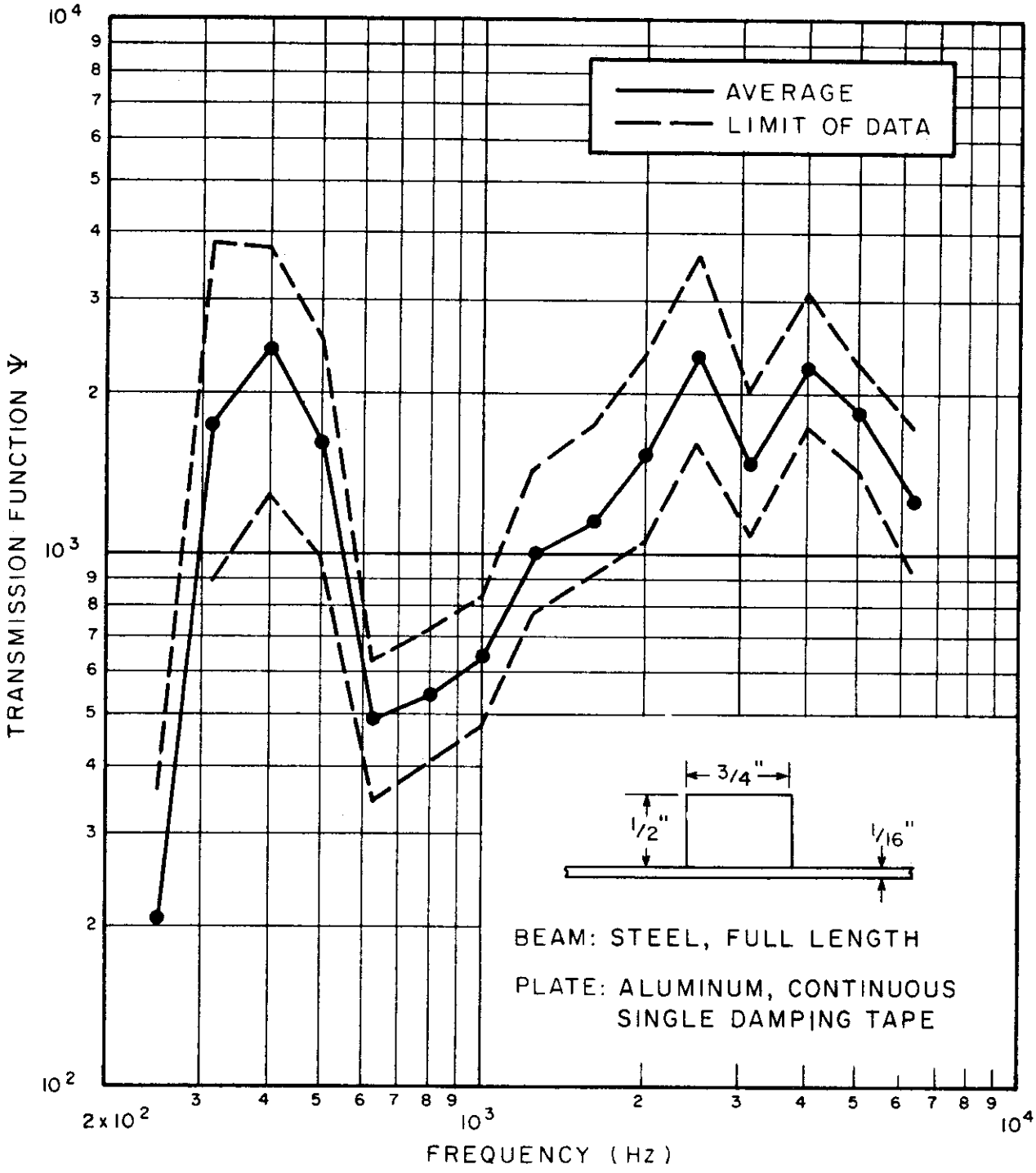

FIG. 16b POWER FLOW ACROSS A BEAM ON A PLATE

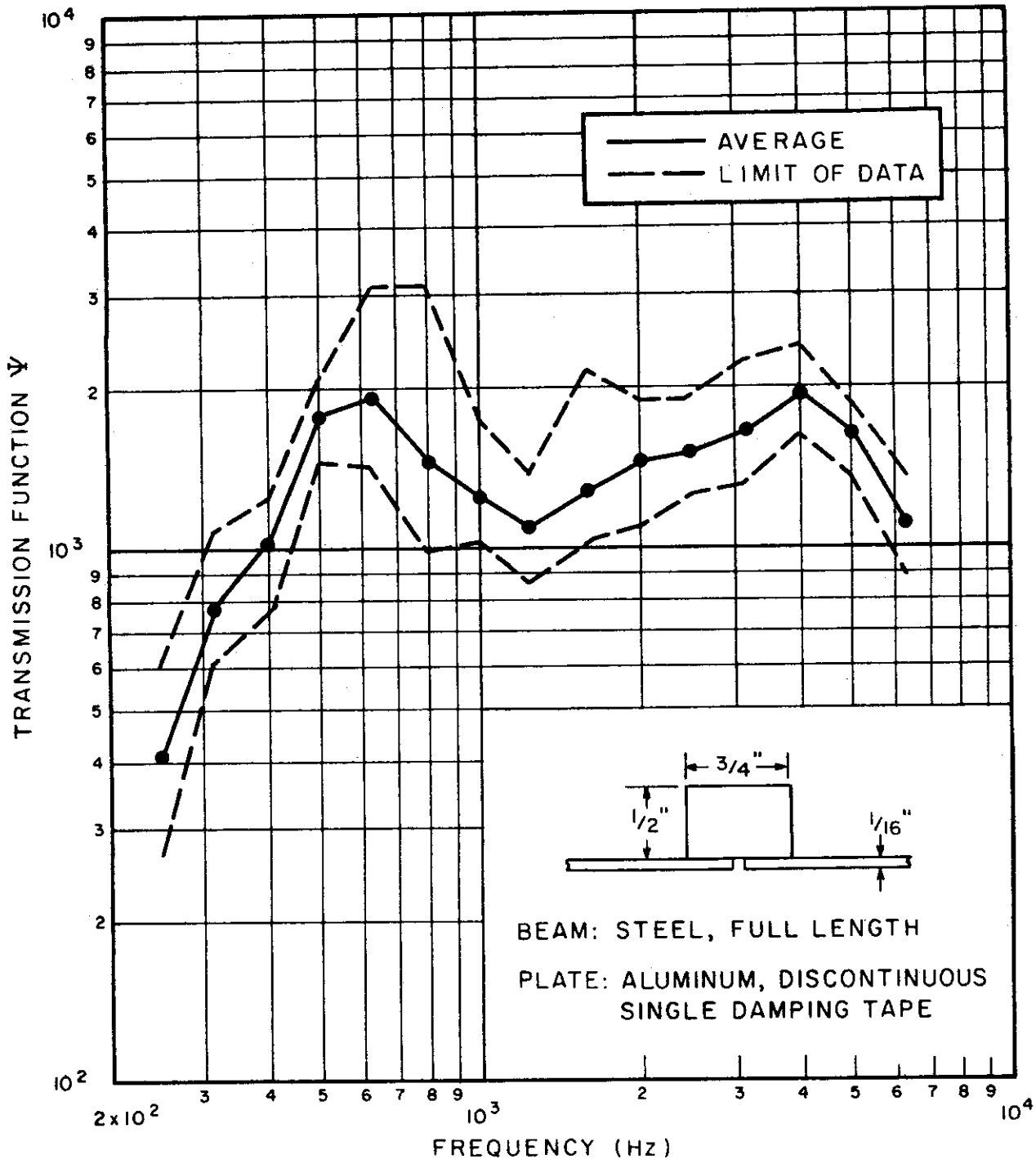

FIG. 16c POWER FLOW ACROSS A BEAM ON A PLATE

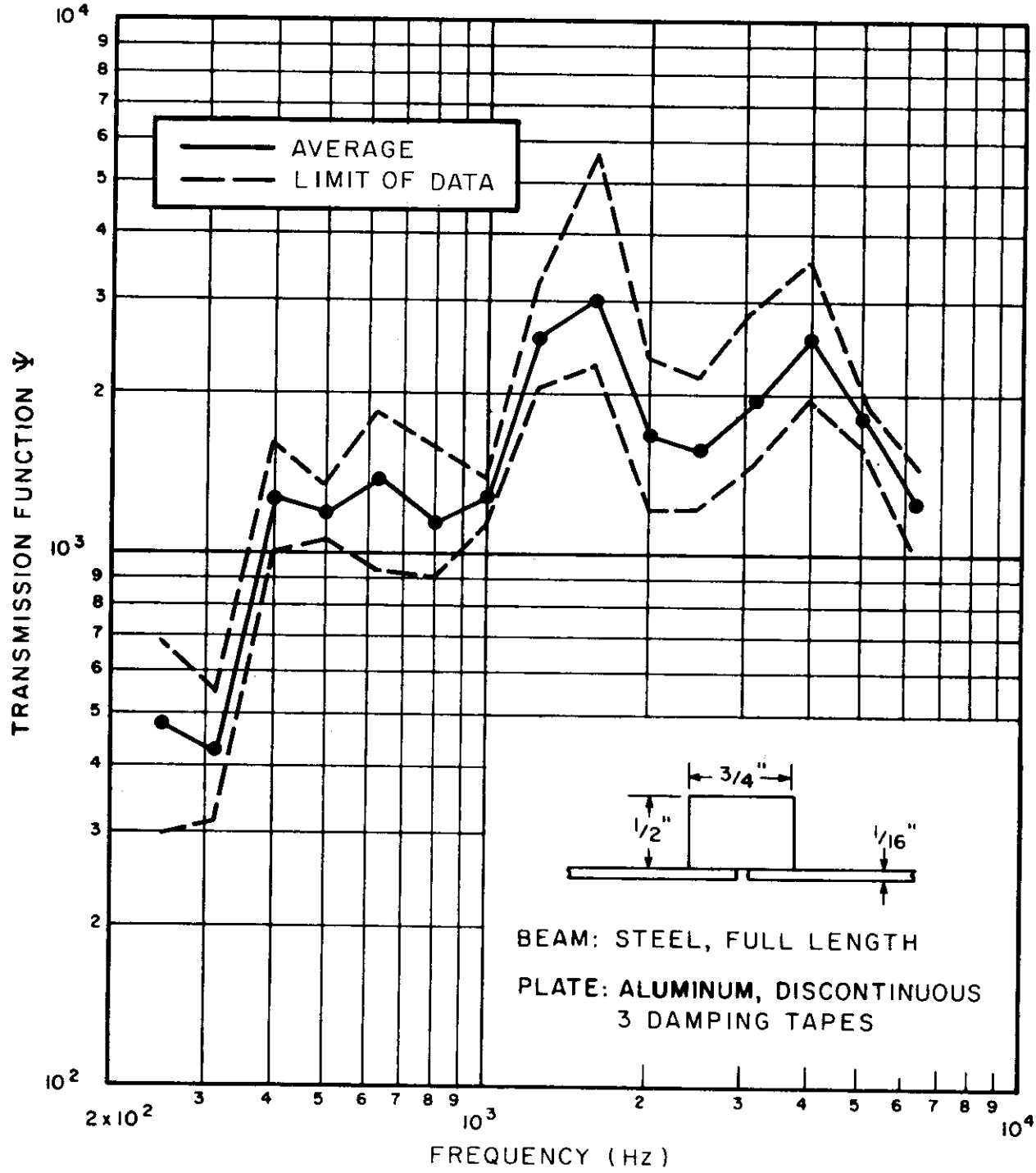

FIG. 16d POWER FLOW ACROSS A BEAM ON A PLATE

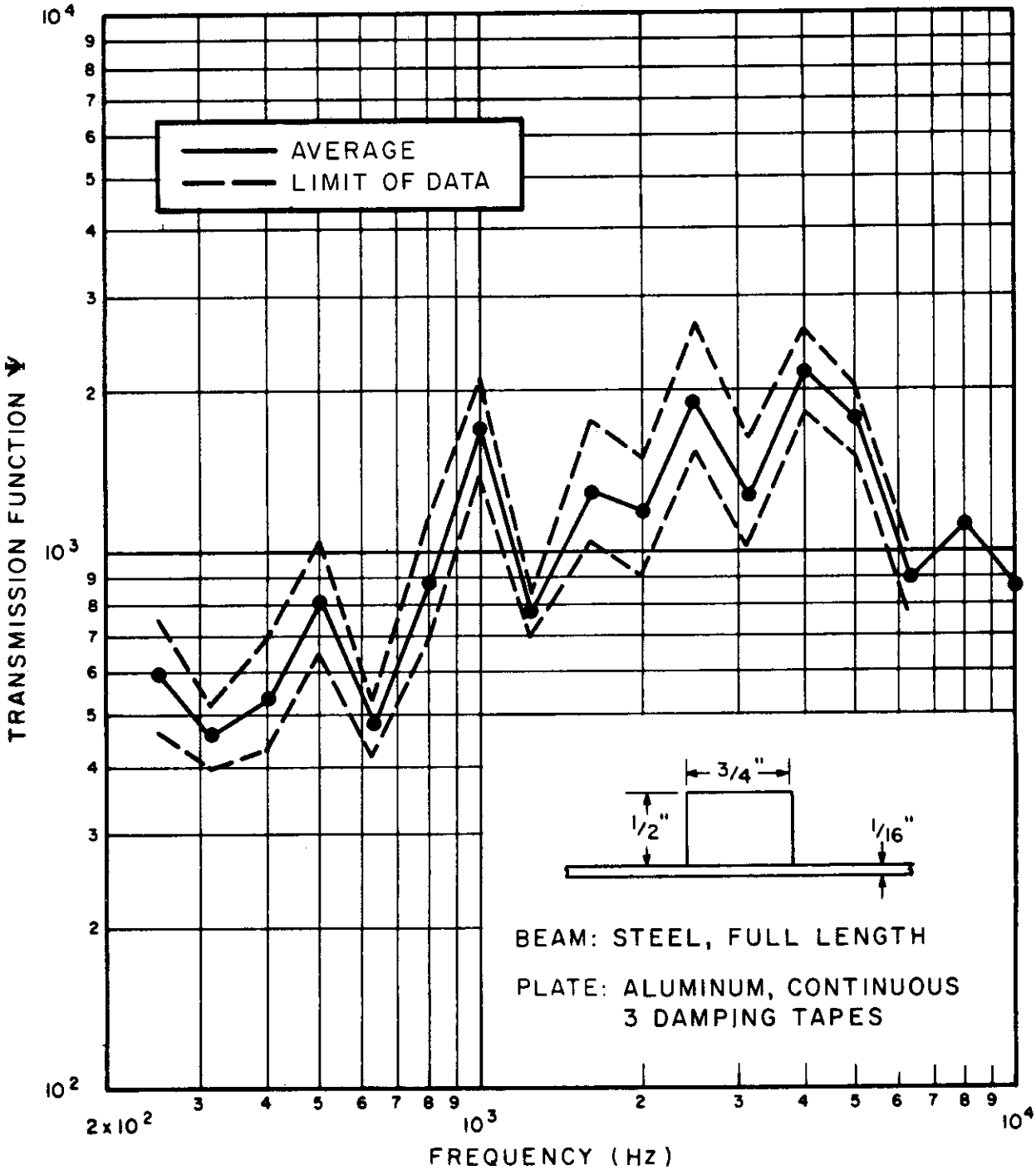

FIG. 16e POWER FLOW ACROSS A BEAM ON A PLATE

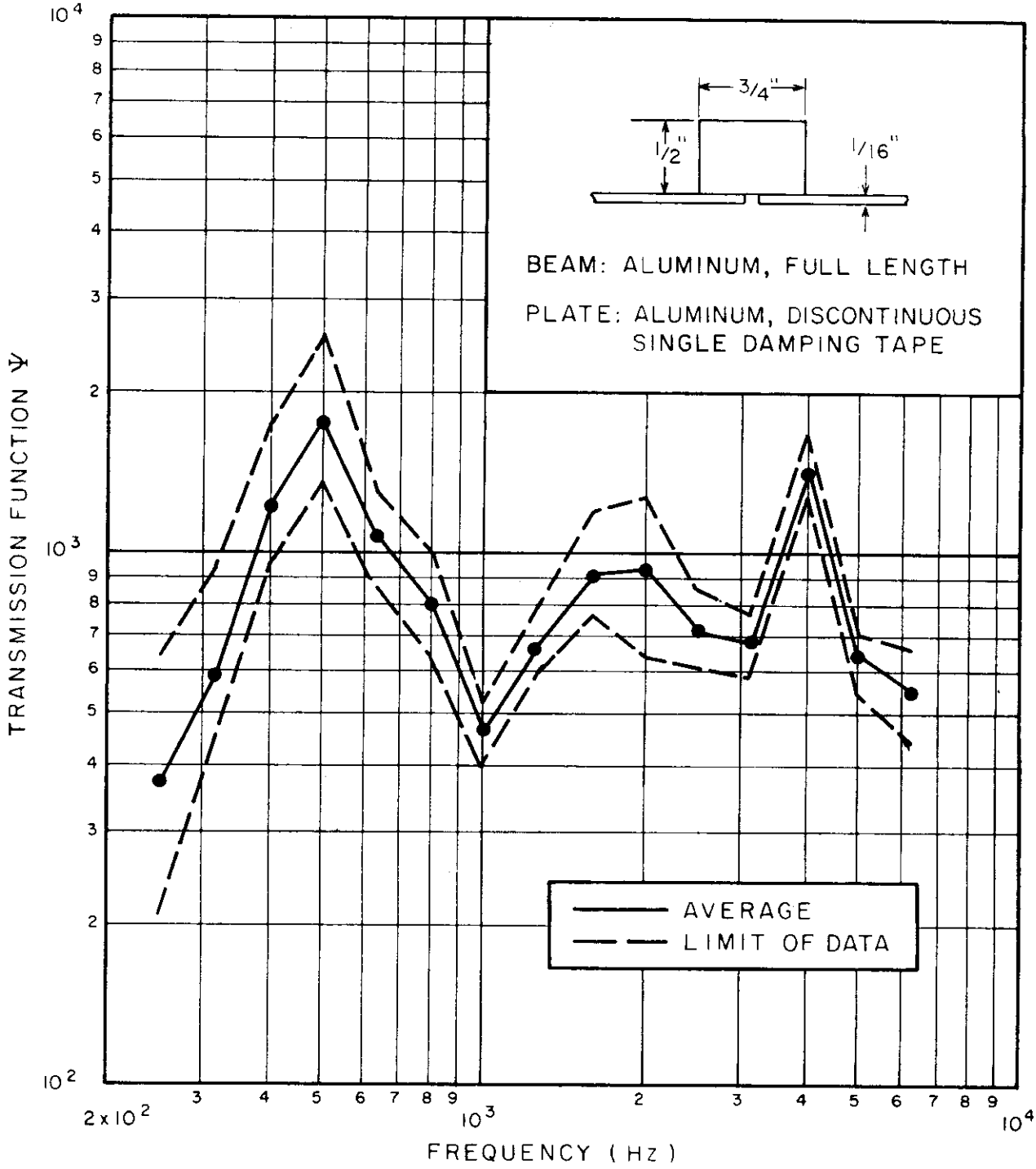

FIG. 16f POWER FLOW ACROSS A BEAM ON A PLATE

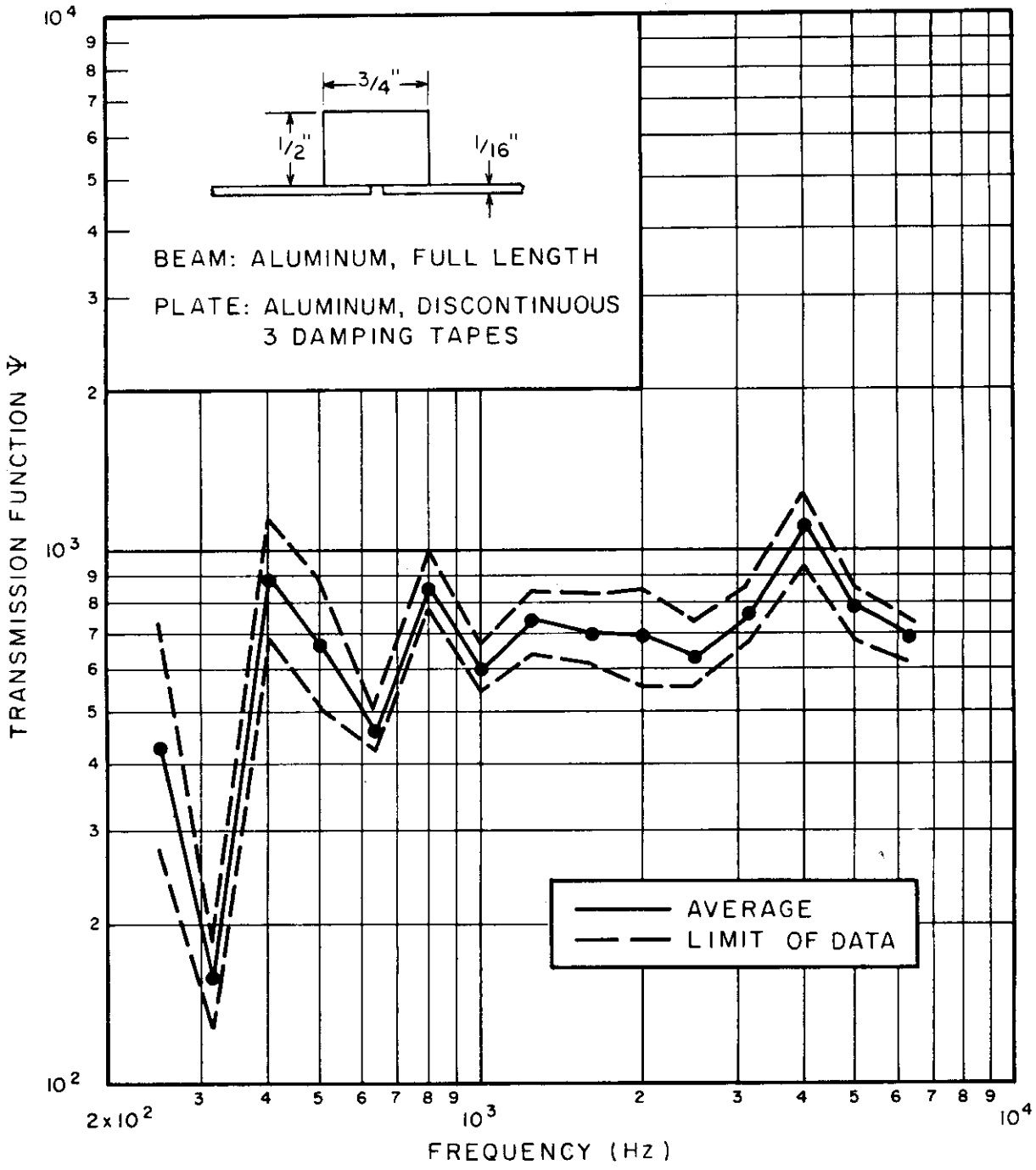

FIG. 16g POWER FLOW ACROSS A BEAM ON A PLATE

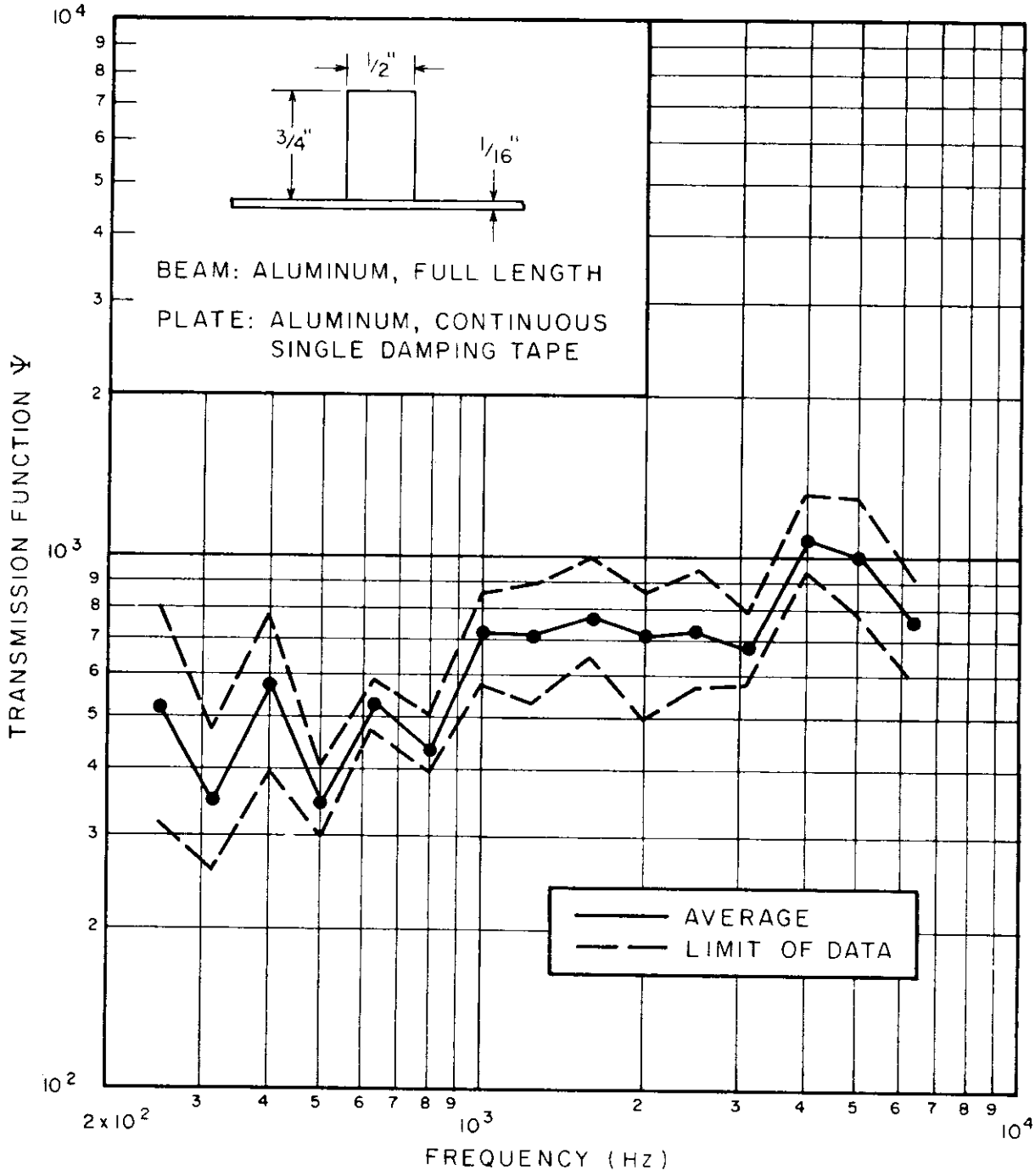

FIG. 16h POWER FLOW ACROSS A BEAM ON A PLATE

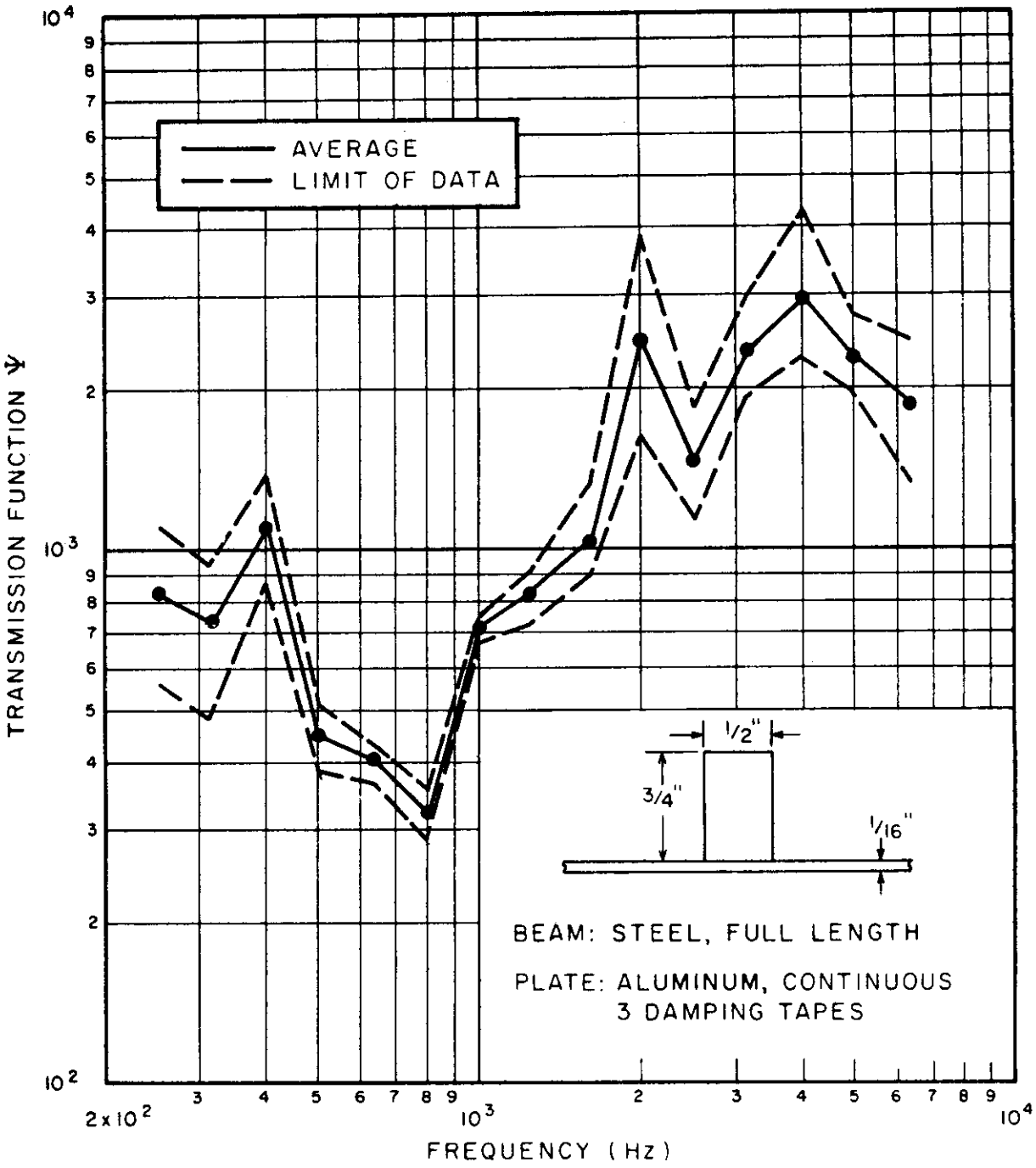

FIG. 161 POWER FLOW ACROSS A BEAM ON A PLATE

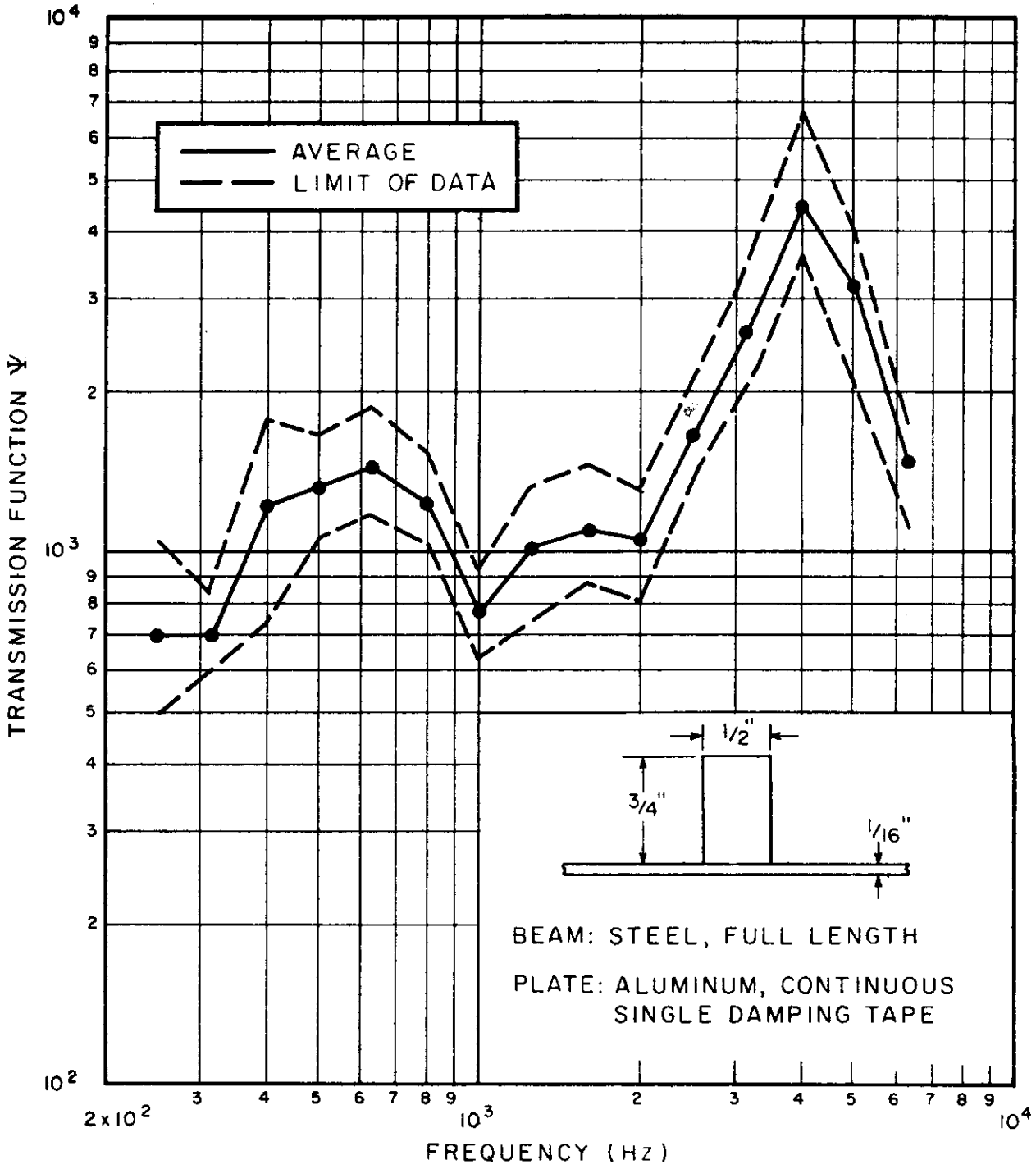

FIG. 16j POWER FLOW ACROSS A BEAM ON A PLATE

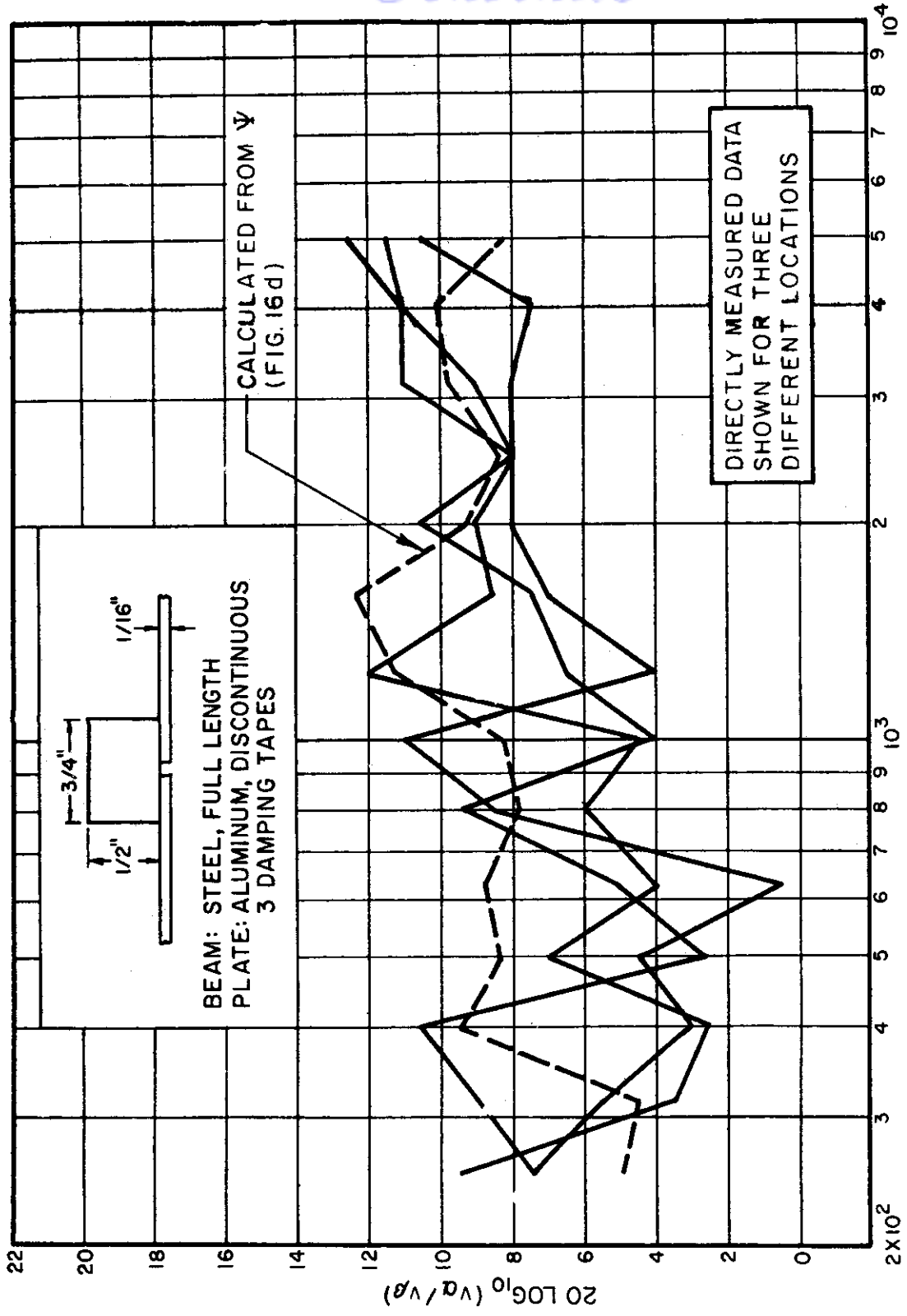

FIG. 17a PLATE VELOCITY RATIO

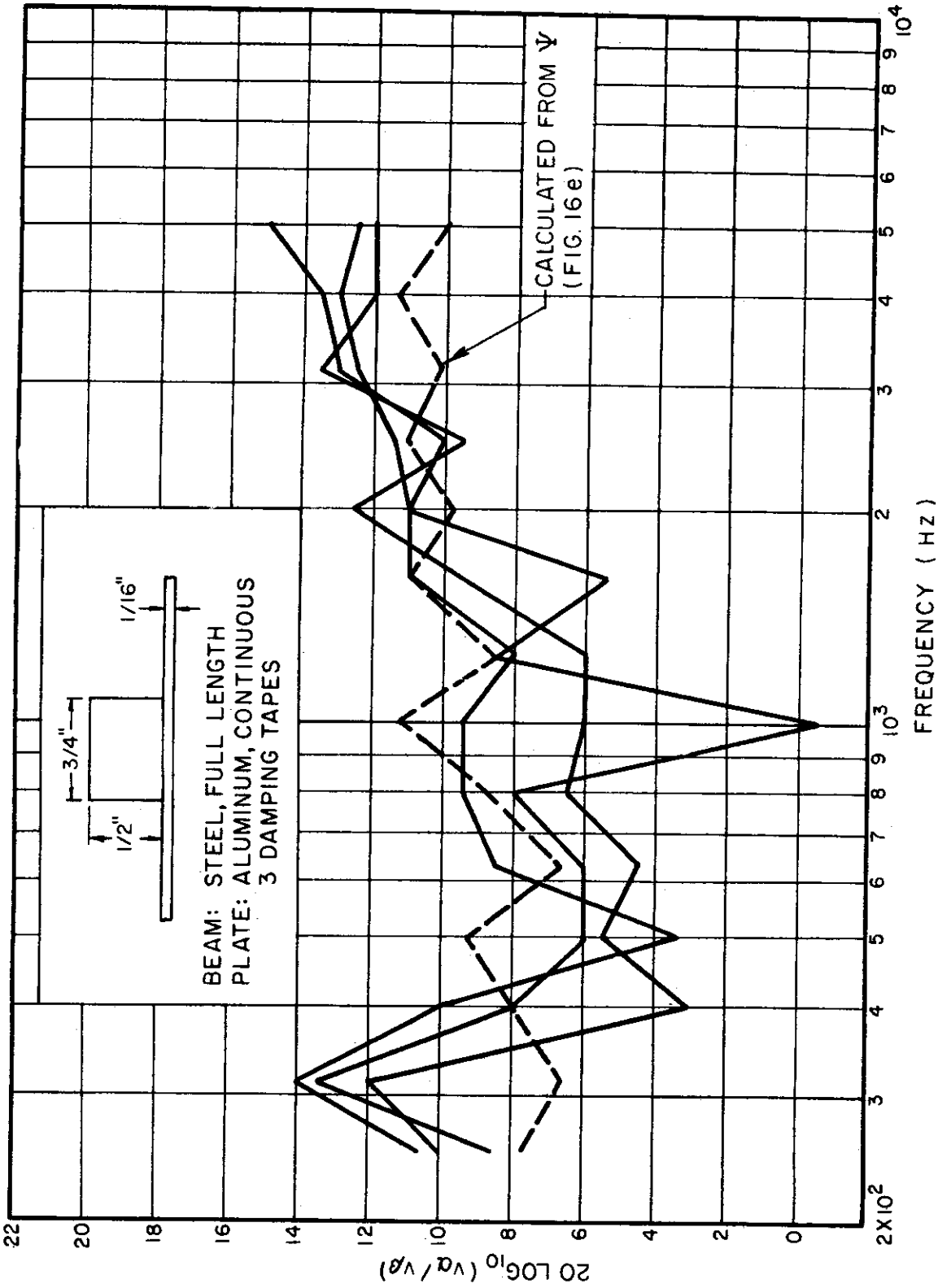

FIG. 17b PLATE VELOCITY RATIO

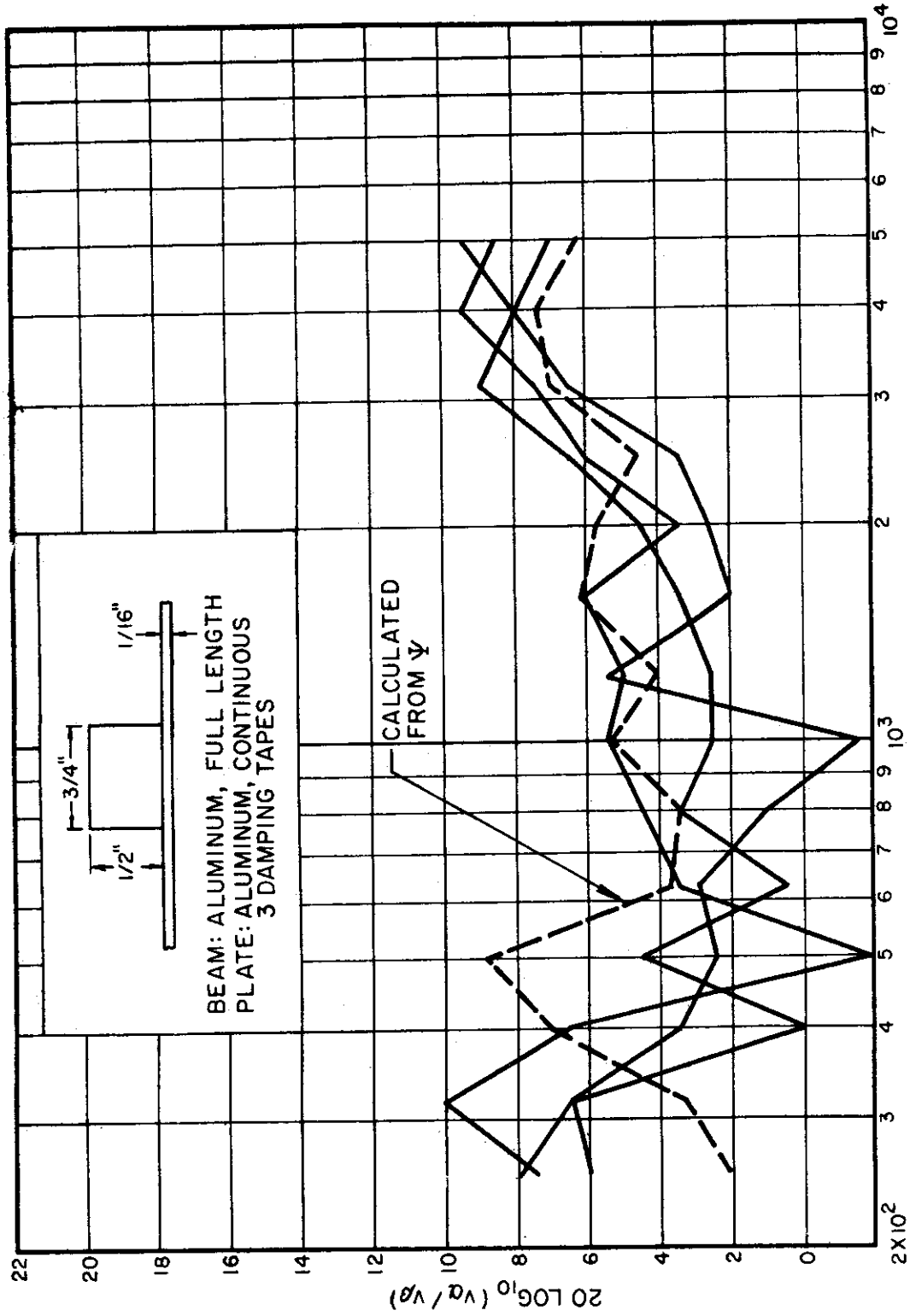

FIG. 17c PLATE VELOCITY RATIO

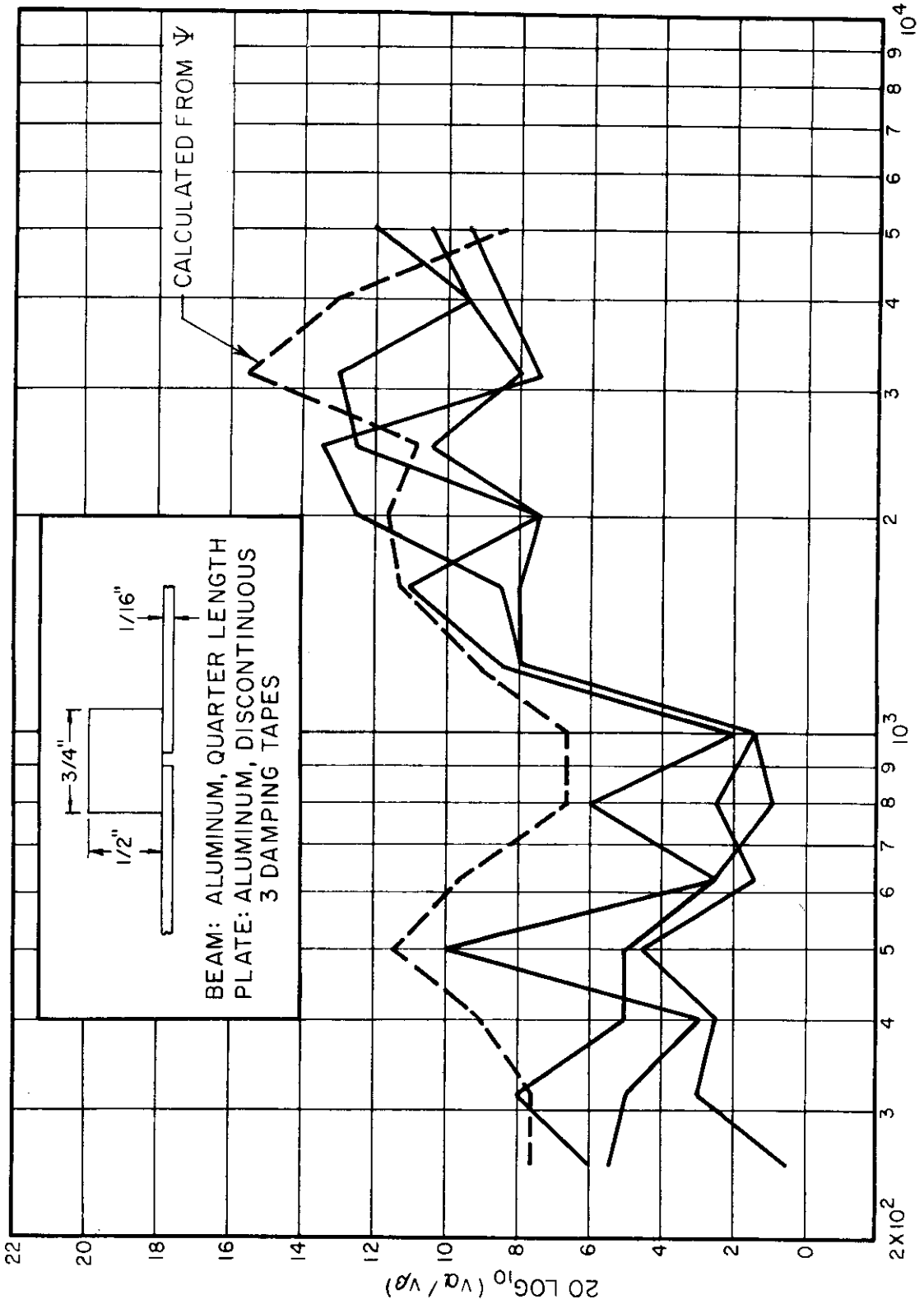

FIG. 17d PLATE VELOCITY RATIO

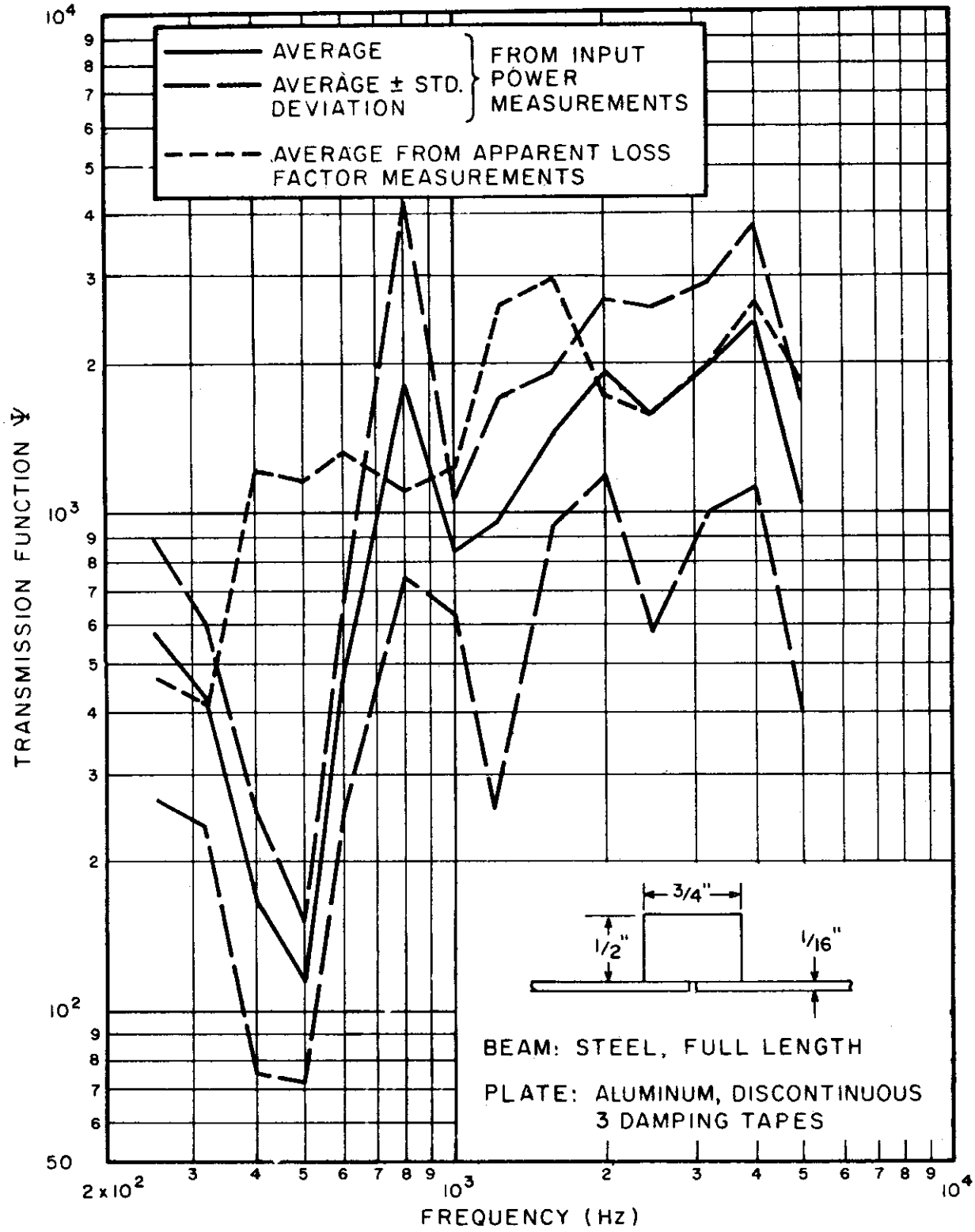

FIG. 18a TRANSMISSION FUNCTION DATA FROM INPUT POWER MEASUREMENTS

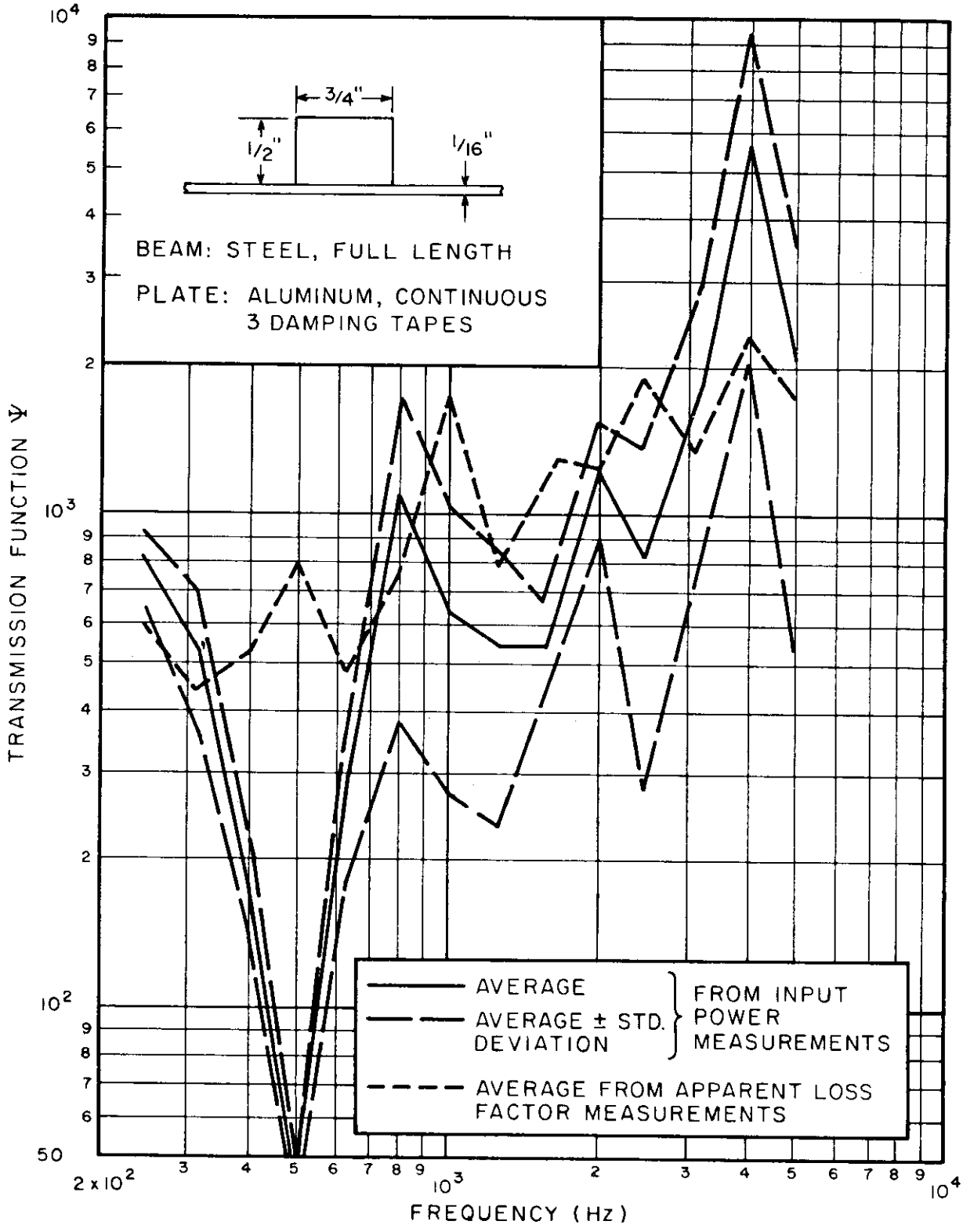

FIG. 18b TRANSMISSION FUNCTION DATA FROM INPUT POWER MEASUREMENTS

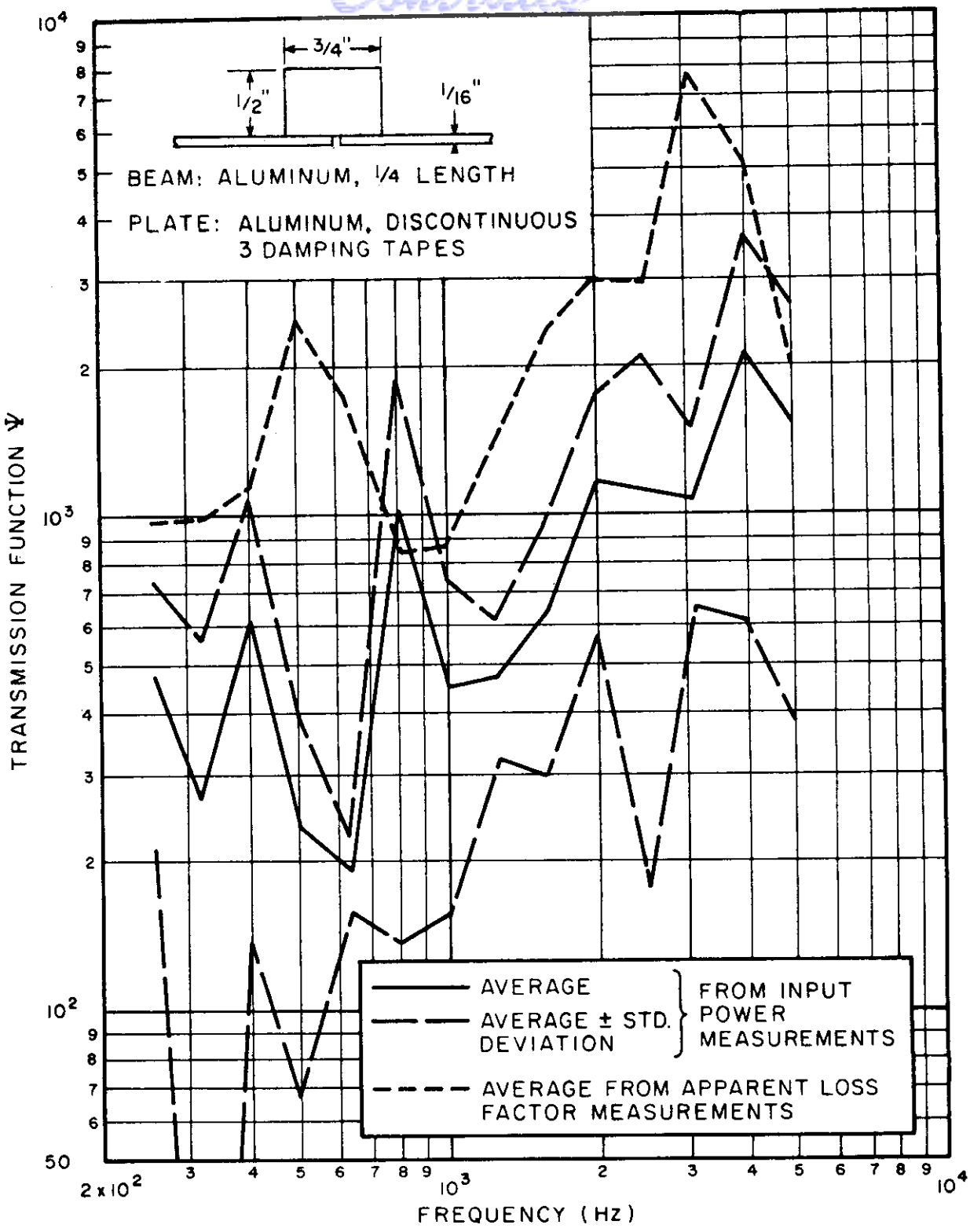

FIG. 18c TRANSMISSION FUNCTION DATA FROM INPUT POWER MEASUREMENTS

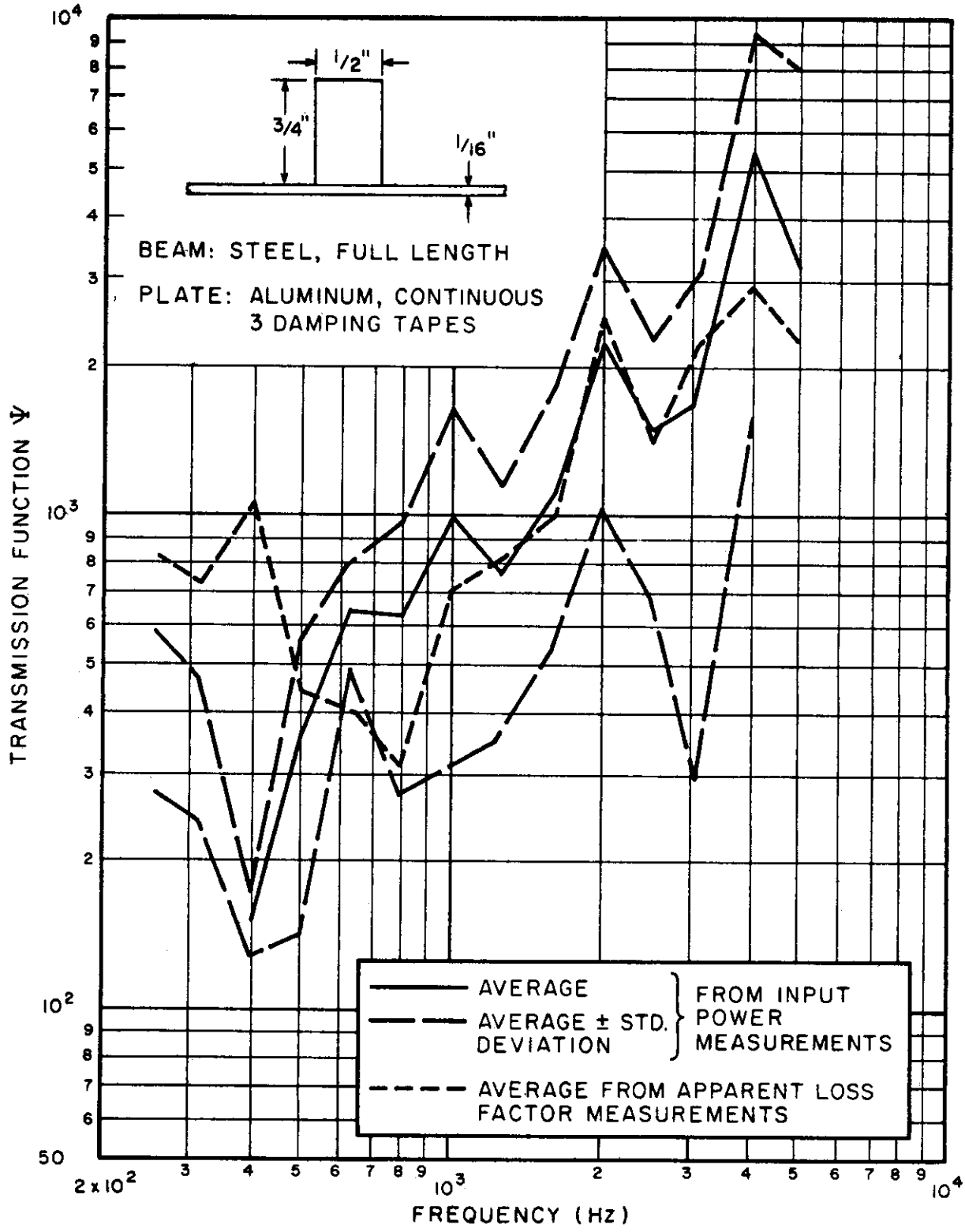

FIG. 18d TRANSMISSION FUNCTION DATA FROM INPUT POWER MEASUREMENTS

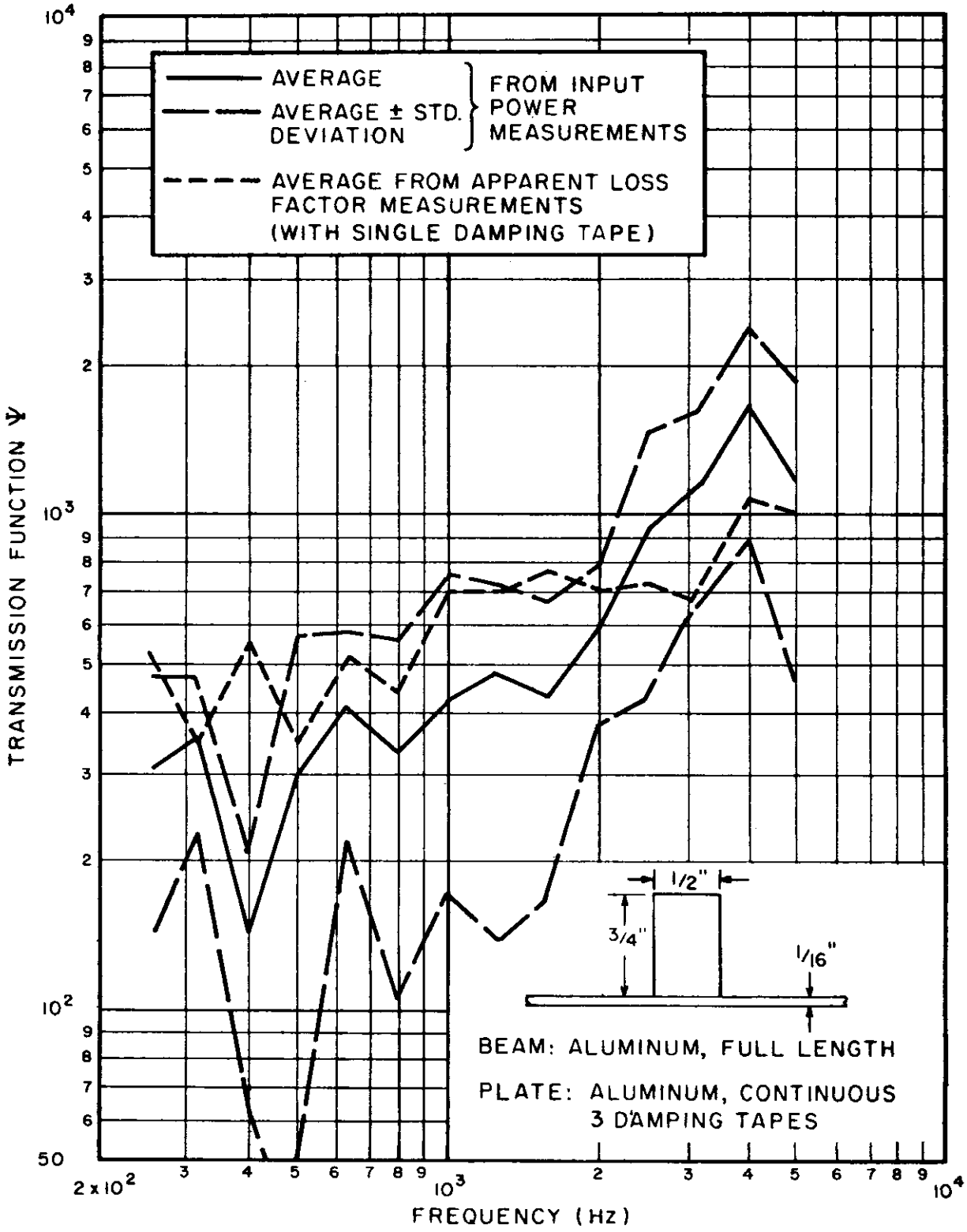

FIG. 18e TRANSMISSION FUNCTION DATA FROM INPUT POWER MEASUREMENTS

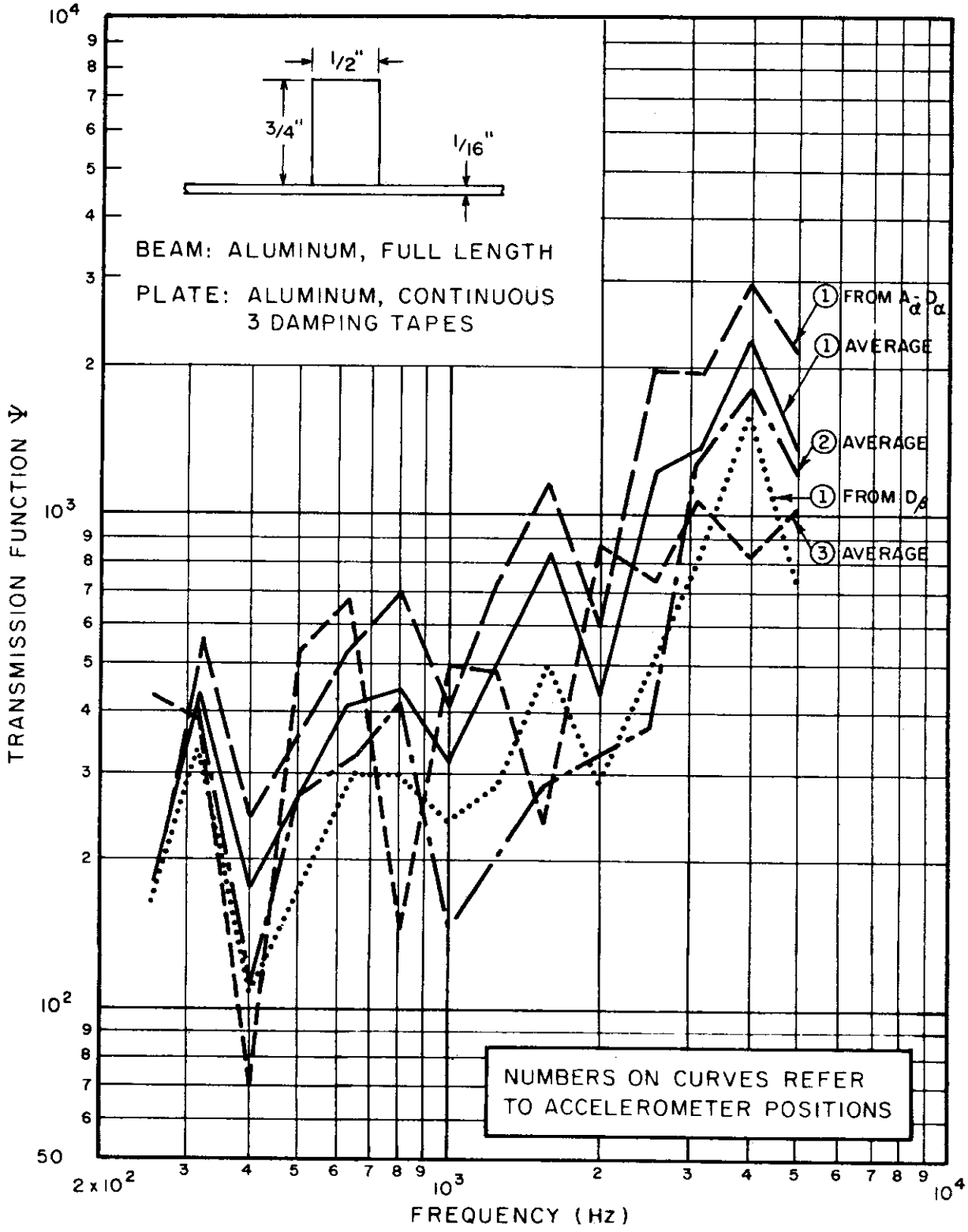

FIG. 19 VARIABILITY OF TRANSMISSION FUNCTION DATA OBTAINED FROM POWER MEASUREMENTS

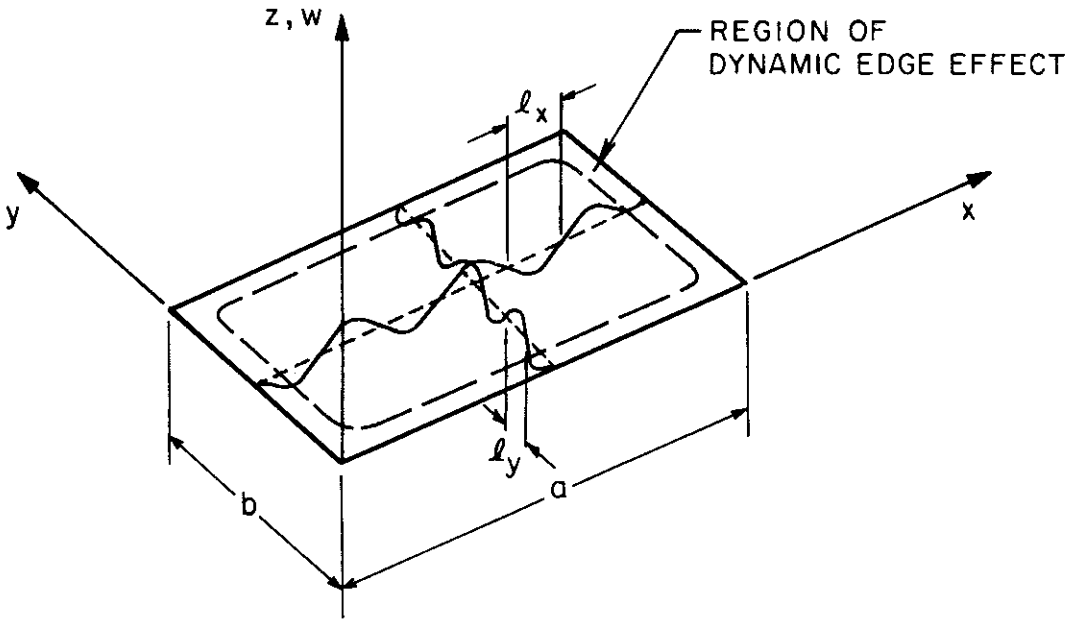

FIG. 20 DYNAMIC EDGE EFFECT REGION IN RECTANGULAR PLATE

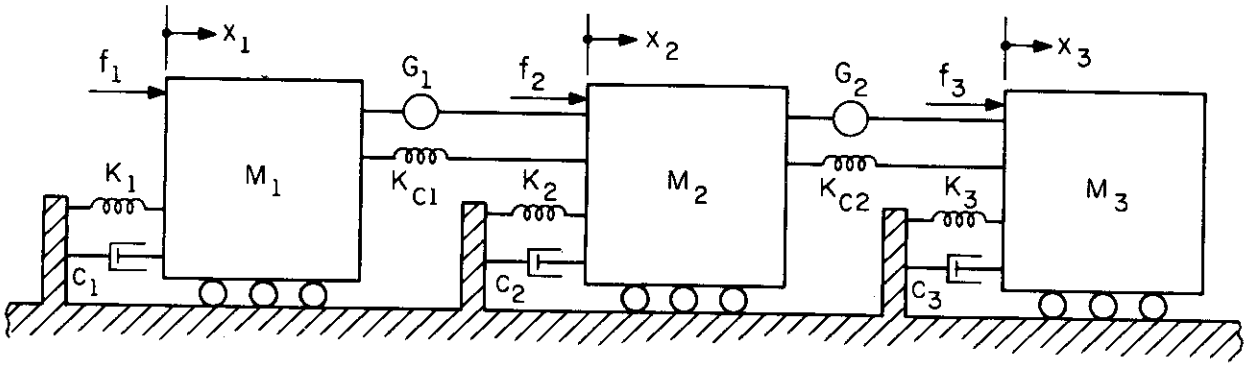

$$\beta_i = M_i / c_i$$

$$\omega_1^2 M_1 = K_1 + K_{c1}$$

$$\omega_2^2 M_2 = K_2 + K_{c1} + K_{c2}$$

$$\omega_3^2 M_3 = K_3 + K_{c2}$$

FIG. 21 THREE COUPLED OSCILLATORS

Unclassified
Security Classification

DOCUMENT CONTROL DATA - R & D

(Security classification of title, body of abstract and indexing annotation must be entered when the overall report is classified)

1. ORIGINATING ACTIVITY (Corporate author)
Bolt Beranek and Newman Inc.
50 Moulton Street
Cambridge, Massachusetts 02138

2a. REPORT SECURITY CLASSIFICATION
Unclassified

2b. GROUP

3. REPORT TITLE

APPLICATION OF STATISTICAL ENERGY ANALYSIS TO VIBRATIONS OF MULTI-PANEL STRUCTURES

4. DESCRIPTIVE NOTES (Type of report and inclusive dates)
Final Report, February 1966 to April 1967

5. AUTHOR(S) (First name, middle initial, last name)
Eric E. Ungar, Nicholas Koronaois, and Jerome E. Manning

6. REPORT DATE
August 1967

7a. TOTAL NO. OF PAGES
108

7b. NO. OF REFS
27

8a. CONTRACT OR GRANT NO.
AF 33(615)-2649

b. PROJECT NO.
1370

c.
Task No. 137005

d.

9a. ORIGINATOR'S REPORT NUMBER(S)
AFFDL-TR-67-79

9b. OTHER REPORT NO(S) (Any other numbers that may be assigned this report)
BBN Report No. 1491

10. DISTRIBUTION STATEMENT
This document is subject to special export controls and each transmittal to foreign governments or foreign nationals may be made only with prior approval of the AF Flight Dynamics Laboratory (FDD).

11. SUPPLEMENTARY NOTES
This report is a supplement to AFFDL-TR-66-52.

12. SPONSORING MILITARY ACTIVITY
AF Flight Dynamics Laboratory, Wright-Patterson Air Force Base, Ohio 45433

13. ABSTRACT

Experimentally determined vibratory mean square velocity distributions on a multi-panel planar structure and on a ring-and-stringer reinforced cylindrical shell are compared with predictions obtained from statistical energy analysis. Generally good agreement is observed.

The flow of mechanical power between two panels that are separated by a reinforcing beam is studied, in order to uncover the important parameters and to provide information on the coefficients of proportionality between power flow and average modal energy difference, which one must know in order to apply statistical energy analysis. No analytical prediction methods are developed for these coefficients, but an empirical measurement technique is presented and is shown to yield consistent results.

Analyses pertaining to dynamic response concentrations in plate and shell structures are summarized, and investigations of response characteristics and response statistics which warrant further pursuit are delineated.

Distribution of this Abstract is Unlimited

DD FORM 1 NOV 65 1473 (PAGE 1)
S/N 0101-807-6811

Unclassified
Security Classification

14. KEY WORDS	LINK A		LINK B		LINK C	
	ROLE	WT	ROLE	WT	ROLE	WT
Vibrations						
Vibratory Systems						
Sound Transmission						